COMPRESSIVE AND TENSILE BEHAVIORS OF STEEL FIBER REINFORCED CONCRETE

A MASTER'S THESIS

IN

CIVIL ENGINEERING

ATILIM UNIVERSITY

BY

ALFADHIL. A. GHEIT. ALFADHIL ABDUSSALAM

JUNE 2015

COMPRESSIVE AND TENSILE BEHAVIORS OF STEEL FIBER REINFORCED CONCRETE

A THESIS SUBMITTED TO
THE GRADUATE SCHOOL OF NATURAL AND APPLIED SCIENCES
OF
ATILIM UNIVERSITY
BY
ALFADHIL. A. GHEIT. ALFADHIL ABDUSSALAM

IN PARTIAL FULFILLMENT OF THE REQUIREMENTS FOR THE DEGREE OF
MASTER OF SCIENCE
IN
CIVIL ENGINEERING DEPARTMENT

Approval of the Graduate School of Natural and Applied Sciences, Atılım University

_____

Prof. Dr. İbrahim Akman

Director

I certify that this thesis satisfies all the requirements as a thesis for the degree of Master of Science.

_____

Assoc. Prof. Dr. Tolga Akış

Head of Department

This is to certify that we have read the thesis "Compressive and Tensile Behaviors of Steel Fiber Reinforced Concrete" submitted by Alfadhil. A. Gheit. Alfadhil Abdussalam and that in our opinion it is fully adequate, in scope and quality, as a thesis for the degree of Master of Science.

Assist. Prof. Dr. Halit Cenan Mertol	Assoc. Prof. Dr. Eray Baran
Supervisor	Co-supervisor

Examining Committee Members

Assoc. Prof. Dr. Tolga Akış	_____
Assoc. Prof. Dr. Eray Baran	_____
Assist. Prof. Dr. Halit Cenan Mertol	_____
Assist. Prof. Dr. Gökhan Tunç	_____
Assist. Prof. Dr. Saeid Kazemzadeh Azad	_____

Date: 23rd of June, 2015

I declare and guarantee that all data, knowledge and information in this document has been obtained, processed and presented in accordance with academic rules and ethical conduct. Based on these rules and conduct, I have fully cited and referenced all material and results that are not original to this work.

Name, Last name: Alfadhil. A. Gheit. Alfadhil Abdussalam

Signature:

ABSTRACT

COMPRESSIVE AND TENSILE BEHAVIORS OF STEEL FIBER REINFORCED CONCRETE

Alfadhil. A. Gheit. Alfadhil Abdussalam
M.S., Civil Engineering Department
Supervisor: Assist. Prof. Dr. Halit Cenan Mertol
Co-supervisor: Assoc. Prof. Dr. Eray Baran
June 2015, 113 pages

Steel fiber reinforced concrete (SFRC) is a concrete mixture containing discontinuous, discrete steel fibers that are randomly dispersed and uniformly distributed. The quality and quantity of steel fibers influence the mechanical properties of concrete. It is in general accepted that the addition of steel fibers significantly increases tensile toughness and ductility, also slightly enhances the compressive strength. The benefits of using steel fibers become apparent after concrete cracking because the tensile stress is then redistributed to fibers.

The objective of this study is to investigate the compressive and tensile behavior of steel fibers in reinforced concrete by conducting an experimental program consisting of load testing on various specimens made from conventional concrete (CC) and steel fiber reinforced concrete (SFRC).

Test series consisted of cylindrical compression (100×200 and 150×300 mm) and prismatic modulus of rupture (150×150×600 mm) specimens. Tensile tests on reinforcing bars surrounded by prismatic concrete specimens were also performed. The variables used in these tests were lengths (500, 1000, and 1500 mm) and cross-sectional dimensions (60×60, 100×100,150×150, 200×200 mm) of the prismatic concrete specimens around reinforcing bar.

Load-deflection behaviors were obtained and evaluated to develop the compressive and tensile stress-strain relationships of SFRC. Experimental load-deflection

relationships obtained from modulus of rupture tests were compared to the predicted load-deflection curves determined using compressive and tensile stress-strain curves obtained in this research. Also the stress-strain relationships available in the literature were used predict the behavior.

Keywords: Steel fiber reinforced concrete, compressive, tensile, stress-strain relationship, flexure.

ÖZ

ÇELİK LİFLİ BETONUN ÇEKME VE BASINÇ ALTINDAKİ DAVRANIŞI

Alfadhil. A. Gheit. Alfadhil Abdussalam

Yüksek Lisans, İnşaat Mühendisliği Bölümü

Tez Yöneticisi: Yrd. Doç. Dr. Halit Cenan Mertol

Ortak Tez Yöneticisi: Doç. Dr. Eray Baran

Haziran 2015, 113 sayfa

Çelik lifli beton, içinde belirli uzunluktaki çelik liflerin gelişigüzel ve düzgün bir şekilde yayılımı ile elde edilen bir beton karışımıdır. Liflerin kalitesi ve miktarı betonun mekanik özelliklerini etkilemektedir. Çelik liflerin betona katılması, betonun çekme tokluğunu ve sünekliğini arttırdığı, basınç dayanımını da ufak da olsa iyileştirdiği genel olarak kabul edilmiştir. Betonun kırılmasından sonra çekme gerilmelerinin lifler arasındaki dağılımı sağlandığından dolayı çelik liflerin yararı daha belirgin olarak görülmektedir.

Bu araştırmanın amacı, çelik lifli betonun çekme ve basınç altındaki davranışının, konvansiyonel ve çelik lifli beton kullanılan çeşitli numuneler üzerinde uygulanan yükleme deneyleri ile incelenmesidir.

Deney numuneleri basınç silindirlerinden (100×200 ve 150×300 mm), prizmatik eğilme dayanımı elemanlarından (150×150×600 mm) oluşmaktadır. Ayrıca çelik donatıyı çevreleyen prizmatik beton numuneler üzerinde çekme deneyleri gerçekleştirilmiştir. Çelik donatı çevresindeki prizmatik numuneler için gerçekleştirilen çekme deneylerinde beton prizmaların uzunlukları (500, 1000, ve 1500 mm) ve kesit boyutları (60×60, 100×100,150×150, 200×200 mm) değişkenler olarak uygulanmıştır.

Yük-deformasyon davranışları elde edilmiş ve çelik lifli betonun basınç ve çekme altındaki gerilme-birim uzama ilişkileri bulunmuştur. Prizmatik eğilme numunelerinden elde edilen yük-deformasyon davranışları, bu araştırmada bulunan basınç ve çekme altındaki gerilme-birim uzama ilişkileri kullanılarak tahmin edilen

yük deformasyon davranışları ile karşılaştırılmıştır. Ayrıca literatürde bulunan farklı gerilme-birim uzama modelleri kullanılarak davranışlar yeniden tahmin edilmiştir.

Anahtar Kelimeler: Çelik lifli beton, basınç, çekme, gerilme-birim uzama ilişkisi, eğilme.

DEDICATION

To my parents

For their endless support, love and prayers

ACKNOWLEDGMENTS

I express my sincere gratitude to my supervisor, Assist. Prof. Dr. Halit Cenan Mertol, for their patience, numerous constructive suggestions, inspirational and motivational advices throughout the time I worked with them.

My gratitude goes also to the laboratory technicians Ali Şener Dursunoğlu, Şuayip Özdemir, Cafer Hastürk, and Eren Öden who made sure all activities went correctly and successfully throughout the laboratory work.

I am grateful to friends, well-wishers and all those who contributed in one way or another to the achievement of this research work.

I would like to express my appreciation to the committee members for this research project.

TABLE OF CONTENTS

LIST OF FIGURES

LIST OF TABLES

1 INTRODUCTION

1.1 General

During the last four decades, fiber reinforced concrete has been increasingly used in civil engineering structures, often in combination with reinforced concrete, and many researches have been undertaken to more fully understand its mechanical properties (Fanella and Naaman (1985)). Steel fiber reinforced concrete (SFRC) is a concrete mixture containing discontinuous, discrete steel fibers that are randomly dispersed and uniformly distributed. The quality and quantity of steel fibers influence the mechanical properties of concrete. It is in general accepted that the addition of steel fibers significantly increases tensile toughness and ductility, also slightly enhances the compressive strength. The benefits of using steel fibers become apparent after concrete cracking because the tensile stress is then redistributed to fibers.

Researches in the early of 1960's by Ramouldi and Baston (1963) and Ramouldi and Mandel (1964) on closely spaced random fibers, mainly steel fibers, started the era of using the fiber composite concretes that we have today. Steel and synthetic fibers have been used to enhance the properties of concrete in practice for many years. However, commercial use of fibers in concrete begun in 1970's particularly in Europe, Japan and the USA. In addition, Shah and Rangan (1971), Swamy (1975), and several other researchers in the United States, Japan, United Kingdom, and Russia performed extensive researches on the use of other types of fibers in addition to steel. Other developments using bundled fiberglass as the main reinforcement in concrete members were introduced by Navy et al. (1971) and Navy and Neuwerth (1977). Nowadays, a wide range of engineering materials including ceramics, plastics, cements, and gypsum, are being used to improve composite properties of concrete.

1.2 Motivation

It is widely known that concrete is brittle in tension and strong in compression. In construction sector, this deficiency can be overcome by providing steel bars to carry the tensile forces to improve tension reinforcement in concrete . The reinforcement can also be in form of pre-stressed so that the concrete will be entirely in compression under load. The purpose of such reinforcements is to ensure that the capacity of the plain concrete does not go above the load capacity of the concrete sections (Cement and Concrete Association of New Zealand (2009)).

When steel fibers are used, the behavior of concrete changes. This change affects not only its strength but also its behavior under tension and compression. These changes affect the overall performance of the members made of SFRC. The flexural behavior of SFRC structural members can be estimated if behaviors under tension and compression of SFRC are known.

1.3 Objectives and Scope

The objective of this study is to investigate the tensile and compressive behaviors of fiber steel in reinforced concrete by:

- Evaluating the previous research published by other researchers related to tensile behavior of SFRC.
- Conducting an experimental program consisting of load testing of specimens with conventional concrete and SFRC to establish the tensile and compressive stress-strain relationships.
- Using the tensile and compressive stress-strain relationships to determine the behavior of tested flexural members were estimated.

1.4 Thesis Organization

In Chapter 2, a detailed literature review related to SFRC is presented. Previous researches on SFRC members under compression, tension and flexure are explained in details.

The materials, test specimens, test sep-up and procedure is described in Chapter 3. Pictures are also presented for some of the specimens during fabrication, load testing, and after the test.

Results obtained from laboratory test are presented and discussed in both graphical and tabular forms in Chapter 4. The results are discussed in details.

In Chapter 5, an analytical work was performed to estimate the behavior of tested flexural specimens using the stress-strain models of SFRC under tension and compression. These models were selected based on the correlation of the model to the test data obtained in the scope of this research.

A brief summary and conclusion is presented in Chapter 6. Also recommendations for the future work is also explained based on the experience gained in this research.

2 BACKGROUND

2.1 General

Conventional concrete is a brittle material with low tensile strength and low strain capacity at fracture. The addition of conventional reinforcement in forms of mesh or bars will result in enhanced the load carrying capacity at the cracked section at the maximum limit state. Also better control cracking, reduced rotation and deflection at the serviceability limit state may be achieved. As mentioned above, the conventional reinforcements cannot prevent the formation and development of micro-cracks. On the other hand, steel fibers are discontinuous and randomly dispersed in the concrete matrix. They improve the stiffness and crack-control performance by arresting and retarding the development of micro-cracks. Common applications of SFRC include overlays in bridge decks, highway and airport pavements, thin-shell structures, seismic, impact, and explosion-resisting structures, and shotcrete applications (Cement and Concrete Association of New Zealand - CCANZ, 2009).

2.2 Types of Steel Fibers

The steel fibers can be classified on the basis of the production process, the shape as well as the material:

- **Based on production process:**
  - cold-drawn wire (Type A);
  - cut sheet (Type B);
  - other processes (Type C).
- **Based on shape:**
  - straight;
  - deformed (hooked, crimped, etc.).
- **Based on material:**
  - steel with low carbon content ($C \leq 0.20$, Type 1);
  - steel with high carbon content ($C > 0.20$, Type 2);
  - stainless steel (Type 3).

Figure 2-1 – Typical shape for hooked end steel fiber (www.imerstore.it/product/4424/Kerabuild-HW-Steel-Fiber-Dramix-RC-80-30-BP-Conf.-da-20-kg.html)

2.3 Properties of Steel Fibers

The steel fibers have a length, l_f, usually ranging from 6 to 70 mm and an equivalent diameter, d_f, ranging from 0.15 to 1.20 mm. Steel fibers are short, have discrete lengths having an aspect ratio (ratio of length to diameter) about 20 to 100. They are manufactured in several different cross sections and are sufficiently small to be randomly dispersed in an unhardened concrete mixture using the usual concrete mixing procedure. Steel fibers are produced by various processes, in various shapes, and geometries. Most of steel fibers however, are round in cross-section with an equivalent diameter ranging between 0.15 and 2 mm and lengths ranging between 7 and 75 mm. The fibers used in the early times were round and smooth, and obtained by cutting or chopping wires to the required lengths. Nowadays, steel fibers have either rough surfaces, can be crimped, hooked at their ends, or deformed along their length.

2.3.1 Fiber Content

In terms of fiber proportion within a concrete mixture, most literature refers to the percentage of fibers by volume expressed by the symbol V_f. The use of 78 kg/m^3 of

fibers results in 1% of fibers per volume of concrete. Typical fiber contents range from 0.25 to 1.5%, with non-structural applications typically requiring fiber contents of 0.5% or less, while quantities greater than 0.5% are typically required for most structural applications (Aoude, 2007). It should be noted that increasing fiber content beyond certain limits in traditional concrete (typically above 1%) can cause problems during mixing and placement.

2.3.2 Fiber Length

According to the National Research Council (CNR-204/2006), the length of steel fibers, $l_{f,}$ usually ranges from 6 to 70 mm. In the ACI 544.4R, steel fibers have lengths ranging between 25 and 60 mm. The definitions for length and the diameter of the fiber are shown in Figure 2-2.

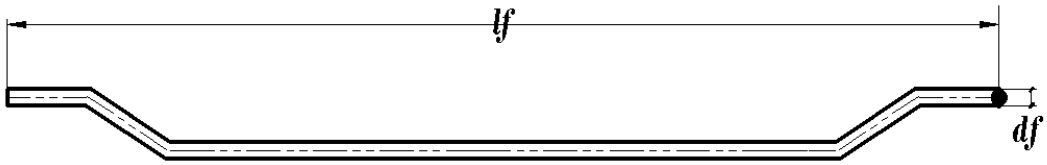

Figure 2-2 – Typical length and diameter for hooked end steel fiber

2.3.3 Fiber Equivalent Diameter

For fibers that are not circular in cross-section, the equivalent diameter is the diameter of a circle having the same area as that of the average cross-sectional area of the fiber.

2.3.4 Fiber Aspect Ratio

The fiber aspect ratio is the major characteristics of the slenderness of an individual fiber. It is defined as fiber (l_f) length divided by the equivalent fiber diameter (d_f) for a particular type of fiber. The aspect ratio is also a measure of fiber stiffness and bond characteristics. The fiber aspect ratio may be calculated as follows:

Fiber aspect ratio = l_f / d_f Equation 2-1

2.3.5 Fiber Reinforcement Index (RI)

Fiber reinforcement index is defined as the weight (W_f) or volume fraction of fiber multiplied by the fiber aspect ratio as shown:

$$RI = W_f \, \mathrm{x} l_f \, / d_f. \qquad \text{Equation 2-2}$$

2.4 Requirements for Steel Fibers

For efficient and effective performance of steel fibers in hardened concrete, the following points are essential in achieving the expected results.

- Fibers should be significantly stiffer than the matrix. This means that the fibers should have modulus of elasticity higher than that of the matrix itself (The Concrete Institute, 2007).
- Fiber content in the matrix should be adequate.
- Fiber-matrix bond must be ensured.
- Length and diameter of fiber must be reasonably sufficient.
- Fibers must have high aspect ratio, i.e. they must be long relative to their diameter.
- The shape and material from which the fiber is made, i.e. whether hooked end, flat end, deformed or flat shape, and whether metallic fibers, glass fibers, polymeric or carbon fibers are used.

2.5 SFRC in Tension

When concrete is subjected to tensile forces, it shows signs of weakness as cracks. SFRC has more resistance to tensile stresses and better post cracking behavior and increased toughness.

Conventional concrete has tensile strength between 8 and 14% of its compressive strength, as a result of cracking at low stress levels occurs. Steel fibers when added to concrete, are able to enhance the tensile strength by preventing the micro cracks from

propagating and widening (Edward, 2008). Ductility is also increased due to the fibers' energy absorption capacity. SFRC is mainly used in the construction of statically redundant structures, where the residual tensile strength may improve the load bearing capacity of the structures as well as its ductility.

For low volume fraction of fibers, the phenomena in the post cracking region is characterized by softening behavior and this implies that the post crack flexural strength provided by the steel fiber is typically less than the capacity of the non-cracked matrix. For higher volume ratio however (higher than 2%), the post-cracking behavior is termed strain-hardening and this means the strength can be higher than that of the non-cracked matrix due to the formation of multiple cracks (Cement and Concrete Association of Switzerland, 2009). In direct tension, the improvement of strength is significant, with increases on the order of 30 to 40% reported for the addition of fiber in mortar or concrete. Test results of direct tension tests are shown in Figure 2-3.

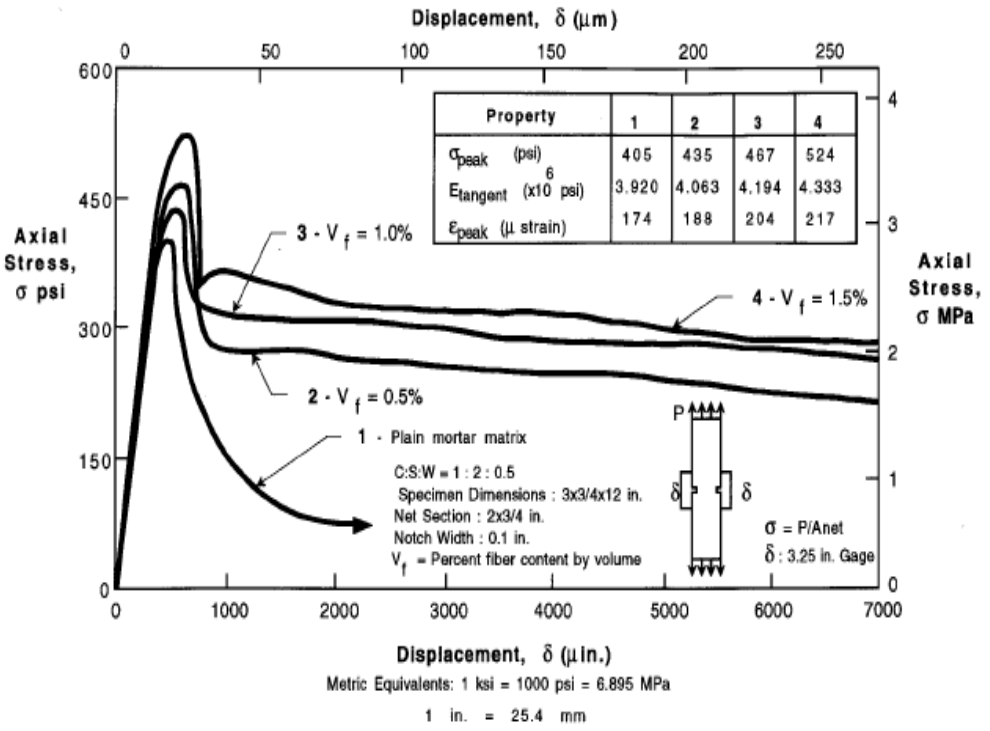

Figure 2-3 – Results of stress-displacement curves from direct tension tests (ACI 544-96)

Several models and expressions have been proposed to predict the tensile behavior of SFRC members subjected to uniaxial tension. The models of Abrishami and Mitchell (1997), Bentur and Mindes (1990), Frank et al. (2013), Henager and Doherty (1976), Lok and Xiao (1998), Sorankom and Mobasher (2009), and Chuang (2006) are some of the models discussed in the literature.

2.5.1 Sabeena et al. (2013)

Sabeena et al. (2013) conducted an experimental work to study the tension stiffening and cracking of hybrid fiber reinforced concrete. Twenty four specimens having 60x60x600 mm dimensions reinforced by 10 mm steel bars were used. The investigated variables were the volume of steel fibers (0.5 and 1%) and volume of polypropylene fibers (0.10%, 0.15% and 0.20%) in the mixture. The specimens were tested under uniaxial tension using tension machine having a capacity of 1000 kN. Sabeena et al. (2013) reported that, the addition of steel fibers and polypropylene fibers improved the tension stiffening effect considerably, and thus, increased the bond stress of reinforcing bars in hybrid fiber reinforced concrete versus plain concrete, also the addition of hybrid fibers reduced the crack width.

2.5.2 Henager and Doherty (1976)

Henager and Doherty (1976) suggested a tensile stress block model for predicting the flexural strength of a singly reinforced beams having steel fibers (Figure 2-4). The model which is similar to the ACI 318-05 maximum strength design method, was improved by calculating the tensile strength of the fibrous concrete separately and then combining the corresponding strength contributed by the reinforcing bar to obtain the maximum moment of the member.

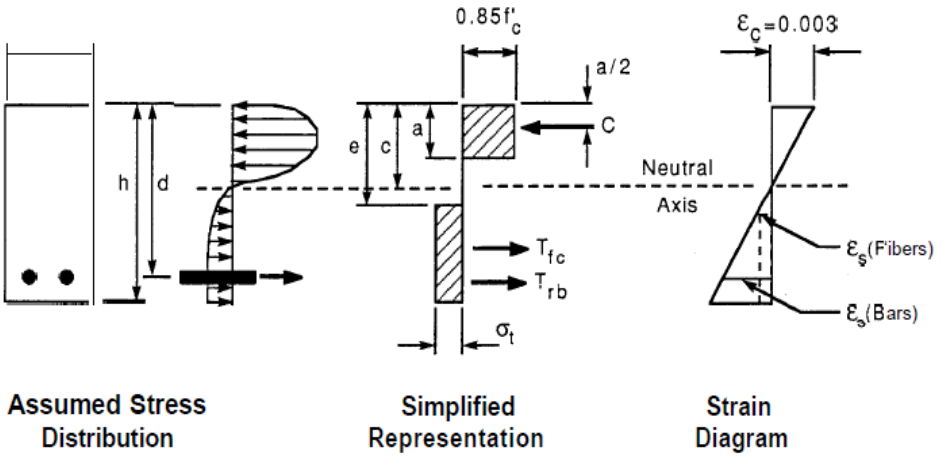

Figure 2-4 – Design assumptions for analysis of a singly-reinforced concrete beams containing steel fibers, (Henager and Doherty, 1976)

$$M_n = A_s f_y \left(d - \frac{a}{2}\right) + \sigma_t b(h-e)\left(\frac{h}{2} + \frac{e}{2} - \frac{a}{2}\right) \qquad \text{Equation 2-3}$$

The parameter σ_t represents the tensile strength contributed by steel fibers and is given as:

$$\sigma_t = 0.00772 \frac{l}{df} \rho_f F_{be} \text{ (MPa)} \qquad \text{Equation 2-4}$$

where, M_n is the ultimate moment capacity of the beam, A_s is the area of reinforcing bars, f_y is the yield strength of steel bars, l is the length of fiber, d_f is the fiber diameter, ρ_f is the percent by volume of fiber, and F_{be} is the bond efficiency of the fiber and it varies from 1.0 to 1.2 depending upon fiber characteristics. Rest of the parameters in the equations are defined in Figure 2-4.

2.5.3 Bentur and Mindes (1990)

Based on a composite-material of steel fiber-reinforced concrete, Bentur and Mindes (1990) suggested the empirical expression given in Equation 2-5 for predicting the flexural strength:

$$\sigma_c = A\sigma_m\left(1 - V_f\right) + BV_f \frac{l}{d} \qquad \text{Equation 2-5}$$

where σ_c is the composite flexural strength, σ_m is the ultimate strength of the matrix, V_f is the volume fraction of fibers adjusted for randomness, l/d is the fiber aspect ratio, l is the fiber length, d is the diameter of fiber, A and B are the constants.

Analytical equations developed by Swamy et al (1974) have a form based on theoretical derivation with the above constants A and B obtained from regression analysis of the tested laboratory data. The test was performed on a 100×100×305 mm beam specimen. The obtained values of the constants A and B lead to the following expressions.

For first cracking composite flexural strength:

$$\sigma_c = 0.843 f_r V_m + 425 V_f \, l/d_f \qquad \text{Equation 2-6}$$

where, f_r is the stress in the matrix (modulus of the plain mortar or concrete), V_m is the volume fraction of matrix (1 - V_f), V_f is the volume fraction of fibers (1 - V_m), $\frac{l}{d}$ is the ratio of length to diameter of fiber (i.e., aspect ratio).

For ultimate composite flexural strength:

$$\sigma_{cu} = 0.97 f_r V_m + 494 V_f \, l/d_f \qquad \text{Equation 2-7}$$

2.5.4 Mitchill et al. (1997)

Mitchill et al. (1997) conducted an experimental study to investigate the effects of steel fibers on the behavior of reinforced concrete elements subjected to pure tension. The variables used in the study included four types of concrete, normal-and high-strength concrete, with and without fibers. Hooked-end steel fibers were used to attain 1% fiber reinforcement by volume of concrete. The fibers had a length of 30 mm and diameter of 0.50 mm. The tensile strength of the fibers was 1200 MPa. All of the reinforcing bars were #15 with a specified yield strength of 400 MPa. Specimens used in the study had 95×170×1500 mm dimensions. All specimens were

tested in vertical direction. The findings of Mitchill et al. (1997) showed that the tension stiffening behavior of both normal- and high-strength reinforced concrete elements increased. After yielding of reinforcing bars only those specimens containing steel fibers showed an increase in load capacity with greater strains.

2.5.5 Lok and Xiao (1998)

Lok and Xiao (1998) proposed a model for predicting the tensile behavior of steel fiber reinforced concrete as shown in Figure 2-5. Expressions representing the proposed model focused entirely on a parameter τ_d, the fiber bond stress, which according to the developed model, contributed to the tensile behavior of SFRC.

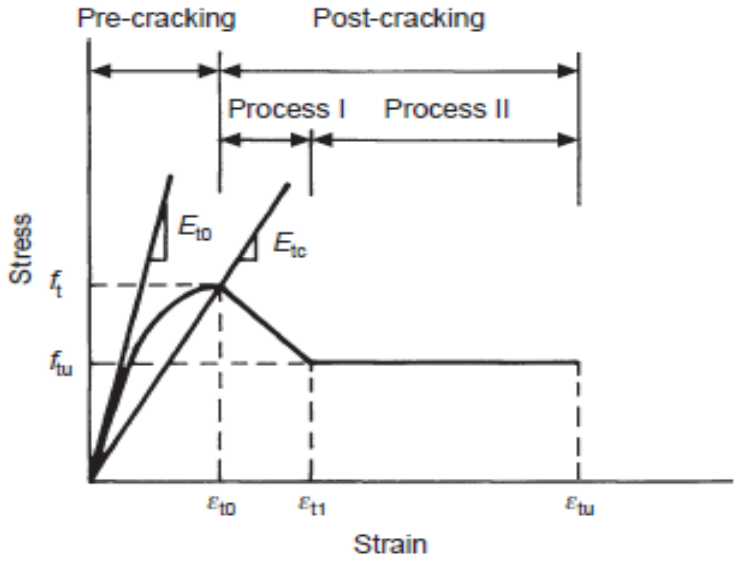

Figure 2-5 – Idealized stress-strain model (Lok and Xiao, 1998)

In the above figure, the tensile behavior (σ) before cracking is expressed by the following equation.

$$\sigma = f_t \left[2 \times \left(\frac{\varepsilon}{\varepsilon_{to}} \right) - \left(\frac{\varepsilon}{\varepsilon_{to}} \right)^2 \right] \qquad \text{Equation 2-8}$$

where, ε_{to} is the strain at ultimate tensile stress, f_t is the ultimate tensile stress to determine from direct tensile test or from following equation:

$$f_t = f_m(1 - V_f) + \frac{\eta_o \eta_1 \tau_d V_f L}{d}$$ Equation 2-9

where, η_o and η_1 are the fiber orientation and fiber length factors respectively, τ_d is the fiber bond stress, V_f is the fiber volume percentage, and $\frac{L}{d}$ is the fiber aspect ratio.

$$\varepsilon_{to} = \frac{2f_t}{E_{to}}$$ Equation 2-10

$$E_{to} = 2E_{tc}$$ Equation 2-11

where, E_{to} is the tensile secant modulus, E_{to} is the initial tangent modulus of concrete in tension, and ε_{to} is the strain at stress f_t.

$$f_{tu} = \eta V_f \tau_d \frac{L}{d}$$ Equation 2-12

$$\varepsilon_{t1} = \tau_d \frac{L}{d} \frac{1}{E_s}$$ Equation 2-13

where, η is the fiber orientation factor (equal to 0.405 for beams and 0.50 for slabs), E_s is the elastic modulus of steel fibers.

$$\tau_d = \frac{f_{tu}}{0.5 V_f \left(\frac{L}{d}\right)}$$ Equation 2-14

2.5.6 Wang (2006)

Wang (2006) proposed an expression to predict the tensile behavior of an SFRC members, based on experimental and analytical research. The ascending part of the model is based on a relationship between the tensile strength of the concrete, while the descending part is based on a stress versus crack width relationship.

$$\sigma = E_t \varepsilon \text{ for } \sigma \leq f_t$$ Equation 2-15

$$E_t = (4000 + 100000 \alpha_f V_f) \sqrt{f_{c'}}$$ Equation 2-16

where, σ is the tensile stress for a SFRC, ε is the tensile strain, E_t is the direct tensile elastic modulus (MPa), $f_{c'}$ is the compressive strength of plain concrete (MPa).

The descending branch was represented by the expression below:

$$\sigma = \frac{1+w}{1+w+\frac{w^2}{1000\alpha_f v_f}} \times f_t \qquad \text{Equation 2-17}$$

where, σ is the tensile stress, f_t is the tensile strength, w is the crack width (mm), V_f is the fiber volumetric ratio, α_f is an experimental constant which considers the fiber type and is 1 for Norvotex fiber and 1.6 for 1% Dramix fiber type.

2.5.7 Soranakom and Mobasher (2009)

Soranakom and Mobasher (2009) suggested a model for estimating the strain-softening behavior of fiber reinforced concrete elements. The model consists of a linear stress-strain behavior up to the point where cracking tensile strain happened after which the post-cracking behavior is characterized by a decaying stress-strain relationship. The contribution of fibers in the post-cracking response is represented by an average constant post-crack tensile parameter, σ_p which is related to the fiber volume fraction and bond behavior of the matrix.

$$\sigma_{cr} = E\varepsilon_{cr} = 0.56\sqrt{f_{c\prime}} \text{ (MPa)} \qquad \text{Equation 2-18}$$

$$E = 4733\sqrt{f_{c\prime}} \text{ (MPa)} \qquad \text{Equation 2-19}$$

where, σ_{cr} is the cracking stress, f_c is the ultimate uniaxial cylinder compression strength. The first crack tensile strain of the SFRC model was obtained assuming Hooke's Law as:

$$\varepsilon_{cr} = \frac{\sigma_{cr}}{E} = \frac{0.56\sqrt{f_{c\prime}}}{4733\sqrt{f_{c\prime}}} = \frac{6.7\sqrt{f_{c\prime}}}{57{,}000\sqrt{f_{c\prime}}} = \text{ 118 microstrain} \qquad \text{Equation 2-20}$$

$$\beta_{tu} = \frac{\varepsilon_{tu}}{\varepsilon_{cr}} = \frac{0.025}{118\times10^{-6}} \approx 212 \qquad \text{Equation 2-21}$$

$$\sigma_p = \mu E\varepsilon_{cr} \ : \mu(0 \le \mu \le 1) \qquad \text{Equation 2-22}$$

According to RILEM Model (2003):

$\varepsilon_{tu} = 0.025$ Equation 2-23

The parameter μ represent the post-crack strength as a fraction of the cracking tensile strength, σ_{cr}.

The idealized tension model proposed by Mobasher and Soranakom (2009) is shown in Figure 2-6.

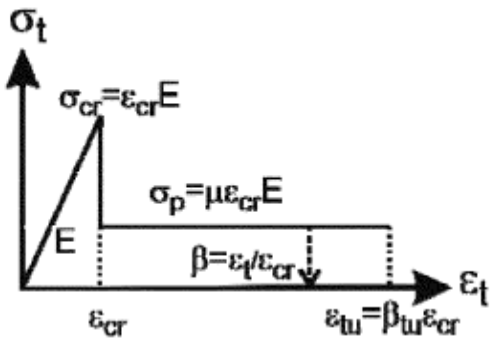

Figure 2-6 – Idealized tension model for strain- softening fiber-reinforced concrete (Mobasher and Soranakom (2009))

2.5.8 Zuccarello et al. (2010)

Zuccarello et al. (2010) performed parametric and experimental study on the tensile behavior of steel fiber reinforced concrete. Portland Cement Type CEM I, 42.5R, was used in the concrete mixture. The fiber length used were 22, 30 and 44 mm. Fibers content in terms of volume was set equal to 1% and 2% corresponding to 78 and 157 kg/m^3, respectively. Water-to-cement ratio was arranged as 0.55 to provide good mechanical strength and adequate workability of the mixtures . Eight prismatic specimens having dimensions of 30×80×350 mm were cast. The study focused also on bridging effect produced by the fibers during tensile tests. For this reason only 22 and 30 mm fibers were used to have a smaller range of values for tensile behavior of SFRC. The results showed that the maximum tensile strength for specimens having short fibers were greater that of having long fibers, whereas the ultimate strain was greater for long fibers.

2.5.9 Frank et al. (2013)

Frank et al. (2013) conducted an analytical study to develop a tension-stiffening model for SFRC. By utilizing the crack analysis procedure developed by Lee et al. (2011), Frank et al. (2013) modified the conventional tension-stiffening of Bentz (2005) to take into account the effect of steel fibers. The tensile stress due to tension stiffening is shown below:

$$f_c, Ts = \frac{f_{cr}}{1+\sqrt{3.6 c_f M \varepsilon_{t,avg}}} \quad \text{Equation 2-24}$$

$$c_f = 0.6 + \frac{1}{0.034}\left[\frac{l_f}{d_f}\right]^{1.5} \frac{100 V_f}{M^{0.8}} \quad \text{for hooked-end fiber} \quad \text{Equation 2-25}$$

where, c_f is the coefficient to consider the effect of steel fibers, $\varepsilon_{t,avg}$ is the average tensile strain of reinforcing bar of reinforced FRC member, V_f is the fiber volumetric ratio, l_f is the fiber length, f_{cr} is the cracking strength of concrete, M is the bond parameter ($= Ac/(\Sigma d_{bs}\,\pi)$), A_c is the cross sectional area of concrete matrix, and d_{bs} is the diameter of reinforcing bar.

In the above expressions:

$$E_c = 3300\sqrt{f_{c'}}6900 \text{ (MPa)} \quad \text{Equation 2-26}$$

$$f_{cr} = 0.33\sqrt{f_{c'}} \text{ (MPa)} \quad \text{Equation 2-27}$$

where, E_c is the elastic modulus of concrete matrix and f_c' is the cylinder compressive strength of concrete.

2.5.10 Vecchio (2013)

Vecchio (2013) tested twelve reinforced concrete (RC) beams without fibers and forty eight large-scale steel fiber-reinforced concrete (SFRC) beam specimens, to investigate their cracking and tension behavior. The test parameters included volumetric fiber ratio, fiber length, fiber aspect ratio, reinforcement ratio, and

reinforcement diameter. They performed “Dog-bone” tension tests and bending tests, to quantify the tensile characteristic of the concrete. They found that the cracking behaviors of SFRC were significantly changing as the reinforcement ratio varied. The reinforcement ratio, reinforcing bar diameter, fiber volume fraction, and fiber aspect ratio influenced the crack spacing and crack width.

Steel fibers added to concrete reinforced with conventional reinforcing bars enhanced the cracking properties and tension-stiffening behavior compared to nonfibrous RC. Steel fibers increased the post-yield load-carrying capacity of a uniaxial concrete tension member reinforced with conventional reinforcement to levels significantly higher than the bare-bar yield load.

2.6 SFRC in Compression

Steel fibers generally reduce the brittle nature of concrete matrix, but they don’t have significant effects on the compressive behavior (Concrete Society, 2007; Baran et al., 2012). The influence of steel fibers in the compressive strength of concrete seems to be minor. However, the ductility and toughness are considerably improved as a function of the increase in the volume fraction, aspect ratio, and type of the fiber used especially in the post-cracking region (Edward, 2008), as shown in Figure 2-7 respectively. Toughness is a measure of the ability of the material to absorb energy during deformation. It can be calculated using the area under the load-deflection or stress-strain curves.

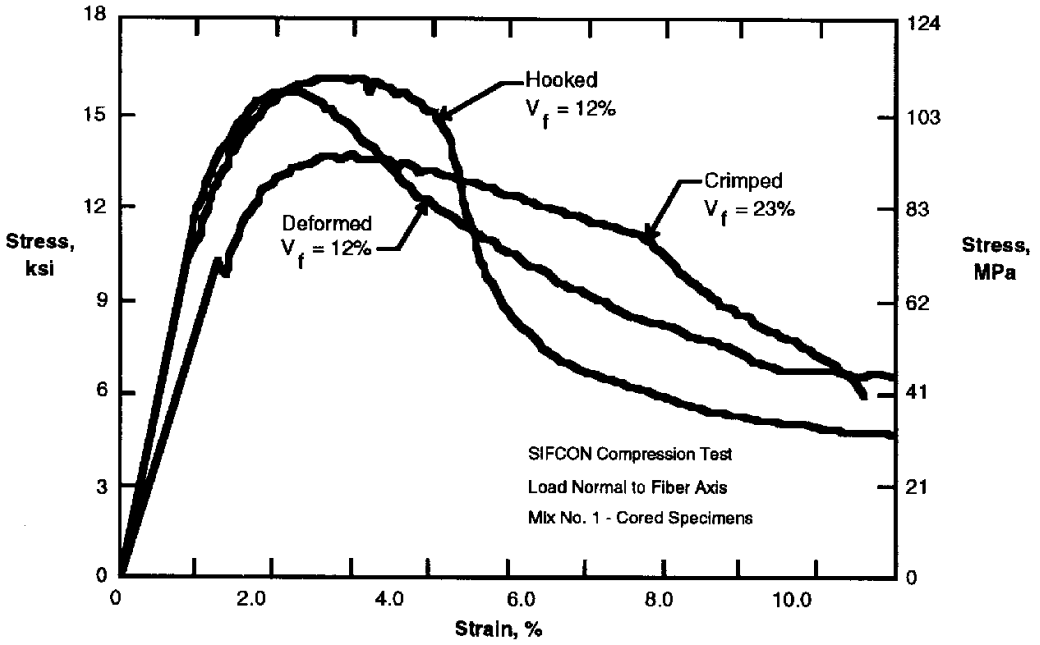

Figure 2-7 – Influence of fiber type on stress-strain curve for concrete in compression (ACI 544-96)

Various analytical expressions have been proposed to model the compressive stress-strain behavior of plain concrete (Popovics (1973), Hognestad (1951), Sargin (1971), CEB-FIP (1993), etc.). The proposed models, however, are in general not suitable for SFRC, because steel fiber reinforced composites have a less steep descending branch than that of conventional concretes, as reported in literatures. The compressive behavior of concrete is influenced by the proportions and properties of its constituent materials. The non-linear equation for conventional concrete proposed by Popovics (1973) is as follows:

$$f_c = f_{ck} \frac{\varepsilon_c}{\varepsilon_{co}} \frac{n}{n-1+\left(\frac{\varepsilon_c}{\varepsilon_{co}}\right)^{nk}} \qquad \text{Equation 2-28}$$

in which, f_c is the stress at any point on the curve, f_{ck} is the concrete compressive strength obtained from the cylinder test and ε_c is the strain corresponding to the stress f_c, and ε_{co} is the strain at peak stress. The ε_{co}, the constants n and k, and modulus of elasticity of concrete (E_c) is defined as follows:

$$\varepsilon_{co} = \frac{f_{ck}}{E_c} \frac{n}{n-1} \qquad \text{Equation 2-29}$$

$$n = 0.8 + \frac{f_{ck}}{17}$$ Equation 2-30

$$k = 0.67 + \frac{f_{ck}}{62}$$ Equation 2-31

$$E_c = 3320\sqrt{f_{ck}} + 6900(\text{MPa})$$ Equation 2-32

The above expressions however, cannot represent the compressive stress-strain behavior of SFRC owing to the fact that the effect of fibers has not been taken into consideration. Little research has been done on the effect of fiber on the descending portion of compressive stress-strain curve. One of the reasons is the difficulty encountered in obtaining a complete stress-strain curve (Shah (1978)). Only a few constitutive models are published for SFRC (Fanella and Naaman, 1985; Barros and Fiqueras, 1999; Ezeldin and Balaguru, 1992). Since the models of the compressive behavior of fiber reinforced concrete, in general, were developed from models for plain concrete, it is necessary to include some parameters in these models to consider the influence of steel fibers on the properties of the stress-strain curve. Some guidelines such as RILEM TC 162-TDF (2003), CNR-DT 204 (2006), proposed the same shape of the stress-strain relationship in compression for ordinary concrete to be used in ultimate limit state design. The compression response is prescribed by a parabolic-rectangular stress-strain model with ultimate compressive strain of 0.0035 and a peak strain of 0.002. Fanella and Naaman (1985), proposed an analytical model to predict the complete stress-strain behavior of fiber-reinforced mortar taking into consideration the fiber shape, volume fraction and fiber geometry. Several authors proposed different analytical equations for modeling the actual stress-strain behavior of SFRC in compression by introducing some parameters relating to fiber properties. Details related to some of these proposed relationships are explained in details in the sections below.

2.6.1 Soroushian and Lee (1989)

The model proposed by Soroushian and Lee (1989) consists of a curvilinear ascending branch followed by a bi-linear descending branch. The expression for this model is as shown below:

$$fc = f_{c_f}\left(\frac{\varepsilon}{\varepsilon_{p_f}}\right)^2 + 2f_{p_f}\left(\frac{\varepsilon}{\varepsilon_{p_f}}\right) \quad for\ \varepsilon \le \varepsilon_{p_f}$$ Equation 2-33

$$\sigma = z\left(\varepsilon - \varepsilon_{p_f}\right) + f_{c_f} > f_o \quad for\ \varepsilon > \varepsilon_{p_f}$$ Equation 2-34

where, ε_{co} = 0.0021,

$$f_{pf} = f_c + 3.6I_f$$ Equation 2-35

$$f_o = 0.12f_{c_f} + 3.6I_f$$ Equation 2-36

$$z = -343f_c\left(1 - 0.66\sqrt{I_f}\right) \le 0$$ Equation 2-37

$$\varepsilon_{p_f} = 0.0007I_f + 0.0021$$ Equation 2-38

where, f_{pf} is the compressive strength of fiber concrete, f_c is the compressive strength for plain concrete, ε_{p_f} is the strain at peak stress f_{pf}, z is the slope of the descending branch, I_f is the fiber reinforcement index, and f_o is the residual stress.

2.6.2 Ezeldin and Balaguru (1992)

Ezeldin and Balaguru (1992) developed an analytical expression to model the compressive stress-strain behavior of normal strength SFRC. The expression, which is based on the one proposed by Carreira and Chu (1985) for uniaxial compression of plain concrete, involves a material parameter β, and it is the slope of the inflection point at the descending branch of the curve.

$$\frac{\sigma_c}{f_{cf}} = \beta \frac{\left(\frac{\varepsilon}{\varepsilon_{pf}}\right)}{\beta - 1 + \left(\frac{\varepsilon}{\varepsilon_{pf}}\right)^{\beta}}$$ Equation 2-39

in which, σ_c is the compressive stress, f_{cf} is the compressive strength for fibrous concrete, ε_c is the strain, ε_{pf} is the strain at peak stress and β is the factor related to the influence of fiber on the descending branch of the curve.

$$f_{c_f} = f_c + 3.51(RI)$$ Equation 2-40

$$RI = W_f \text{x } l_f/d_f$$ Equation 2-41

$$\varepsilon_{p_f} = \varepsilon_{co} + 446x10^{-6}(RI)$$ Equation 2-42

$$\varepsilon_{co} = 0.002$$

For hooked end fibers:

$$\beta = 1.093 + 0.7132(RI)^{-0.926}$$ Equation 2-43

Based on the experimental results of Fanella and Naaman (1985) for straight steel fiber-reinforced mortar, the following equation was proposed:

$$\beta = 1.093 + 7.4818(RI)^{-1.387}$$ Equation 2-44

where, *RI* is the fiber reinforcement index by weight of straight fibers.

According to the experiments performed by Luiz et al. (2010):

$$\beta = (0.0536 - 0.5754V_f)f_c$$ Equation 2-45

$$\varepsilon_{pf} = (0.00048 - 0.01886V_f)lnf_c$$ Equation 2-46

Values of β apply to reinforcing index values ranging from 0.75 to 2.5 for hooked-end steel fibers, and from 2 to 5 for straight fibers. A particular case of the equation proposed by Carreira and Chu (1985) was proposed by Desayi and Krishnan (1964), in which, $\beta = 2$. Another particular case is the one proposed by Tulin and Gerstle (1964) for $\beta = 3$ as reported by Nataraja et al. (1999).

2.6.3 Nataraja et al. (1999)

Based on their extensive experimental works on the effect of steel fibers on the shape of compressive stress-strain curve of concrete, Nataraja et al. (1999), formulated an analytical model to generate both the ascending and descending branches of the stress-strain curve. They adopted the equation of Carreira and Chu (1985) for

uniaxial compression of plain concrete, the same expression used by Ezeldin and Balaguru (1992).

$$\frac{f_c}{f_{c_f}} = \beta \frac{\left(\frac{\varepsilon_c}{\varepsilon_{o_f}}\right)}{\beta - 1 + \left(\frac{\varepsilon_c}{\varepsilon_{o_f}}\right)^{\beta}} \qquad \text{Equation 2-47}$$

where, f_{cf} is the compressive strength of fibrous concrete and ε_{of} is the peak strain corresponding to the peak stress, f_c and ε_c are the stress and strain values at any point on the curve.

$f_{cf} = f_c + 2.1604(RI)$ Equation 2-48

$\varepsilon_{o_f} = \varepsilon_c + 0.0006(RI)$ Equation 2-49

$\beta = 0.5811 + 1.93(RI)^{-0.7406}$ Equation 2-50

$\varepsilon_c = 0.0022$ Equation 2-51

$RI = W_f \times l_f / d_f$ Equation 2-52

2.6.4 Barros and Fiqueiras (1999)

The expressions proposed by Barros and Fiqueiras (1999) is similar to that of Ezeldin and Balaguru (1992), which is based on one parameter only. The same equation was proposed by Vipulanandan and Paul (1990) mainly intended to predict polymer concrete behavior, and used by Mebarkia and Vipulanandan (1992) for glass-fiber reinforced polymer.

$$\sigma_c = f_{cm} \frac{\left(\frac{\varepsilon_c}{\varepsilon_{c1}}\right)}{(1-p-q) + q\left(\frac{\varepsilon_c}{\varepsilon_{c1}}\right) + p\left(\frac{\varepsilon_c}{\varepsilon_{c1}}\right)^{\frac{1-q}{p}}} \qquad \text{Equation 2-53}$$

$q = 1 - p - \frac{E_{p_f}}{E_c}$, Equation 2-54

$p + q = \epsilon[0, 1]$ Equation 2-55

$\frac{1-q}{p} > 0$ Equation 2-56

$E_{pf} = \frac{f_{cf}}{\varepsilon_{pf}}$ Equation 2-57

$$E_c = 21500\sqrt[3]{\frac{f_{c_f}}{10}}$$ Equation 2-58

where, f_{cm} is the average compressive strength of concrete determined from test on cylinder.

For hooked end fiber with l_f = 30 mm, d_f = 0.5 mm, l_f/d_f = 60:

$$\varepsilon_{pf} = \varepsilon_{co} + 0.0002W_f$$ Equation 2-59

$$P = 1 - 0.919^{-0.394Wf}$$ Equation 2-60

For hooked end fiber with l_f = 60 mm and d_f = 0.8 mm; l_f/d_f = 75:

$$\varepsilon_{p_f} = \varepsilon_{co} + 0.00026\ W_f$$ Equation 2-61

$$p = 1 - 0.722^{-0.144Wf}$$ Equation 2-62

where, ε_{co} is the strain at peak for plain concrete and W_f is the fiber weight fraction in the matrix.

According to CEB-FIP Model Code (1993):

$$\varepsilon_{co} = 0.002$$ Equation 2-63

The values of ε_{p_f} and p above are applicable for f_{c_f} values ranging from 30 to 60 MPa and for fiber content ranging from 1 to 3%.

2.6.5 Wang (2006)

Wang (2006) proposed an expression to model the stress-strain behavior of SFRC in compression by modifying Popovic's (1973) expression for plain concrete. The expression was modified by introducing a parameter relating to the volume percentage of steel fiber.

$$f_c = f_{ck}\frac{\varepsilon_c}{\varepsilon_{co}}\frac{n}{n-1+\left(\frac{\varepsilon_c}{\varepsilon_{co}}\right)^{nk}}$$ Equation 2-64

$$\alpha = 0.92 - 25000{V_f}^3$$ Equation 2-65

where, V_f is the volume percentage of steel fiber used.

To obtain new values of *n* and *k*, their corresponding values in the above expression are multiplied by the parameter of α.

$$n = \alpha\left(0.8 + \frac{f_{ck}}{17}\right)$$ Equation 2-66

$$k = \alpha\left(0.67 + \frac{\varepsilon_{ck}}{62}\right)$$ Equation 2-67

where, f_{ck} and ε_{ck} are peak stress and peak strain, respectively.

3 EXPERIMENTAL PROGRAM

3.1 General

In this chapter, the test program performed at Structural Mechanics Laboratory at Civil Engineering Department at Atilim University is described. The concrete mixture proportions of test specimens, mixing and casting sequences, test set-up and test procedure are discussed in detail. Photos have taken during preparation, casting, and testing of specimens are also are included.

3.2 Test Specimens

Total of four batches (two SFRC and two conventional concrete) were cast to evaluate the effectiveness of SFRC compared to conventional concrete (CC). Three cylinders having 100×200 mm and three cylinders having 150×300 mm dimensions, three prismatic flexural (modulus of rupture) beams having 150×150×600 mm dimensions, and a number of square prismatic tension specimens having various cross-sections and lengths with single 12 mm diameter reinforcing bar at the center of the cross-section were cast per each batch. Five prismatic SFRC tension specimens having 100×100×500, 100×100×1000, 100×100×1500, 150×150×1000, and 200×200×1000 mm dimensions were cast first batch. For the second batch six prismatic CC tension specimens having 100×100×500, 100×100×1000, 100×100×1500, 150×150×1000, 200×200×1000, and 60×60×1000 mm dimensions were prepared. Six prismatic CC tension specimens having three 60×60×500 mm and three 100×100×500 mm were cast for the third batch. For the last batch, six prismatic SFRC specimens having three 60×60×500 mm and three 100×100×500 mm were prepared. The main parameters in the testing program were the type of concrete (CC or SFRC), specimen size for compression cylinders, cross-section size and length for the square prismatic tension specimens with reinforcing bar. Details of the prismatic tension specimens with single 12 mm diameter reinforcing bar is shown in Table 3-1. General views of the tension specimens are shown in Figure 3-1 and Figure 3-2.

Table 3-1- Details of prismatic tension specimens with single 12 mm diameter reinforcing bar

Batch Number	Specimen Designation	Concrete Type	Cross Section (mm)	Length (mm)
First Batch	SFRC 100×100×500-01	SFRC	100×100	500
	SFRC 100×100×1000-01	SFRC	100×100	1000
	SFRC 100×100×1500-01	SFRC	100×100	1500
	SFRC 150×150×1000-01	SFRC	150×150	1000
	SFRC 200×200×1000-01	SFRC	200×200	1000
Second Batch	CC 100×100×500-01	CC	100×100	500
	CC 100×100×1000-01	CC	100×100	1000
	CC 100×100×1500-01	CC	100×100	1500
	CC 150×150×1000-01	CC	150×150	1000
	CC 200×200×1000-01	CC	200×200	1000
	CC 60×60×1000-01	CC	60×60	1000
Third Batch	CC 100×100×500-02	CC	100×100	500
	CC 100×100×500-03	CC	100×100	500
	CC 100×100×500-04	CC	100×100	500
	CC 60×60×500-01	CC	60×60	500
	CC 60×60×500-02	CC	60×60	500
	CC 60×60×500-03	CC	60×60	500
Fourth Batch	SFRC 100×100×500-02	SFRC	100×100	500
	SFRC 100×100×500-03	SFRC	100×100	500
	SFRC 100×100×500-04	SFRC	100×100	500
	SFRC 60×60×500-01	SFRC	60×60	500
	SFRC 60×60×500-02	SFRC	60×60	500
	SFRC 60×60×500-03	SFRC	60×60	500

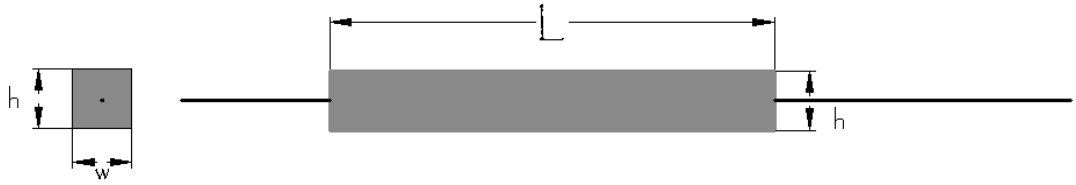

Figure 3-1 – Schematic view of prismatic tension specimens with reinforcing bar

Figure 3-2 – General view of prismatic tension specimens with reinforcing bar

3.3 Materials

3.3.1 Concrete

The materials for concrete used in this research include ordinary Portland Cement (PC 32.5), clean tap water, superplasticizer, river sand of 0 to 4 mm size, fine aggregate of size ranging from 4 to 16 mm, and coarse aggregate of size ranging from 15 to 25 mm. The proportions of materials used in this research are presented in Table 3-2. Proportioning of materials was performed using a digital weighing scale where quantity of each material was measured before mixing are shown in Figure 3-3.

Table 3-2 – Concrete mixture proportions

Materials	**Quantity (kg)**	
	Conventional Concrete (CC)	**SFRC**
Cement	40	40
Sand	90	90
Fine aggregate	44	44
Coarse aggregate	58	58
Steel fiber	-	7.7
Water	20	22
Superplasticizer	0.1	0.1

Figure 3-3 – Materials proportioning

3.3.2 Steel Fibers

Dramix ZP 305 type steel fibers were used in the concrete mix for the SFRC specimens. The manufacturer specified mechanical properties of the steel fibers are shown in Table 3-3. A photograph of the fibers is shown in Figure 3-4

Table 3-3 – Properties of steel fibers

Effective Length (mm)	Equivalent Diameter (mm)	Aspect Ratio	Young's Modulus (MPa)	Tensile Strength (MPa)	Density (kg/m^3)
30	0.55	55	210000	1345	7850

Figure 3-4 – Dramix ZP 305 steel fiber used in the research

3.3.3 Reinforcement

Deformed reinforcing steel bars having 12 mm diameter and nominal yield strength of 420 MPa were used for the prismatic tension specimen with reinforcing bar. The stress-strain relationships of the reinforcement bars for various lengths obtained from tension tests in the laboratory is shown in Figure 3-5.

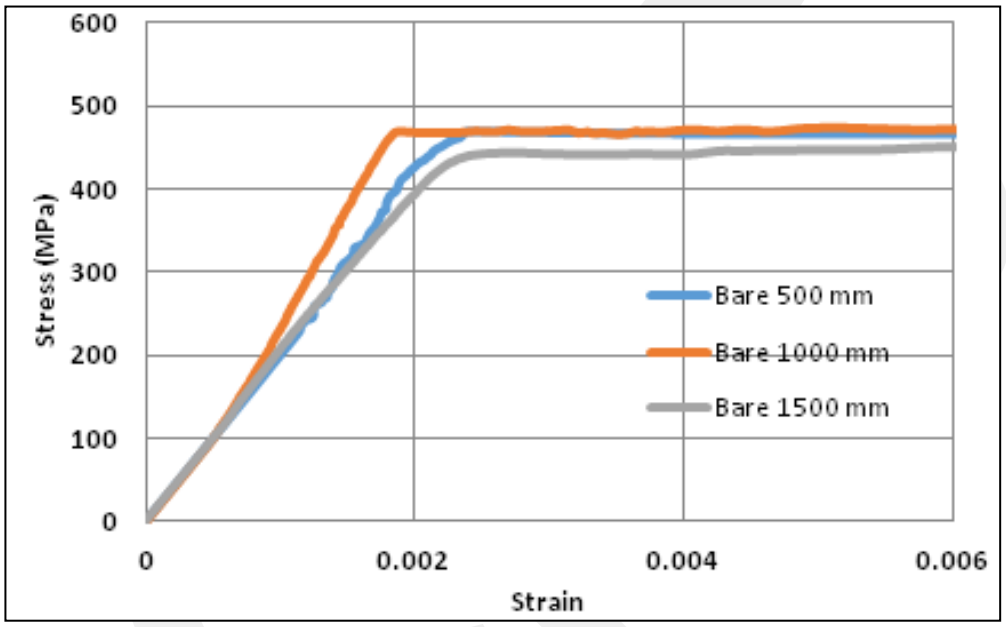

Figure 3-5 – Measured stress-strain relationships of ϕ12 reinforcing bars

3.4 Specimen Preparation

3.4.1 Formwork and Reinforcement Bars

For the cylinder and flexural prismatic specimens, steel moulds readily available in the laboratory were used. For the prismatic tension specimens with reinforcing bar, formwork was prepared for various cross-section sizes and lengths. The reinforcing bars for these specimens were cut into the specified lengths based on the specimen dimensions. Typical formworks for prismatic tension specimens with reinforcing bar is shown in Figure 3-6.

Figure 3-6 – Typical formworks for prismatic tension specimens with reinforcing bar

3.4.2 Concrete Mixing

A stationary drum mixer was used to mix the materials. Aggregates and cement were placed into the mixer and mixed for about one minute. Steel fiber was simultaneously discharged into the mixer while it rotates at a considerable speed. About 80% of water was added to the mixture while mixing was in progress. Finally, the remaining water and superplasticizer were added to the mixing constituents. The ingredients were mixed until a homogenous mixture with a desired workability was obtained. A photograph during mixing of constituents for one of the casts is presented in Figure 3-7.

Figure 3-7 – Mixing of materials and placing concrete in formwork

3.4.3 Casting and Curing

For each concrete batch, three 100×200 mm and three 150×300 mm cylindrical compression specimens were prepared to measure the concrete compressive strength based on ASTM C39. Three prismatic beam specimens having 150×150×600 mm dimensions were also prepared to measure the modulus of rupture based on ASTM C78. All specimens and cylinder were cast using steel molds and plywood formwork followed by curing twenty four hours after casting. Before casting, all formwork and molds were properly cleaned and then lubricating oil was applied on their inner surfaces for easy removal of formworks and molds. An external vibrator was used for the plywood specimens to obtain a well compacted composite and also to prevent segregation of fibers. The concrete mixture used for the specimens had a target compressive strength of 30 MPa, but slight modifications were performed on the amount of water and superplasticizer in some specimens in order to get proper workability. A photograph taken during casting is shown in Figure 3-8.

Figure 3-8 – Placing concrete in formwork

After casting, specimens were allowed to set and dry in formworks and molds prior to curing. Adequate curing was provided until testing day which was minimum 28 days after the day of casting. Proper curing was achieved by making the specimens sufficiently wet using water followed by covering them with wet burlap to minimize loss of moisture due to evaporation as shown in Figure 3-9.

Figure 3-9 – Curing of specimens

3.4.4 Test Setup and Procedure

The cylinders having 100×200 and 150×300 mm dimensions were tested under compression to evaluate the compressive behavior based on ASTM C39 as shown in Figure 3-10. These tests were performed at least 28 days after the day of casting. The test was conducted on a hydraulic compression testing machine with 1000 kN capacity. Before testing, each 150×300 mm cylinder was capped with a sulphur based composition both on the top and bottom face and each 100×200 mm cylinder was cut both at the top and bottom face in order to provide parallel loading surfaces of the cylinder. This helps the specimens achieving proper contact with the testing machine as well as equal distribution of compressive loads on the cylinders. For 150×300 mm cylinders, the load cell of the compression machine is used to collect the load values. For 100×200 mm cylinders, a 500 kN load cell was used to collect the test data. Two 30 mm displacement transducers were used to measure the length change of cylinder specimens. The load was applied slowly by lowering the top testing plate of the machine to bring it into contact with the specimen. Load was applied at the rate of approximately 0.25 MPa/sec by adjusting the lever attached to the testing machine. Each cylinder was subjected to compressive load until failure occurred. The average values of the compressive loads obtained from cylinders for each concrete batch divided by the initial cross sectional area of the cylinder were evaluated as the concrete compressive strength for that particular beam. The photographs of capping of concrete cylinder samples are shown in Figure 3-11.

Figure 3-10 – Testing of cylinders

Figure 3-11 – Capping of 150×300 mm cylinders

The flexural (modulus of rupture) beams having 150×150×600 mm dimensions were tested under four-point bending to evaluate the flexural behavior based on ASTM C78 as shown in Figure 3-12. These test were also performed at least 28 days after the day of casting. The test was conducted on a hydraulic compression testing machine with 1000 kN capacity. A 100 kN capacity load cell on the top and center of the beam was used to measure the applied load. Two 20 mm displacement transducers were used at the mid-span on both sides of the beam to measure the deflection due to the applied load.

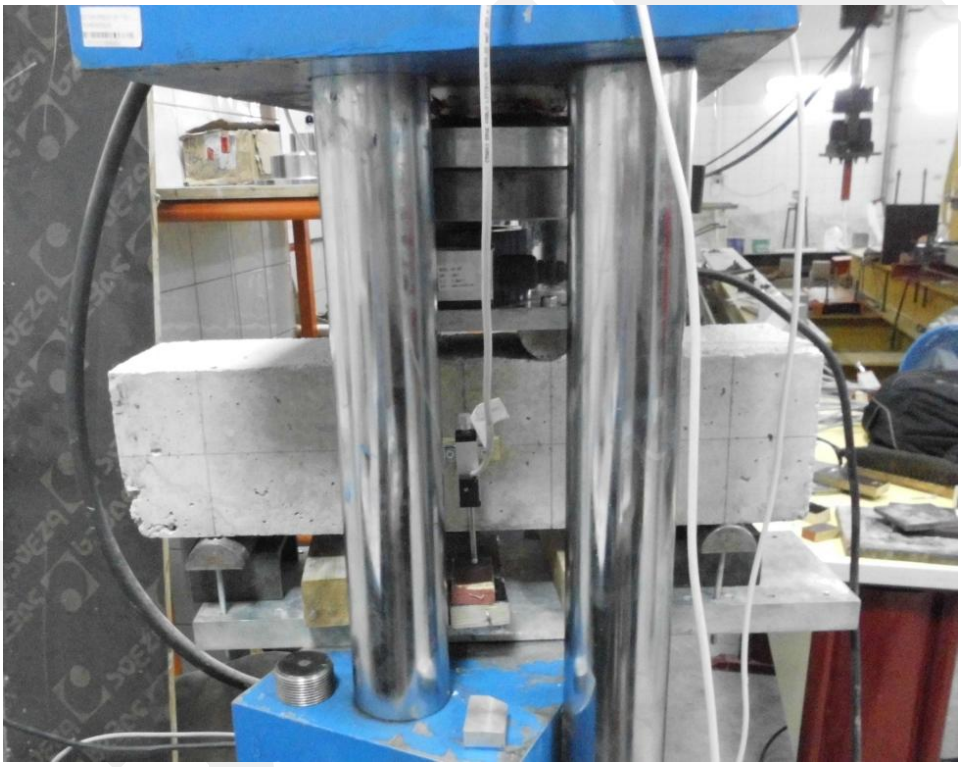

Figure 3-12 – Flexural beam tests (four-point bending)

The prismatic tension specimens with bars were tested in tension to evaluate the tensile characteristics of specimens. The set-up consisted of a loading frame transmitting the load through a set of tension grips (chucks) at both sides of the reinforcing bar. This resulted in tension being transferred from the steel reinforcing bar to the reinforced concrete section. The load was applied by using hydraulic jack and measured by using a 100 kN load cell. Schematic view of the test set-up for

prismatic tension specimens is shown in Figure 3-13. Photographs of the test set-up are shown in Figure 3-14, Figure 3-15, and Figure 3-16.

1- Steel bar with 12 mm diameter
2- Chuck
3- Grip
4- Specimen
5- Steel girder
6- Hydraulic jack
7- Load cell with 10 ton capacity

Figure 3-13 – Schematic view of the test set-up for prismatic tension specimens with bar

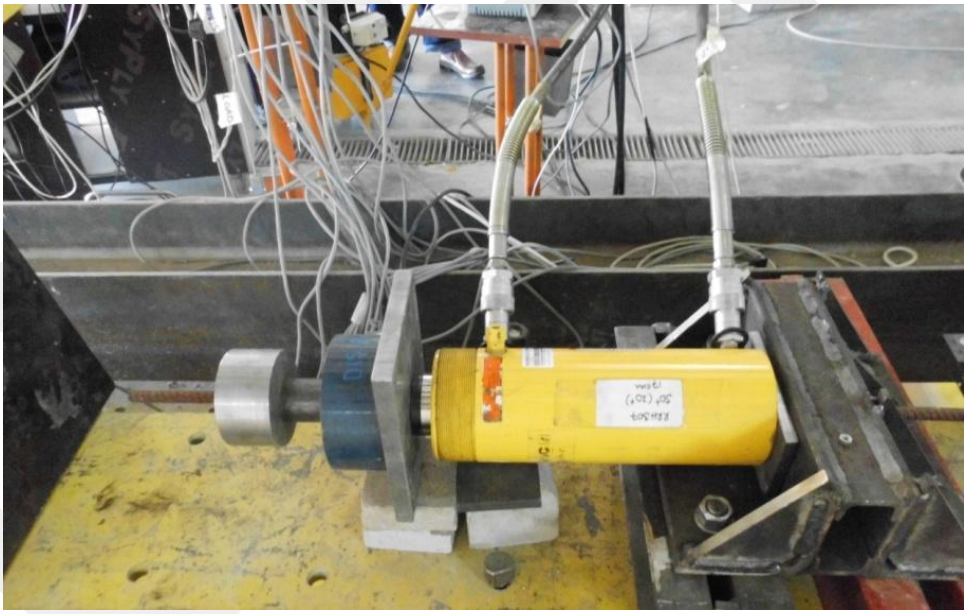

Figure 3-14 – Test set-up for prismatic tension specimens with bar - end 1 (hydraulic jack, load cell, and chuck)

Figure 3-15 – Test set-up for prismatic tension specimens with bar - end 2 (displacement transducers)

Figure 3-16 – Test set-up for prismatic tension specimens with bar

During testing, the longitudinal displacement of specimens throughout the length (from one end to the other) were measured and recorded continuously using four 50 mm displacement transducers. Two of these displacement transducers were attached at the top surface of the specimen whereas the other two were attached at the bottom face of the beam as shown in Figure 3-15 and Figure 3-16. The readings of load cell and the displacement transducers were recorded continuously throughout the test using a data acquisition system.

This test set-up was used in horizontal position for the tests of the first two batches. In the analysis of the test data, it was observed that the bending of the specimen due to its own weight affected the readings obtain from the displacement transducers. Although this effect can be eliminated based on some calculations in the analysis stage of the test data, the research group agreed on changing the position of the test setup from horizontal to vertical. The last two batches were tested in horizontal test set-up as shown in Figure 3-17.

Figure 3-17 – Test set-up for prismatic tension specimens with bar (vertical direction)

4 TEST RESULT AND DISCUSSIONS

4.1 Introduction

In this chapter, test results obtained from 100×200 and 150×300 mm cylinders under compression, 150×150×600 mm prismatic beams under flexure, and square prismatic tension specimens having various cross-sections and lengths with single 12 mm diameter reinforcing bar at the center of the cross-section are presented in tabular and graphical forms. Comments were made based on visual observations during the test periods and comparisons were performed based on the collected test data throughout the tests. Although all specimens were prepared using the same two mixture designs (CC and SFRC), the test results obtained from the same mixture but different time casts were slightly different.

4.2 Compression Test Results

Based on the visual observation made during the compression tests on 100×200 and 150×300 mm cylinders, cylinders made of conventional concrete showed a sudden and brittle mode of failure immediately after reaching the maximum values which can be considered as their respective peak strength values. On the other hand, specimens containing steel fibers sustained a considerable amount of strain under significant level of deformation. Typical failure modes of CC and SFRC cylinders are shown in Figure 4-1 and Figure 4-2.

Figure 4-1 – Typical failure mode of CC cylinders under compression

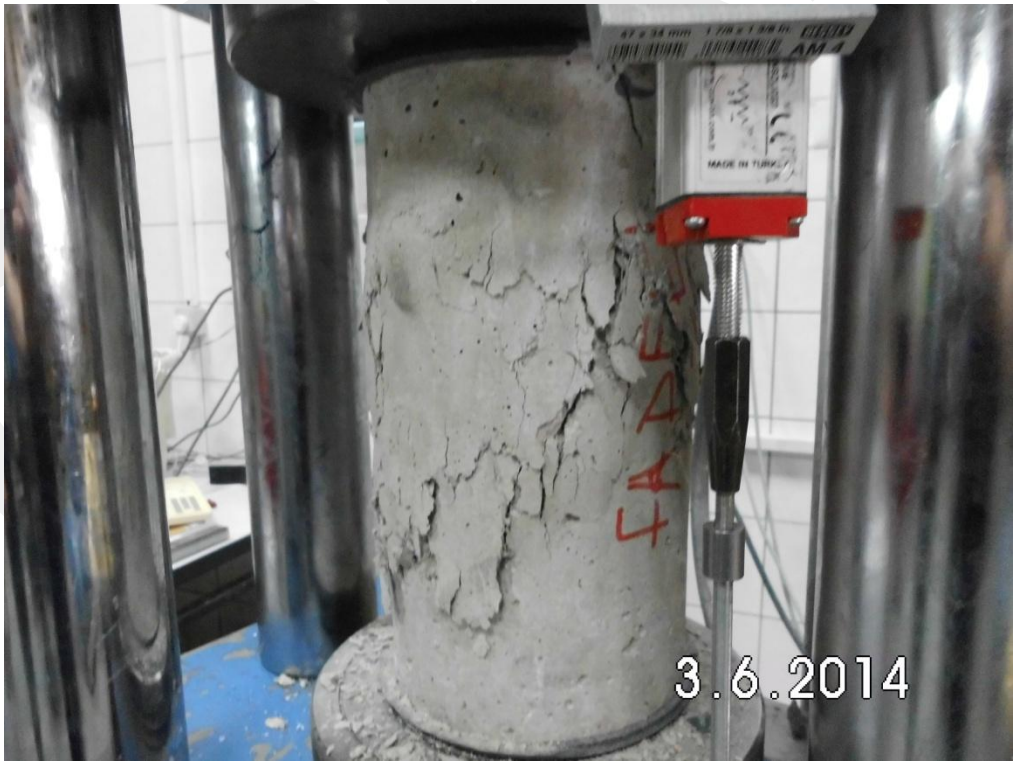

Figure 4-2 – Typical failure mode of SFRC cylinders under compression

The load and deformation values were recorded during the tests. Stress values were calculated by dividing the load values to the area of the specimens and strain values were calculated by dividing the deformation to the length of the specimens. The stress-strain curves obtained from compression tests of CC specimens are shown in Figure 4-3 and Figure 4-4. In Figure 4-3, stress-strain diagrams of five cylinders cast in the second batch are shown with an average concrete compressive strength of approximately 34 MPa. Figure 4-4 shows stress-strain diagram of one cylinder cast in the third batch with an average concrete compressive strength of 29 MPa. The stress-strain relationship data related to the rest of the cylinders cast in the second and third batches could not be collected due to problems associated with the data acquisition system.

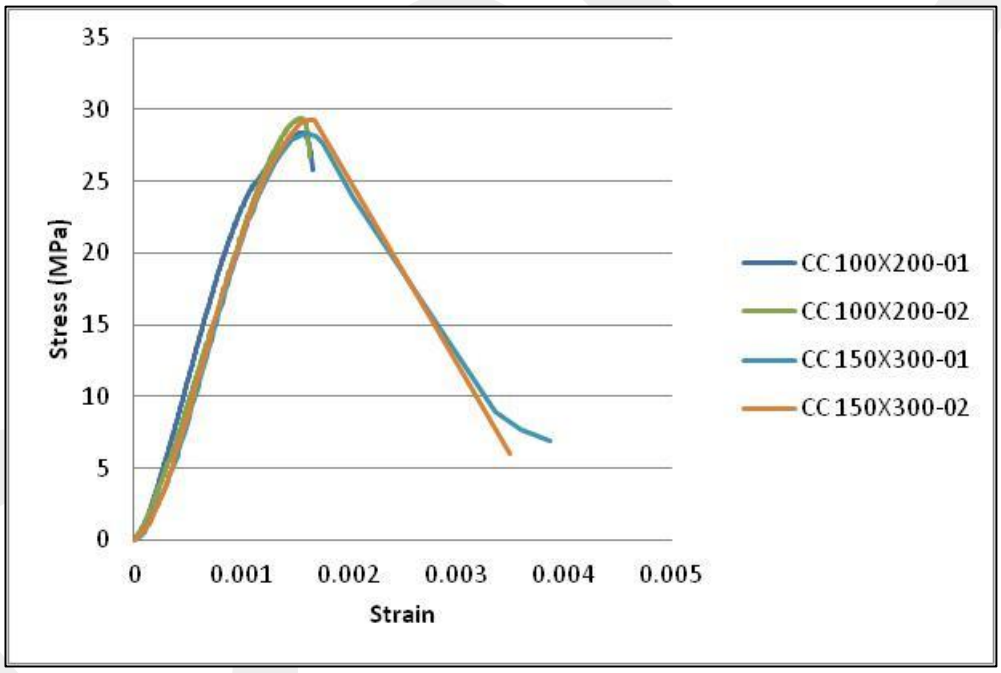

Figure 4-3 – Compressive stress-strain relationships of CC cylinders cast in second batch

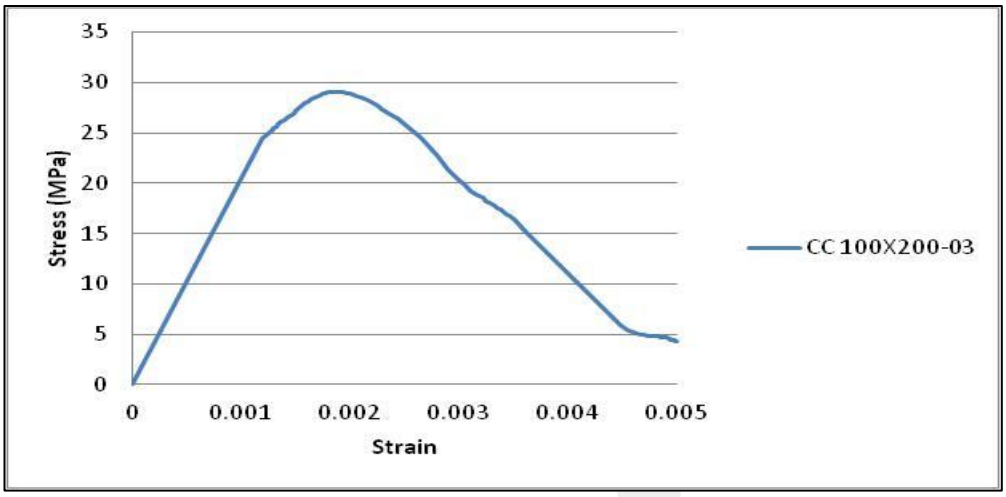

Figure 4-4 – Compressive stress-strain relationship of CC cylinder cast in third batch

The stress-strain curves obtained from compression tests of SFRC specimens are shown in Figure 4-5 and Figure 4-6. In Figure 4-5, stress-strain diagrams of four cylinders cast in the first batch are shown with an average concrete compressive strength of approximately 34 MPa. Figure 4-6 shows stress-strain diagrams of three cylinders cast in the fourth batch with an average concrete compressive strength of 33 MPa. The stress-strain relationship data related to the rest of the cylinders cast in the first and fourth batches could not be collected due to problems associated with the data acquisition system.

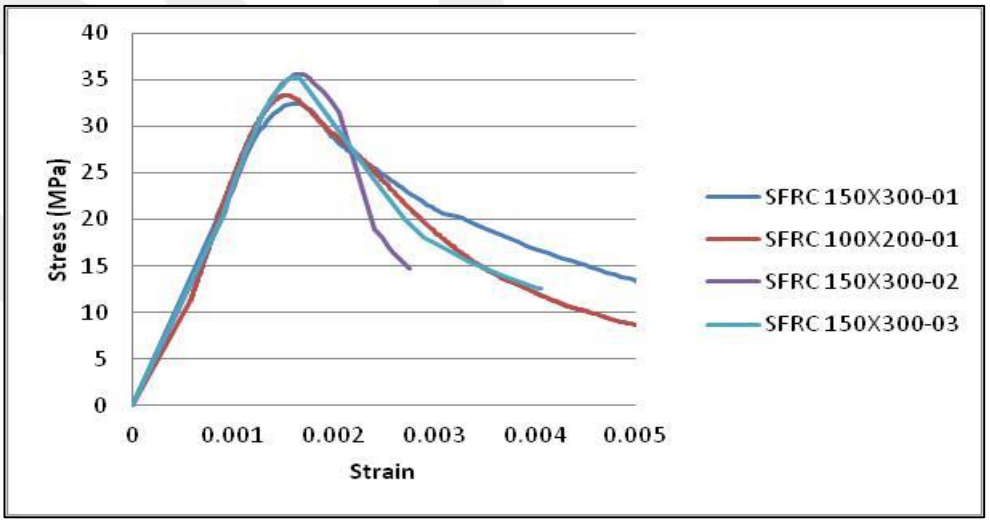

Figure 4-5 – Compressive stress-strain relationships of SFRC cylinders cast in first batch

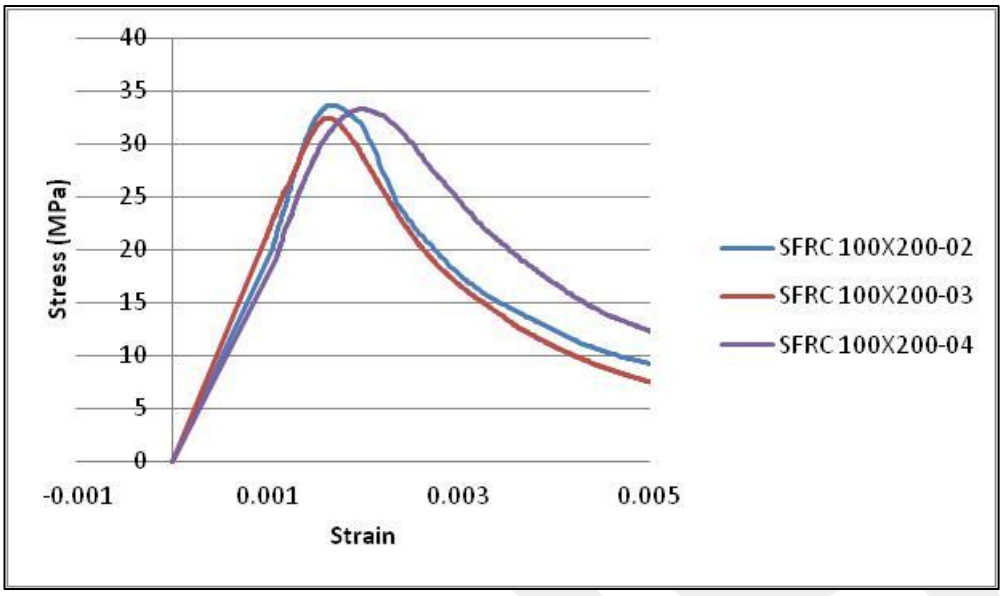

Figure 4-6 – Compressive stress-strain relationships of SFRC cylinders cast in fourth batch

Based on the comparisons of these stress-strain relationships of CC and SFRC specimens, no significant difference was observed between 100×200 and 150×300 mm cylinders. When the stress-strain relationships of CC and SFRC specimens are compared, although there was no significant difference in the ascending branches, the descending branches of SFRC specimens showed a more ductile behavior.

4.3 Flexural (Modulus of Rupture) Test Results

Based on the visual observation made during the flexural tests on 150×150×600 mm prismatic beams, beams made of conventional concrete showed a sudden and brittle mode of failure immediately after cracking of concrete. On the other hand, specimens containing steel fibers sustained a considerable amount of deflection even after cracking. Typical failure modes of CC and SFRC flexural beams are shown in Figure 4-7 and Figure 4-8.

Figure 4-7 – Typical failure mode of CC flexural beams

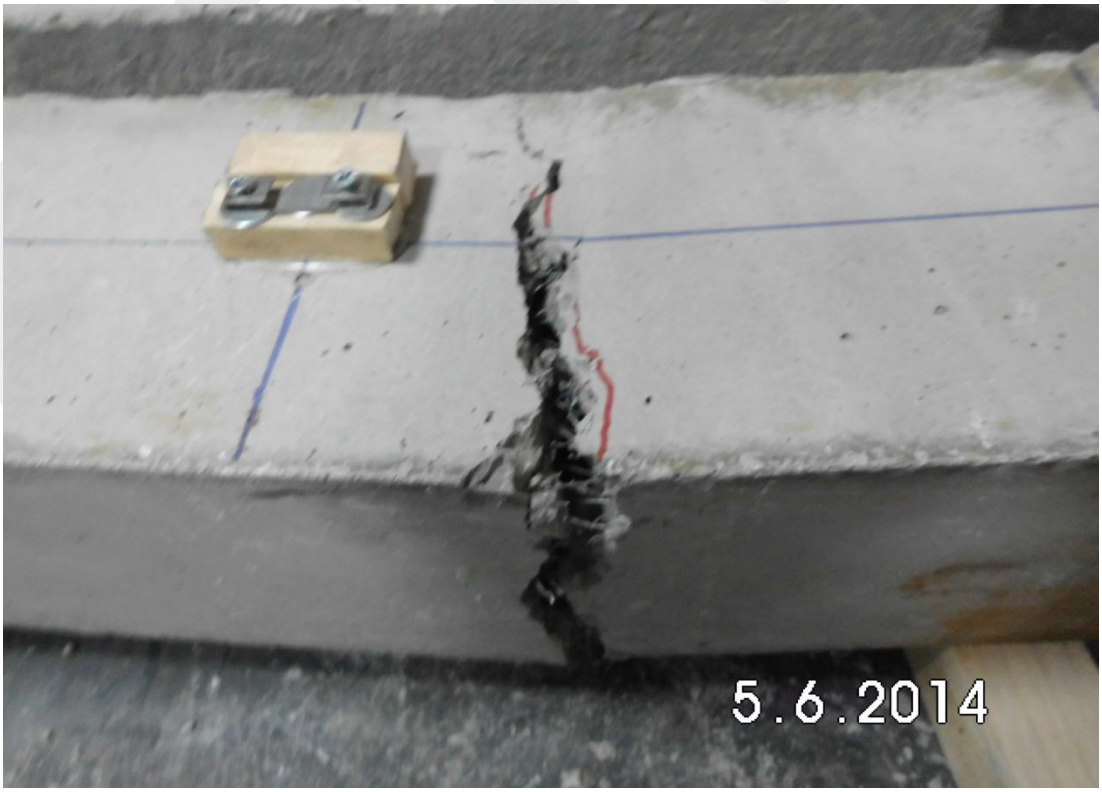

Figure 4-8 – Typical failure mode of SFRC flexural beams

The load-deflection curves obtained from four-point bending tests of CC specimens are shown in Figure 4-9 and Figure 4-10. The cracking loads of CC beams cast in the second and third batches are shown in Table 4-1 and Table 4-2. It can be concluded from the figures that after cracking, the load carrying capacity of the beams drop dramatically to zero for CC beams under flexure.

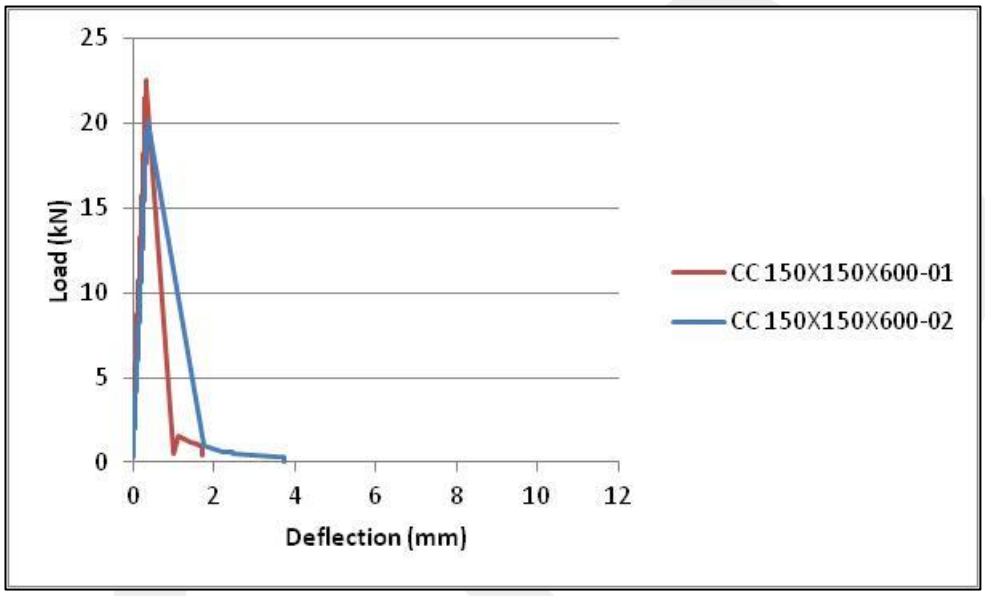

Figure 4-9 – Flexural load-deflection relationships of CC beams cast in second batch

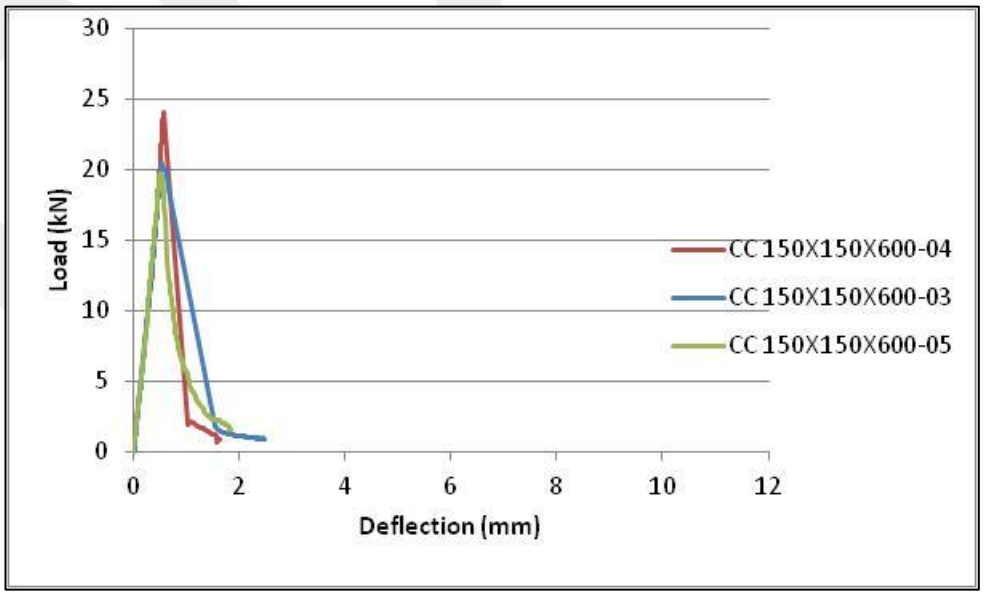

Figure 4-10 – Flexural load-deflection relationships of CC beams cast in third batch

Table 4-1 – Cracking loads of CC beams cast in second batch

	CC150×150×600-02	CC150×150×600-01
Cracking Load (kN)	20.0	22.7

Table 4-2 – Cracking loads of CC beams cast in third batch

	CC150×150×600-03	CC150×150×600-04	CC150×150×600-05
Cracking Load (kN)	20.0	24.0	20.0

The load-deflection curves obtained from four-point bending tests of SFRC specimens are shown in Figure 4-11 and Figure 4-12. The cracking and maximum loads of SFRC beams cast in the first and fourth batches are shown in Table 4-3 and Table 4-4. It can be concluded from the figures that after cracking, the load carrying capacity of the beams increased to a maximum value then dropped gradually for SFRC beams under flexure.

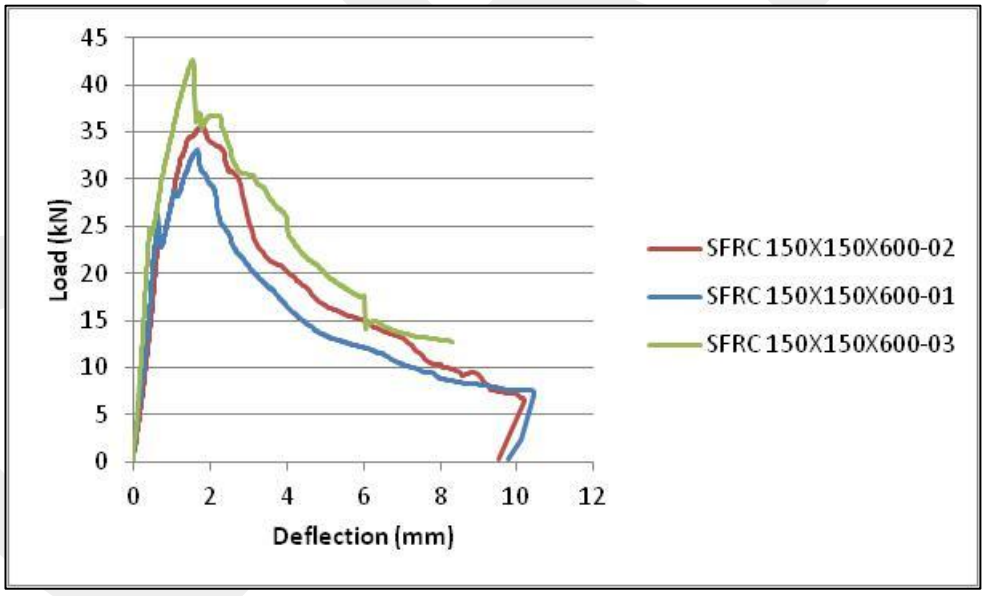

Figure 4-11 – Flexural load-deflection relationships of SFRC beams cast in first batch

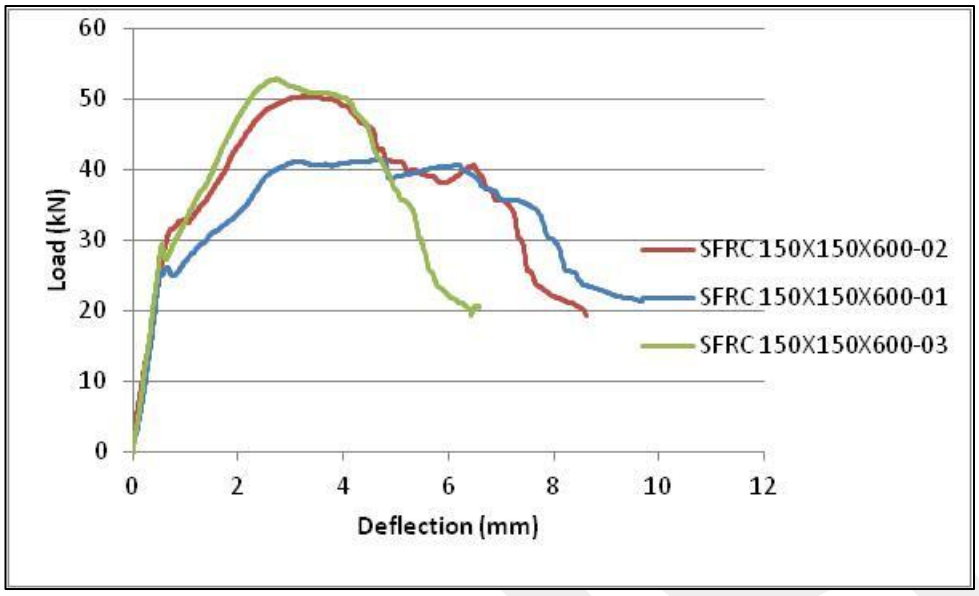

Figure 4-12 – Flexural load-deflection relationships of SFRC beams cast in fourth batch

Table 4-3 – Cracking and maximum loads of SFRC beams cast in first batch

	SFRC150×150×600-01	**SFRC150×150×600-02**	**SFRC150×150×600-03**
Cracking Load (kN)	26.4	23.6	24.7
Maximum Load (kN)	33	35.7	42.6

Table 4-4 – Cracking and maximum loads of SFRC beams cast in fourth batch

	SFRC150×150×600-04	**SFRC150×150×600-05**	**SFRC150×150×600-06**
Cracking Load (kN)	26.0	31.0	29.0
Maximum Load (kN)	41.0	51.0	53.0

When the CC and SFRC specimens under flexure are compared, SFRC specimens had higher cracking load values than that of CC specimens. Also the flexural SFRC specimens carried more load after cracking whereas, flexural CC specimens did not carry any more load after cracking.

4.4 Tension Test Results

Typical crack patterns for CC and SFRC prismatic tension specimens having various cross-sections and lengths with single 12 mm diameter reinforcing bar at the center of the cross-section are shown in Figure 4-13 to Figure 4-16.

Figure 4-13 – Typical crack patterns for CC tension specimens (CC100×100×1000-01)

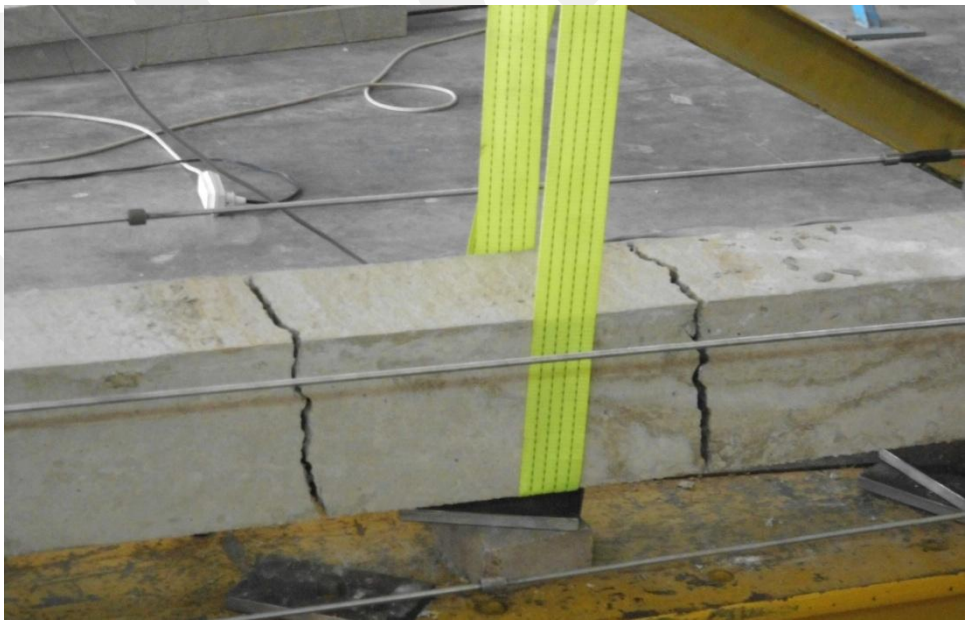

Figure 4-14 – Typical crack patterns for CC tension specimens (CC150×150×1000-01)

Figure 4-15 – Typical crack patterns for SFRC tension specimens (SFRC100×100×500-01)

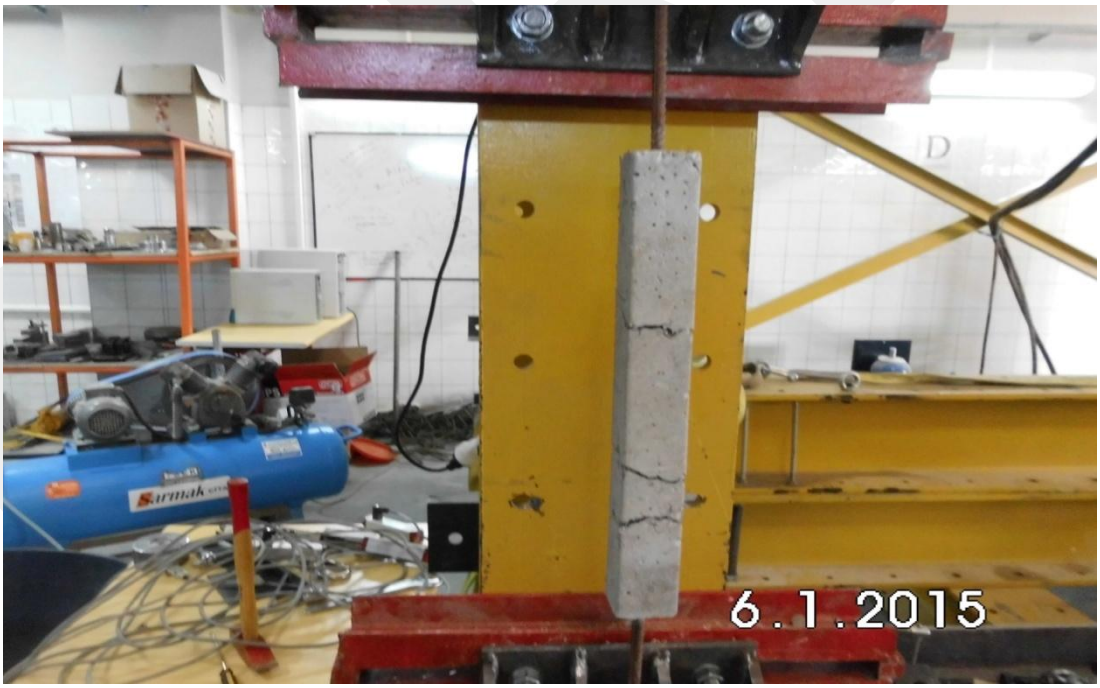

Figure 4-16 – Typical crack patterns for SFRC tension specimens (SFRC60×60×500-01)

As can be seen from these figures, only transverse cracks was observed during the tests for CC and SFRC specimens. The spacing of the cracks for SFRC specimens were more close than the CC specimens.

The load and elongation values were recorded during the tests. Strain values were calculated by dividing the elongation values to the gage length of the specimens. The load-strain curves obtained from five tension tests of CC specimens of the second batch are shown in Figure 4-17 to Figure 4-21. Note that the test set-up for this batch was horizontally oriented. The dimension of the specimens were 100×100×1000, 100×100×1500, 150×150×1000, 100×100×500, and 60×60×1000 mm.

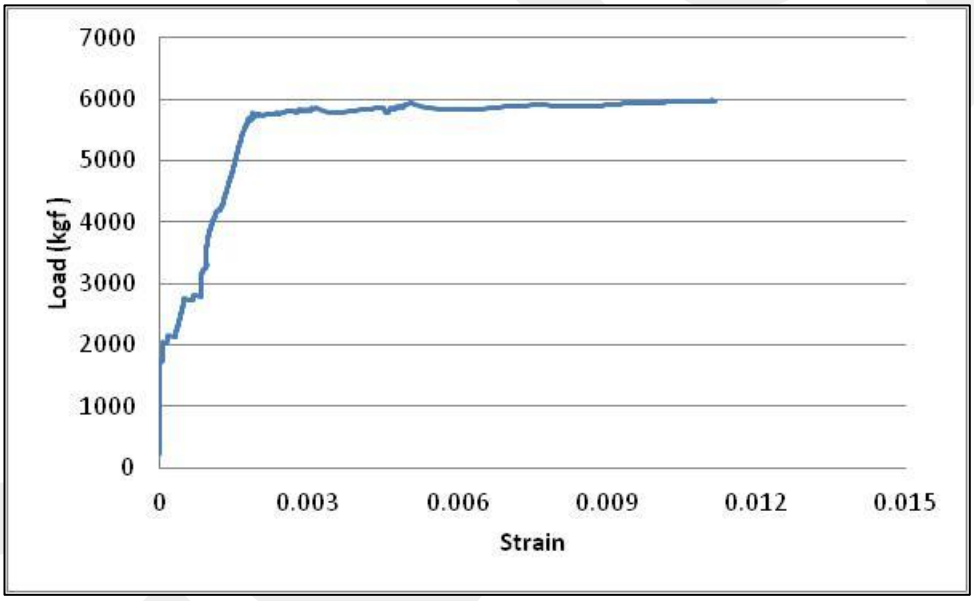

Figure 4-17 – Tensile load-strain graph for CC tension specimen of batch 2 (CC100×100×1000-01)

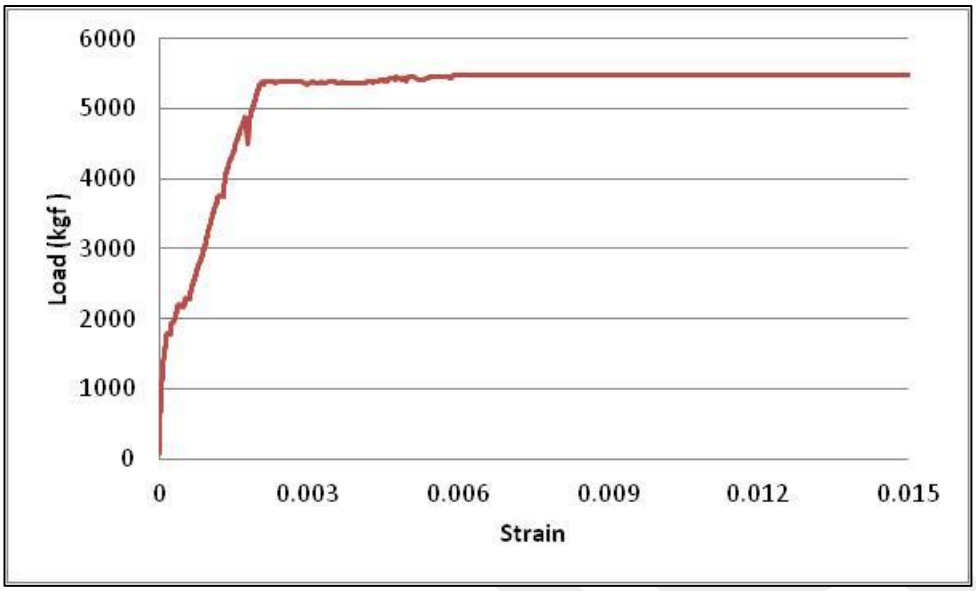

Figure 4-18 – Tensile load-strain graph for CC tension specimen of batch 2 (CC100×100×1500-01)

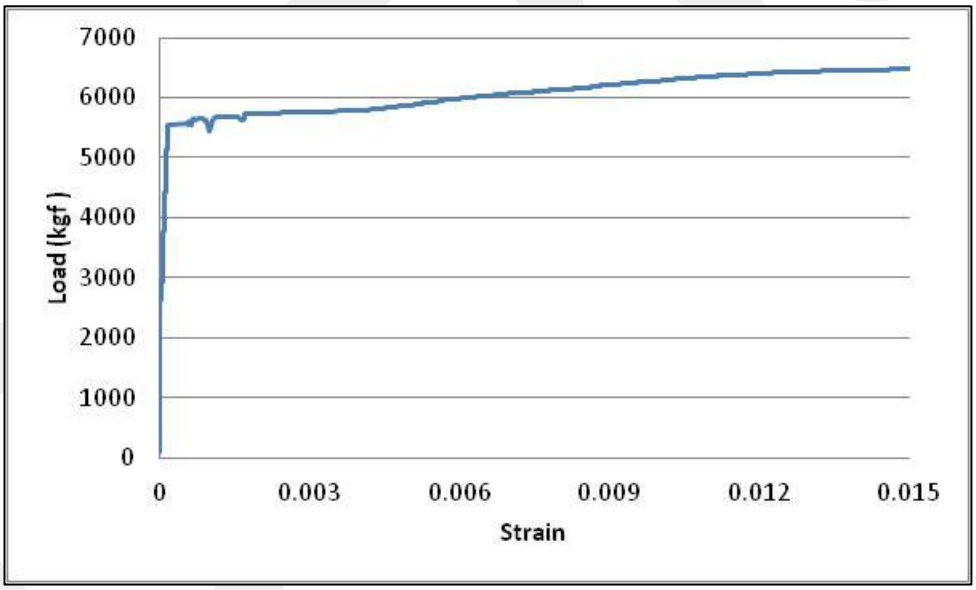

Figure 4-19 – Tensile load-strain graph for CC tension specimen of batch 2 (CC150×150×1000-01)

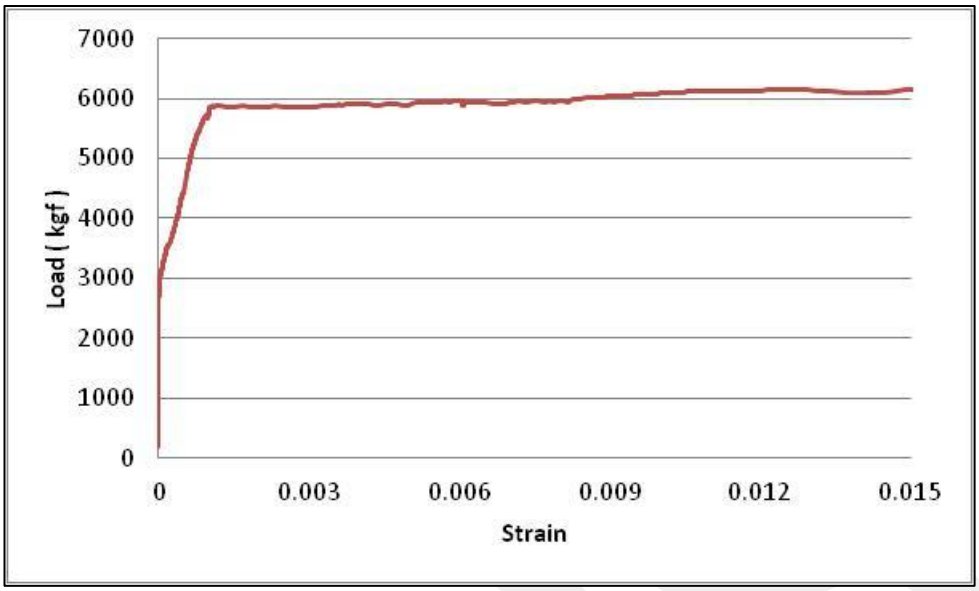

Figure 4-20 – Tensile load-strain graph for CC tension specimen of batch 2 (CC100×100×500-01)

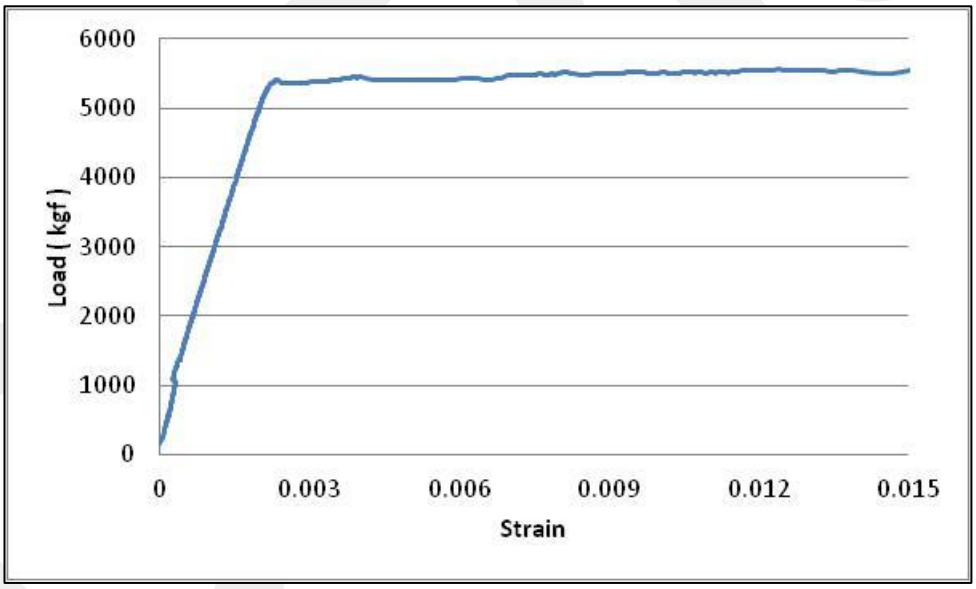

Figure 4-21 – Tensile load-strain graph for CC tension specimen of batch 2 (CC60×60×1000-01)

The load-strain curves obtained from six tension tests of CC specimens of the third batch are shown in Figure 4-22 to Figure 4-27. Note that the test set-up for this batch was vertically oriented. Three of the specimens had 60×60×500 mm and other three specimens had 100×100×500 mm dimensions.

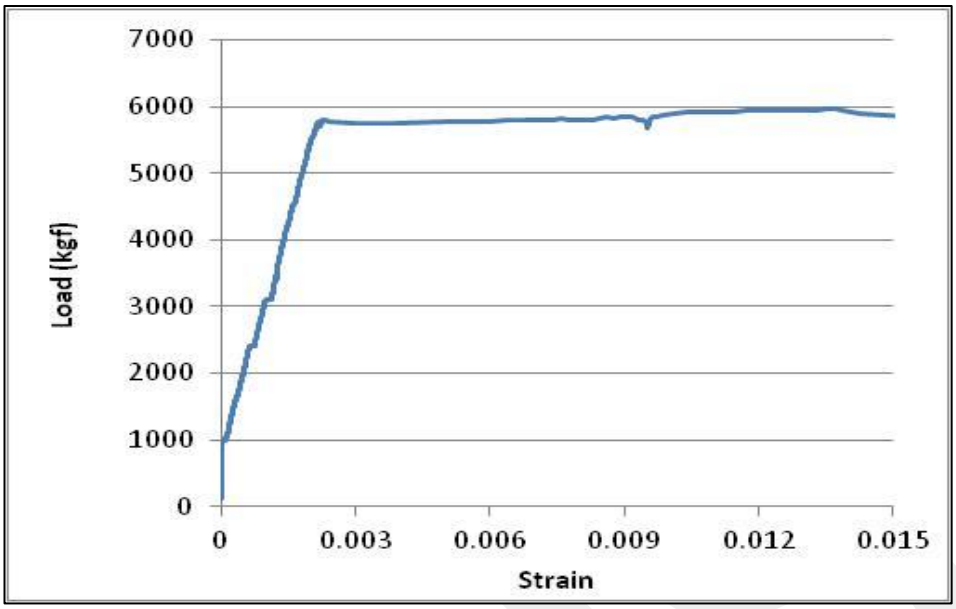

Figure 4-22 – Tensile load-strain graph for CC tension specimen of batch 3 (CC60×60×500-01)

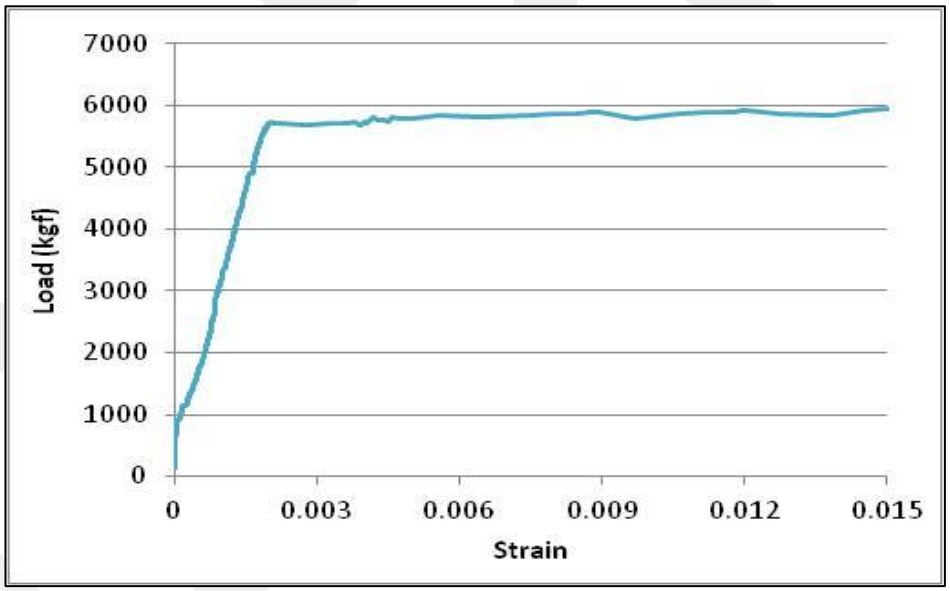

Figure 4-23 – Tensile load-strain graph for CC tension specimen of batch 3 (CC60×60×500-02)

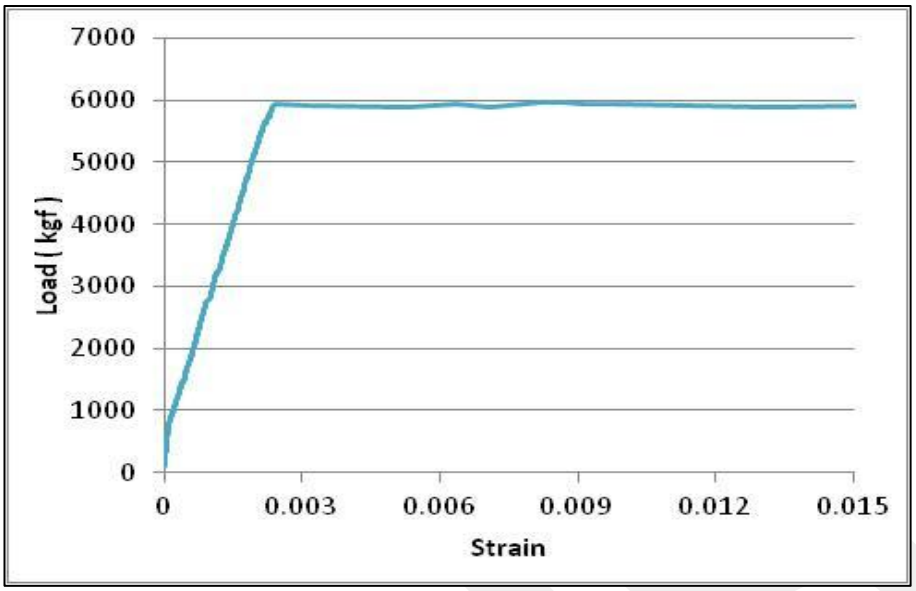

Figure 4-24 – Tensile load-strain graph for CC tension specimen of batch 3 (CC60×60×500-03)

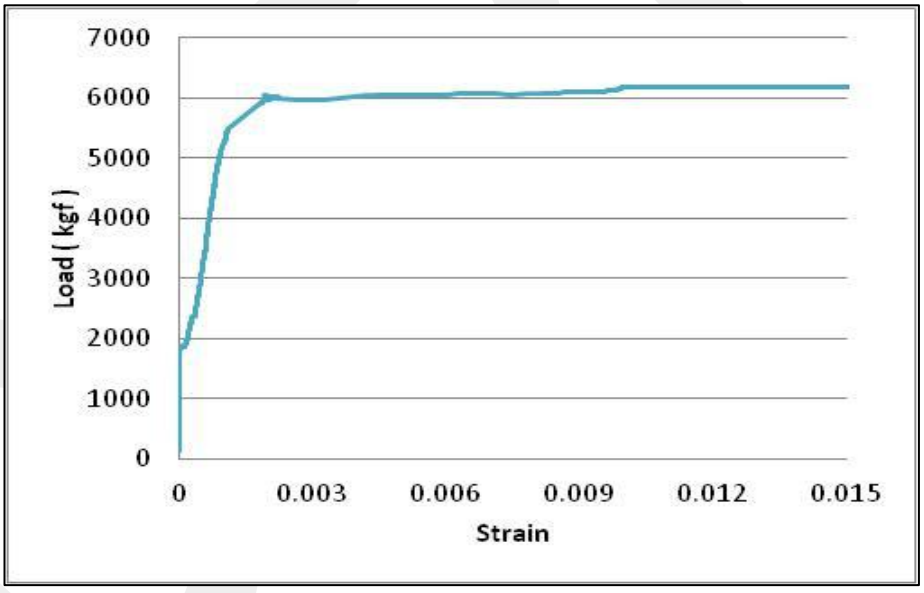

Figure 4-25 – Tensile load-strain graph for CC tension specimen of batch 3 (CC100×100×500-02)

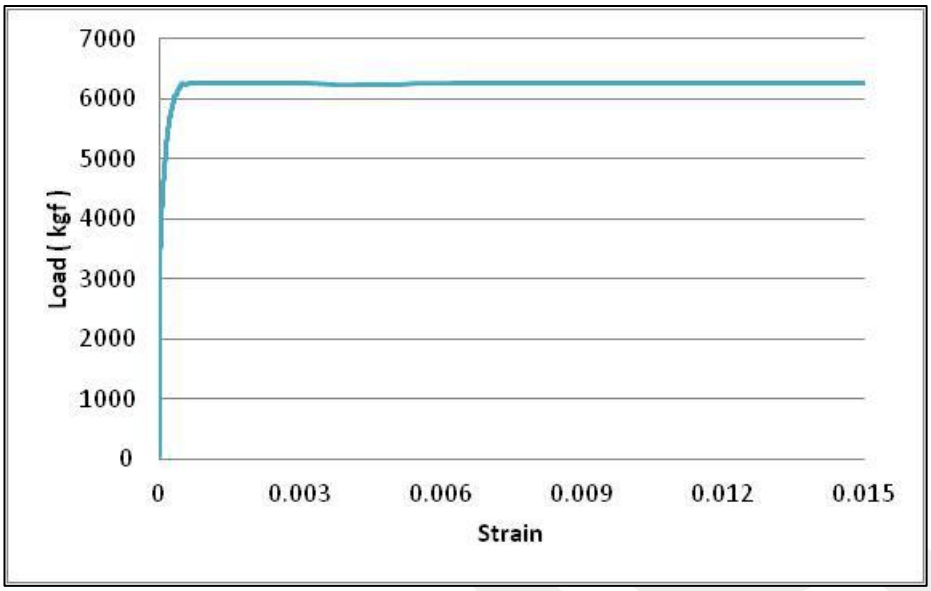

Figure 4-26 – Tensile load-strain graph for CC tension specimen of batch 3 (CC100×100×500-03)

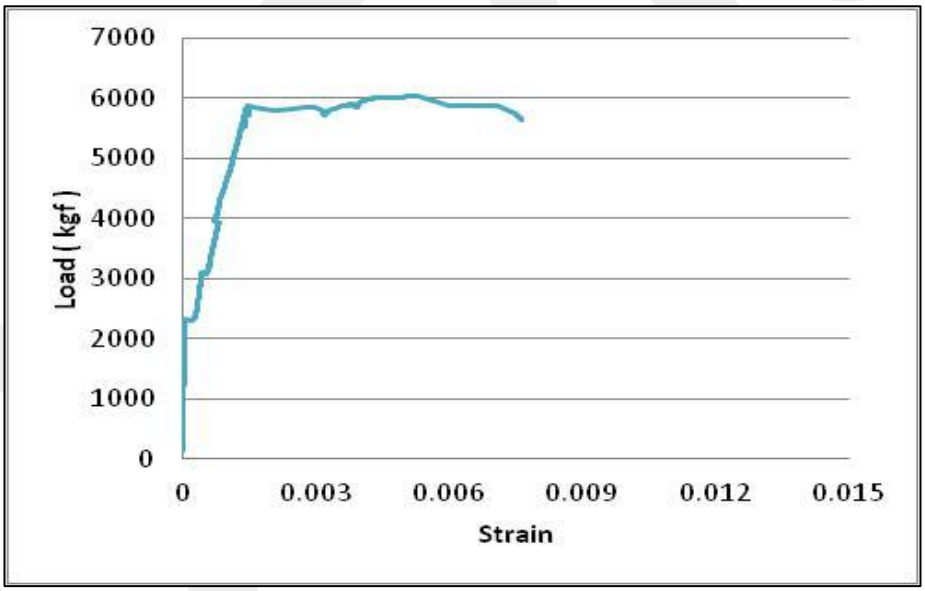

Figure 4-27 – Tensile load-strain graph for CC tension specimen of batch 3 (CC100×100×500-04)

The load-strain curves obtained from three tension tests of SFRC specimens of the first batch are shown in Figure 4-28 to Figure 4-30. Note that the test set-up for this batch was horizontally oriented. The dimension of the specimens were 100×100×1500, 150×150×1000, and 100×100×500 mm.

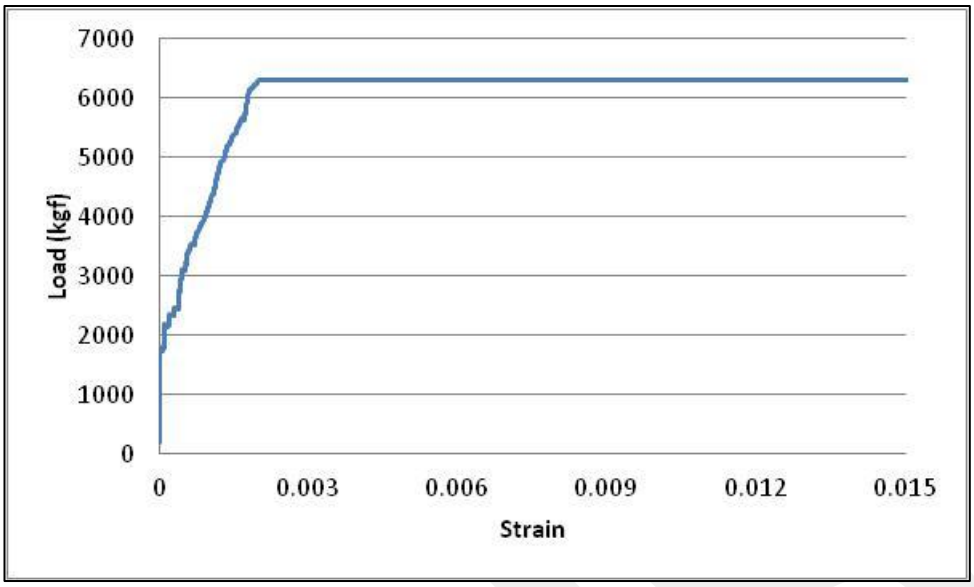

Figure 4-28 – Tensile load-strain graph for SFRC tension specimen of batch 1 (SFRC100×100×1500 -01)

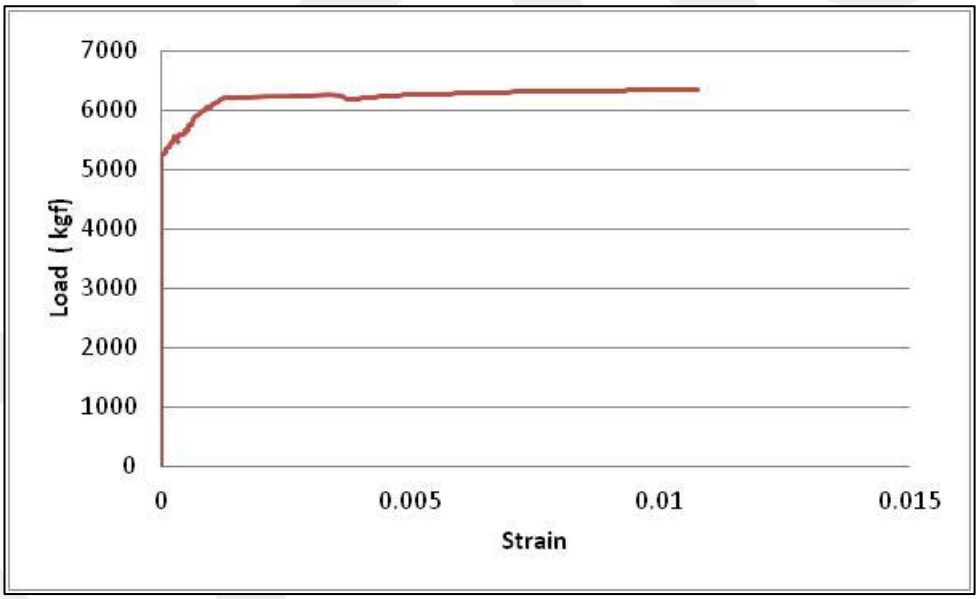

Figure 4-29 – Tensile load-strain graph for SFRC tension specimen of batch 1 (SFRC150×150×1000-01)

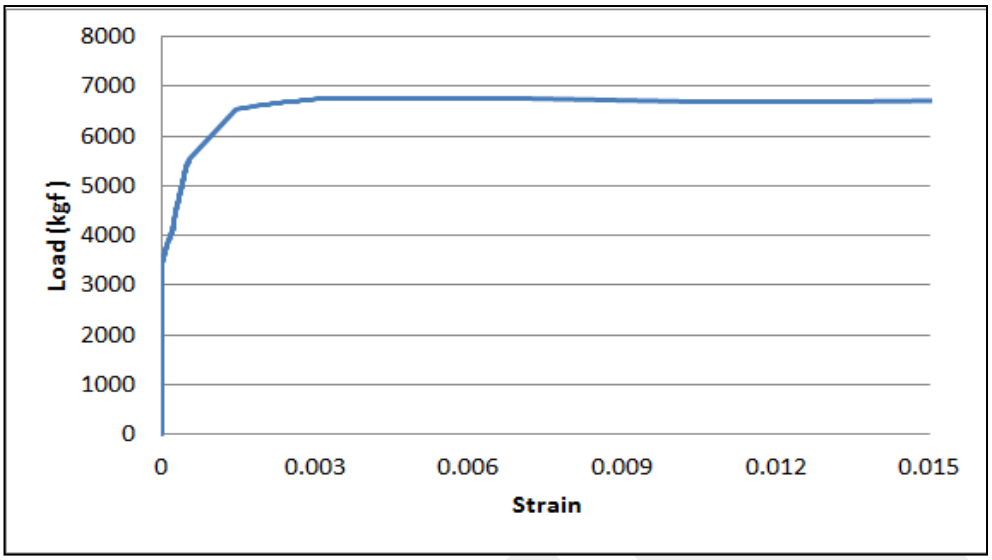

Figure 4-30 – Tensile load-strain graph for SFRC tension specimen of batch 1 (SFRC100×100×500-01)

Five specimens were cast for the first batch however, the test data of only three was obtained, the data of 100×100×1000 mm specimen could not be recovered during test and the 200×200×1000 mm specimen was not cracked, due to the huge size of the cross-section compared to the bar diameter.

During tests, it was observed that the initial cracking load of the specimens with larger cross-section was greater than that of the specimens with smaller cross-section.

The load-strain curves obtained from six tension tests of SFRC specimens of the fourth batch are shown in Figure 4-31 to Figure 4-36. Note that the test set-up for this batch was vertically oriented. Three of the specimens had 60×60×500 mm and other three specimens had 100×100×500 mm dimensions.

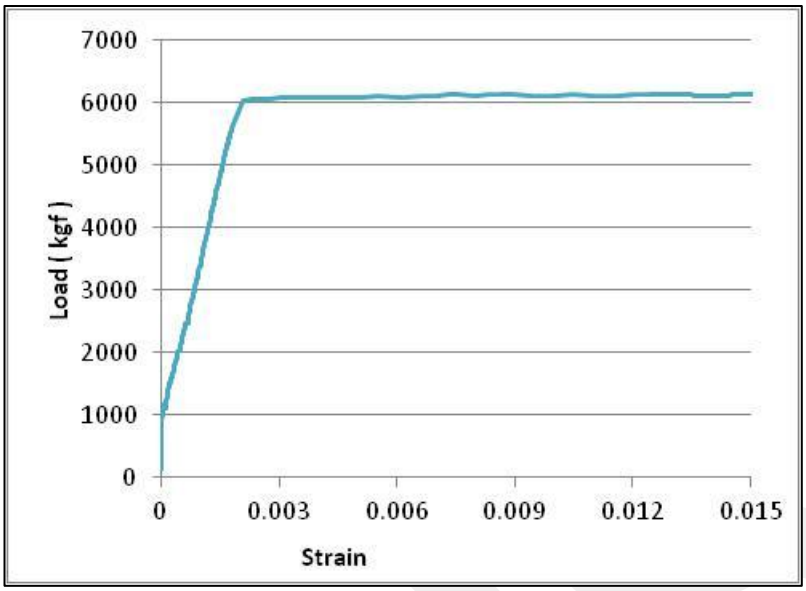

Figure 4-31 – Tensile load-strain graph for SFRC tension specimen of batch 4 (SFRC60×60×500-01)

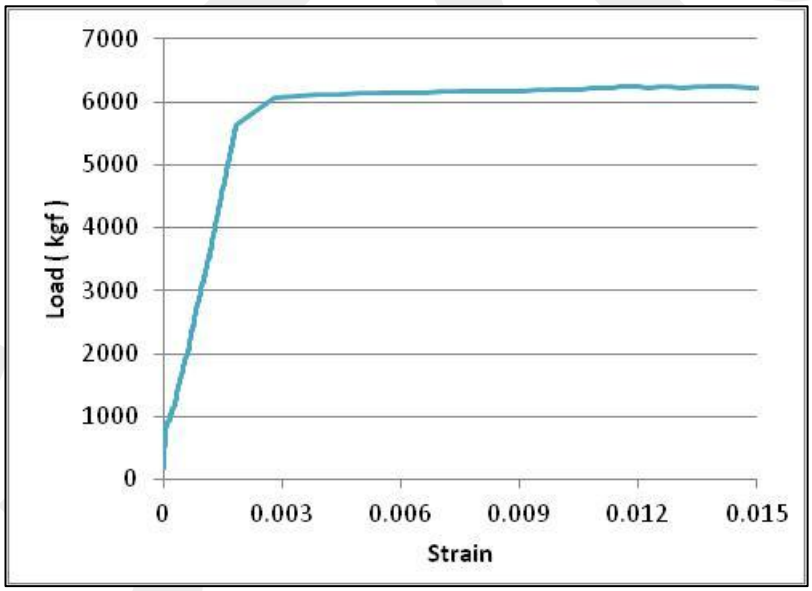

Figure 4-32 – Tensile load-strain graph for SFRC tension specimen of batch 4 (SFRC60×60×500-02)

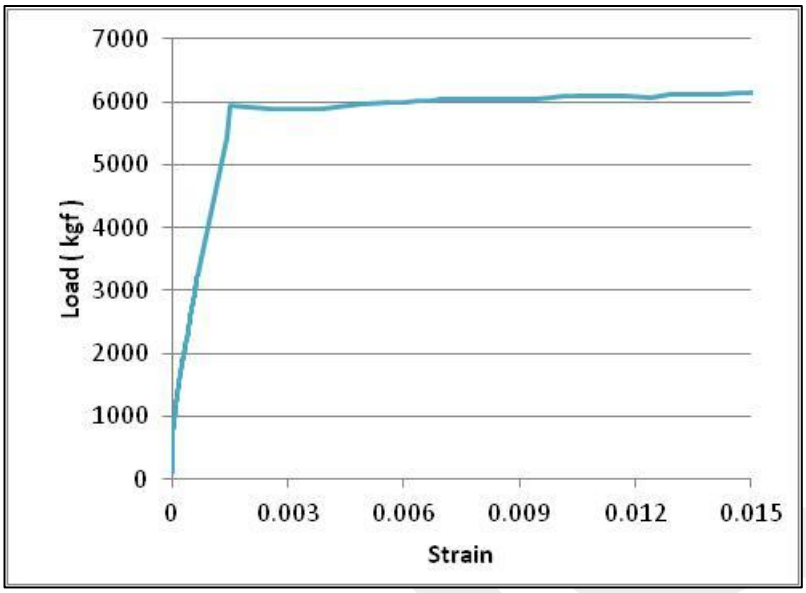

Figure 4-33 – Tensile load-strain graph for SFRC tension specimen of batch 4 (SFRC60×60×500-03)

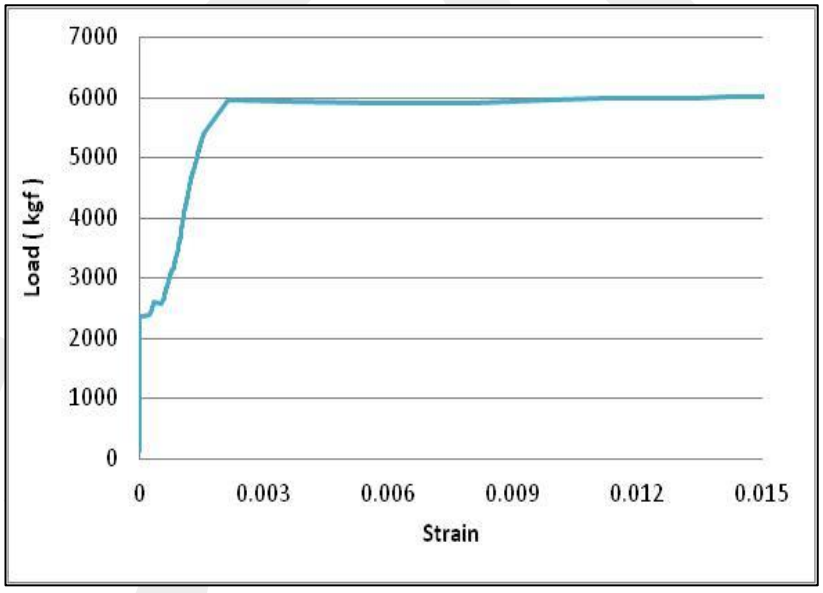

Figure 4-34 – Tensile load-strain graph for SFRC tension specimen of batch 4 (SFRC100×100×500-02)

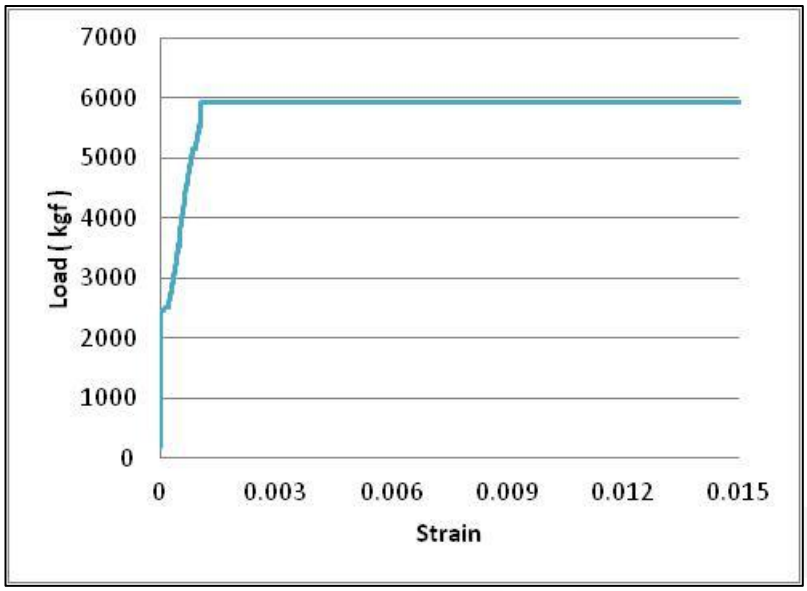

Figure 4-35 – Tensile load-strain graph for SFRC tension specimen of batch 4 (SFRC100×100×500-03)

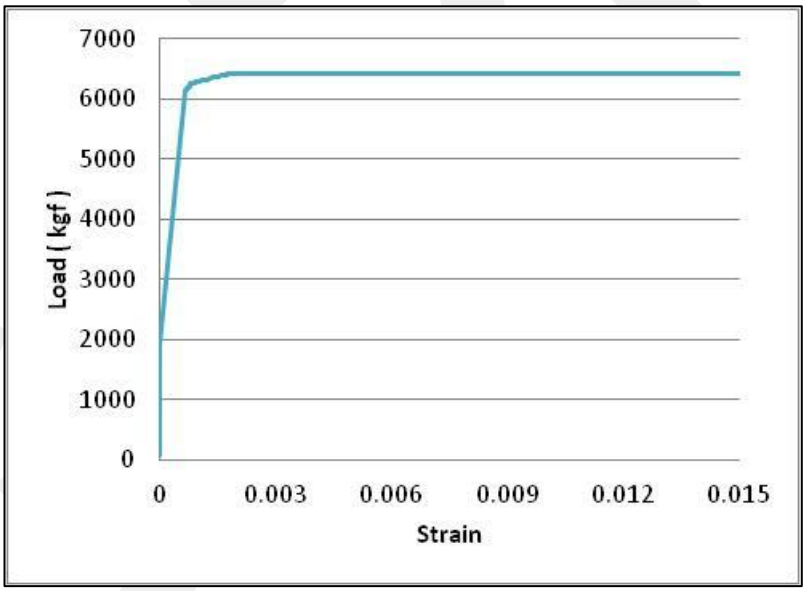

Figure 4-36 – Tensile load-strain graph for SFRC tension specimen of batch 4 (SFRC100×100×500-04)

It was noted that, the test set-up in vertical position was better compared to that of horizontal position due to additional bending deformations introduced to the specimen related to its own weight in horizontal position. However in this research, the effects of additional bending deformations for test set-up in horizontal direction were eliminated by using four displacement transducers.

The initial crack load, yield load, and crack spacing of the CC specimens are tabulated in Table 4-5. The graphical presentations of this table is shown in Figure 4-37 and Figure 4-38. The average initial crack and yield load were 730 and 5755 kgf for 60×60 specimens, 2345 and 5880 kgf for 100×100 specimens, and 2560 and 5530 kgf for 150×150 specimen. The results show that as the cross-section of the specimens increase, the initial crack load increases. However, the cross-sectional dimensions do not have any significant effects on the yield load of CC specimens. Also the change in the length of the specimens does not have any significant effects on the initial crack and yield loads of the CC specimens. The average crack spacings were 52.5 mm for 60×60 specimens, 180 mm for 100×100 specimens, and 400 mm for 150×150 specimen. The results show that as the cross-section of the specimens increase, the crack spacing increases. The change in the length of the specimens also does not have any significant effect on the crack spacing of the CC specimens.

Table 4-5 – Comparison of CC tension specimens

Specimen	Initial Crack Load (kgf)	Yield Load (kgf)	Crack Spacing (mm)
CC60×60×500-01	960	5820	35
CC60×60×500-02	920	5780	50
CC60×60×500-03	840	5950	60
CC60×60×1000-01	200	5470	65
CC100×100×500-01	2670	5890	250
CC100×100×500-02	1900	6010	180
CC100×100×500-03	3500	6200	150
CC100×100×500-04	2500	5930	150
CC100×100×1000-01	2050	5780	150
CC100×100×1500-01	1450	5470	200
CC150×150×1000-01	2560	5530	400

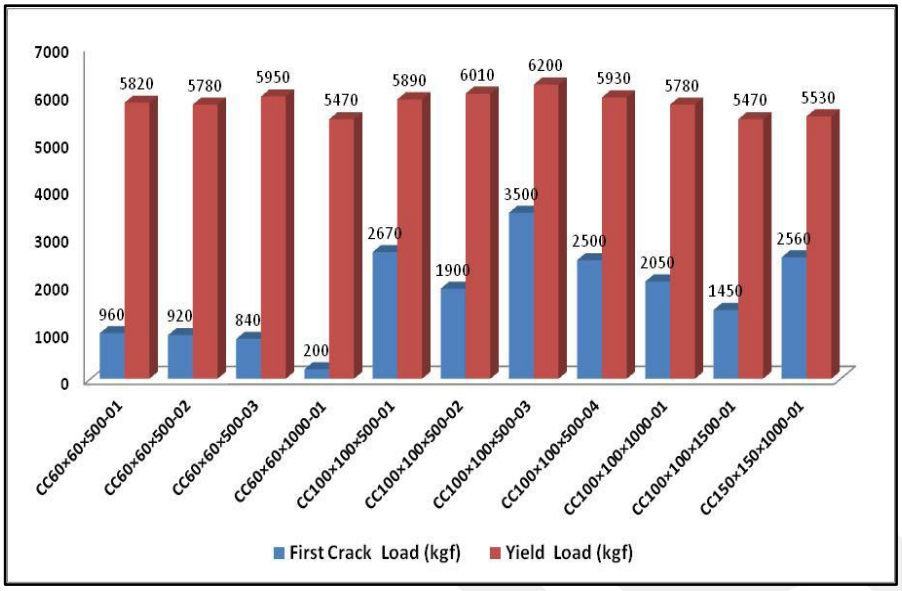

Figure 4-37 – Graphical presentation of initial crack and yield load of CC specimens

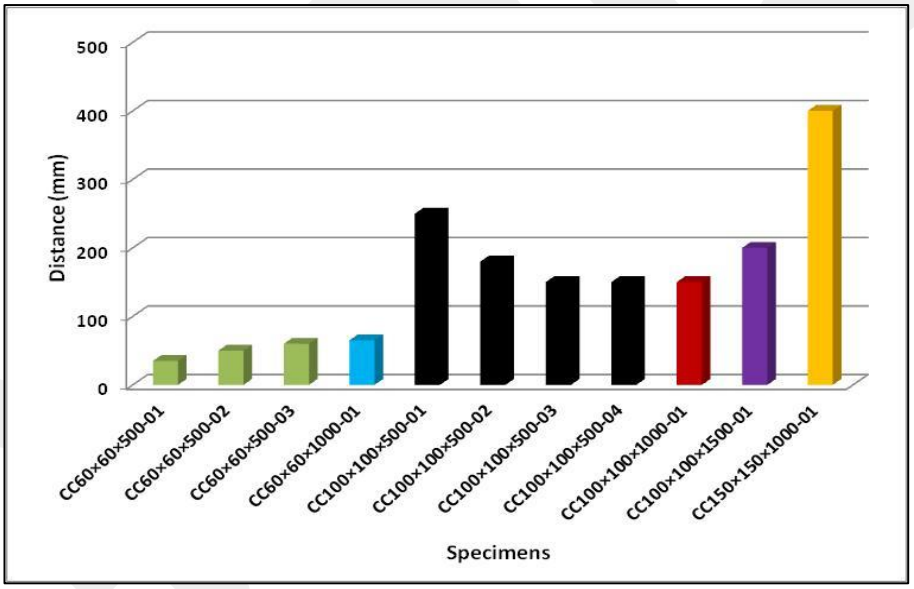

Figure 4-38 – Graphical presentation of crack spacing of CC specimens

The initial crack load, yield load, and crack spacing of the SFRC specimens are tabulated in Table 4-6. The graphical presentations of this table is shown in Figure 4-39 and Figure 4-40. The average initial crack and yield load were 967 and 6017 kgf for 60×60 specimens, 2417 and 6199 kgf for 100×100 specimens, and 5210 and 6090 kgf for 150×150 specimen. The results show that as the cross-section of the specimens increase, the initial crack load increases. However, the cross-sectional dimensions do not have any significant effects on the yield load of SFRC specimens.

Also the change in the length of the specimens does not have any significant effects on the initial crack and yield loads of the SFRC specimens. The average crack spacings were 200 mm for 60×60 specimens, 229 mm for 100×100 specimens, and 400 mm for 150×150 specimen. The results show that as the cross-section of the specimens increase, the crack spacing increases. The change in the length of the specimens also does not have any significant effect on the crack spacing of the SFRC specimens.

Table 4-6 – Comparison of SFRC tension specimens

Specimen	First Crack Load (kgf)	Yield Load (kgf)	Crack Spacing (mm)
SFRC60×60×500-01	1000	6000	250
SFRC60×60×500-02	900	6050	230
SFRC60×60×500-03	1000	6000	120
SFRC100×100×500-01	3500	6580	255
SFRC100×100×500-02	2350	6000	250
SFRC100×100×500-03	2500	5960	250
SFRC100×100×500-04	2100	6200	250
SFRC100×100×1500-01	1633	6254	140
SFRC150×150×1000-01	5210	6090	400

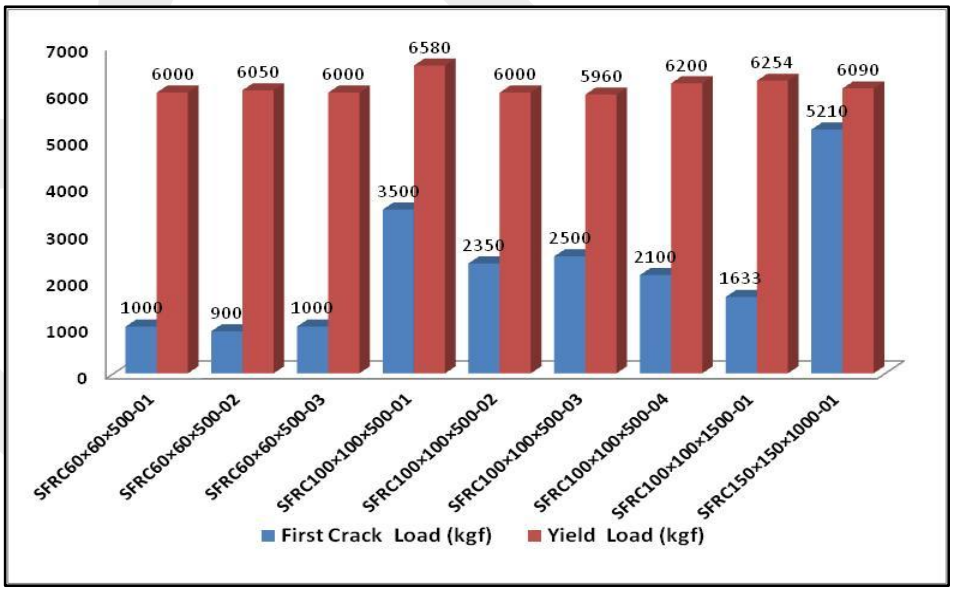

Figure 4-39 – Graphical presentation of initial crack and yield load of SFRC specimens

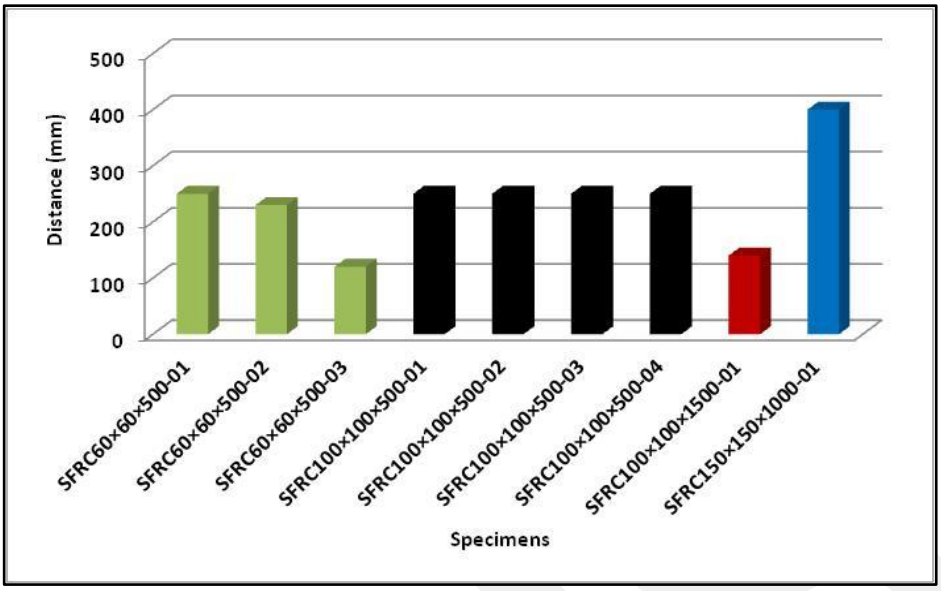

Figure 4-40 – Graphical presentation of crack spacing of SFRC specimens

The CC and SFRC specimens having 60×60 mm cross-sections were compared in Figure 4-41 and Figure 4-42. The average initial crack loads were 730 and 967 kgf and the average yield load loads were 5755 and 6017 kgf for CC and SFRC specimens, respectively. It can be concluded that, SFRC specimens having 60×60 mm cross-sections had greater initial crack and yield loads than that of CC specimens. The average crack spacings were 52.5 and 200 mm for CC and SFRC specimens, respectively. The results indicate that the spacing of cracks for SFRC specimens are greater than that of CC specimens having 60×60 mm cross-sections.

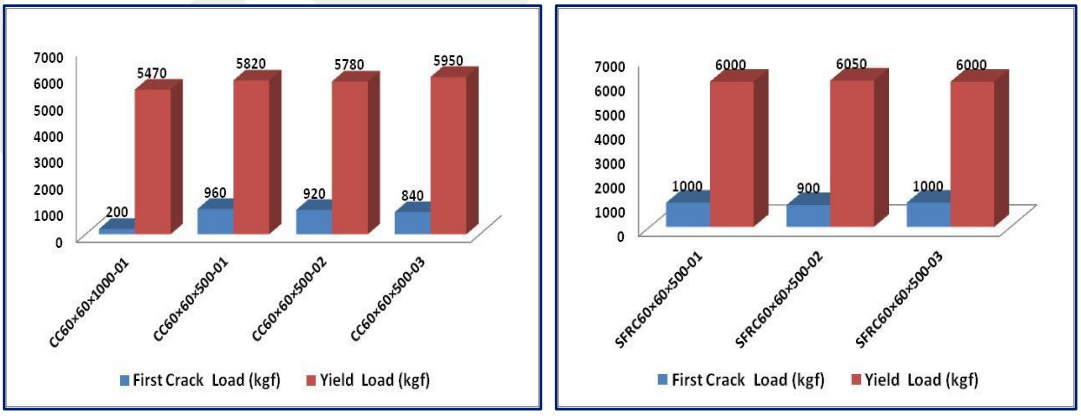

Figure 4-41 – Comparison of initial crack and yield load of CC and SFRC specimens having 60×60 mm cross-section

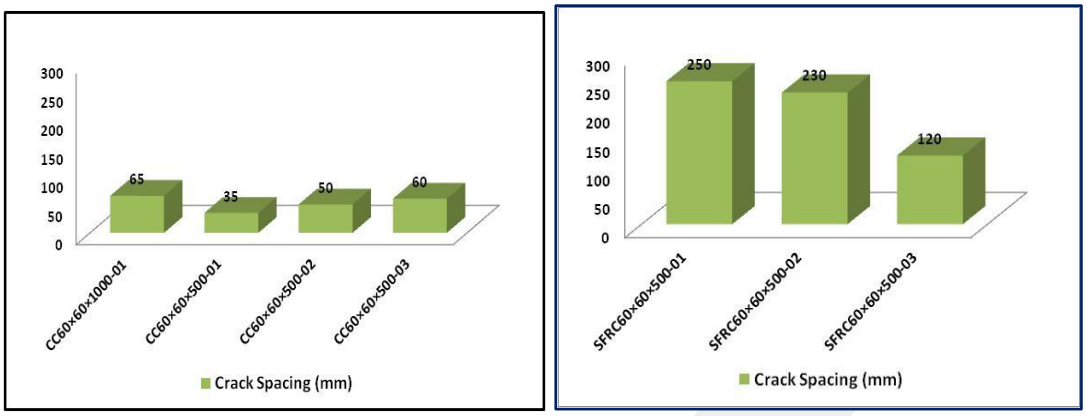

Figure 4-42 – Comparison of crack spacing of CC and SFRC specimens having 60×60 mm cross-section

The CC and SFRC specimens having 100×100 mm cross-sections were compared in Figure 4-43 and Figure 4-44. The average initial crack loads were 2345 and 2417 kgf and the average yield load loads were 5880 and 6199 kgf for CC and SFRC specimens, respectively. It can be concluded that, SFRC specimens having 100×100 mm cross-sections had greater initial crack and yield loads than that of CC specimens. The average crack spacings were 180 and 229 mm for CC and SFRC specimens, respectively. The results indicate that the spacing of cracks for SFRC specimens are greater than that of CC specimens having 100×100 mm cross-sections.

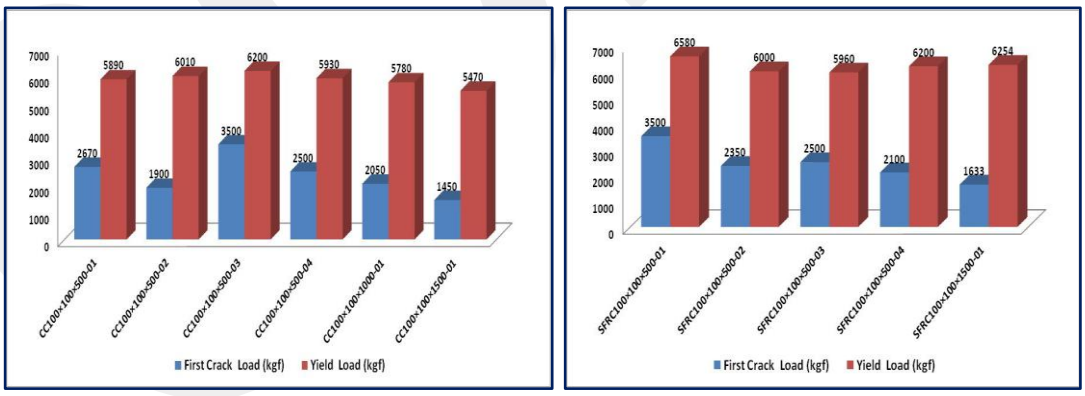

Figure 4-43 – Comparison of initial crack and yield load of CC and SFRC specimens having 100×100 mm cross-section

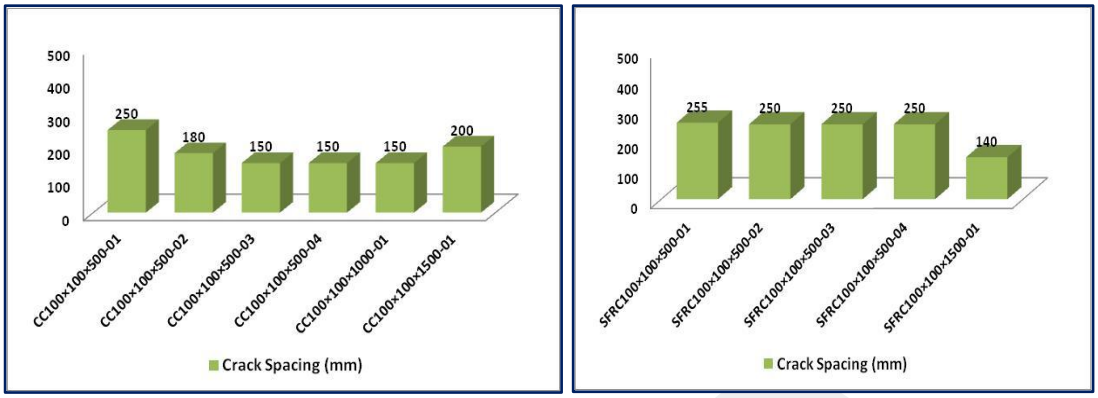

Figure 4-44 – Comparison of crack spacing of CC and SFRC specimens having 100×100 mm cross-section

5 ANALYTICAL WORK

5.1 Introduction

In this chapter, the stress-strain relationships in tension and compression of CC and SFRC specimens were compared to the available models in the literature. Based on the comparison results, the best models and/or best modified models were used to estimate the load-deflection curves obtained in flexural tests in the research.

5.2 Stress-Strain Relationships in Compression

5.2.1 Test Results

The stress-strain relationships in compression of the CC and SFRC specimens were obtained by compression tests as explained in Chapter 4. These relationships are shown in Figure 4-3 to Figure 4-6.

5.2.2 SFRC Models and Comparisons

The literature review showed that SFRC compression models proposed by Ezeldin and Balaguru (1992), Nataraja et al. (1999), and Wang (2006) were the mostly used predictions to estimate the load-deflection behavior of SFRC beams under flexure. Therefore, these three models for SFRC were used in the analytical part of this research. For 34 MPa specified concrete compression strength, the stress-strain relationships of these three models are shown in Figure 5-1.

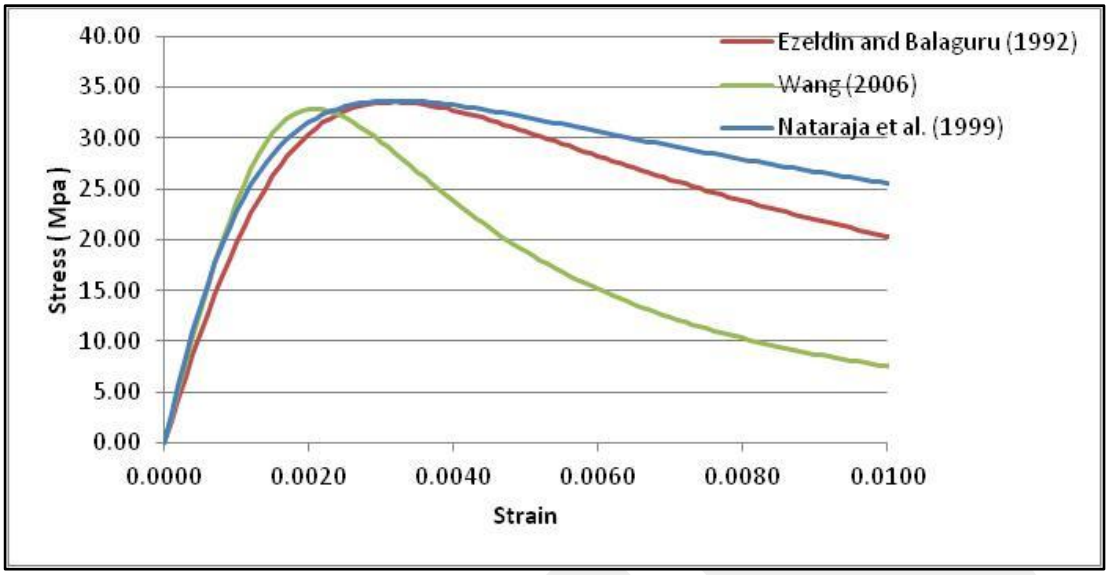

Figure 5-1 – SFRC compression models for 34 MPa concrete compression strength

These models were compared to the data of the tests performed in the scope of this research. The comparisons of the used models and the tested SFRC specimens are shown in Figure 5-2, Figure 5-3, and Figure 5-4. These figures indicate that the tested specimens may be estimated best using the model proposed by Wang (2006).

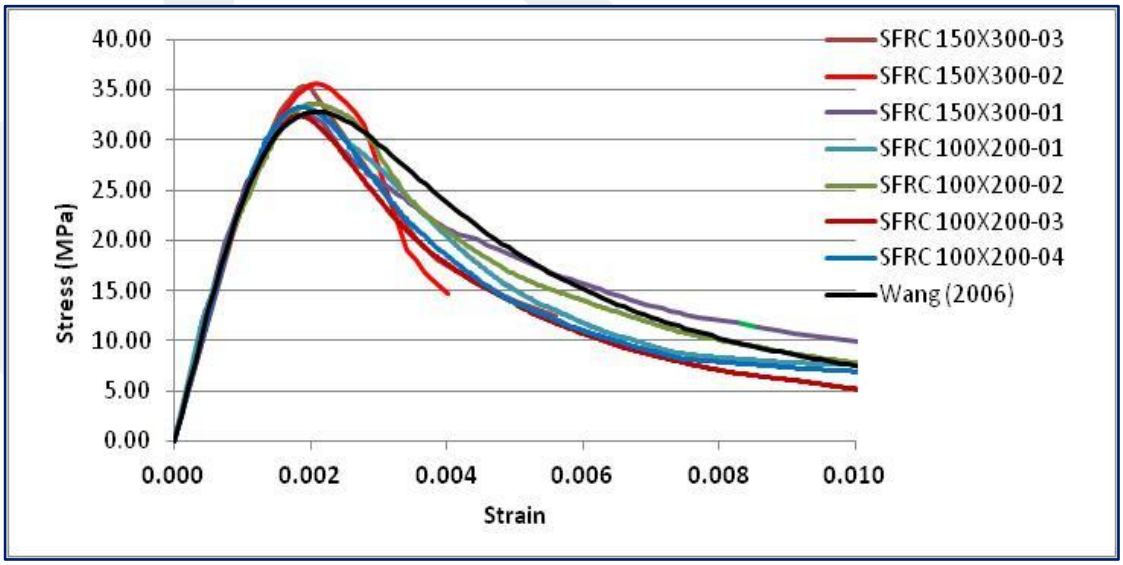

Figure 5-2 – Comparison of stress-strain curves of the tested SFRC specimens to the model proposed by Wang (2006)

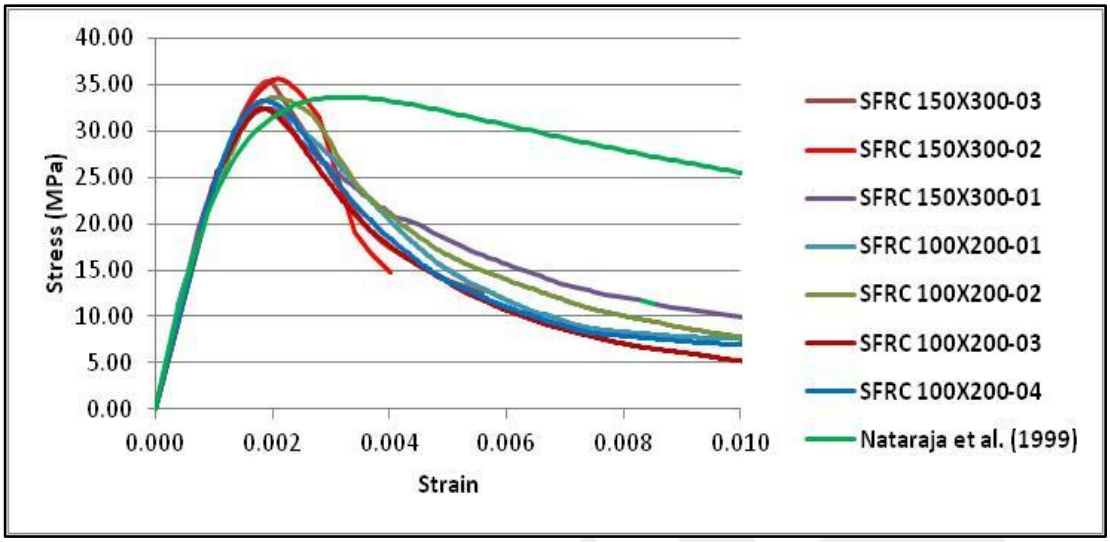

Figure 5-3 – Comparison of stress-strain curves of the tested SFRC specimens to the model proposed by Nataraja et al. (1999)

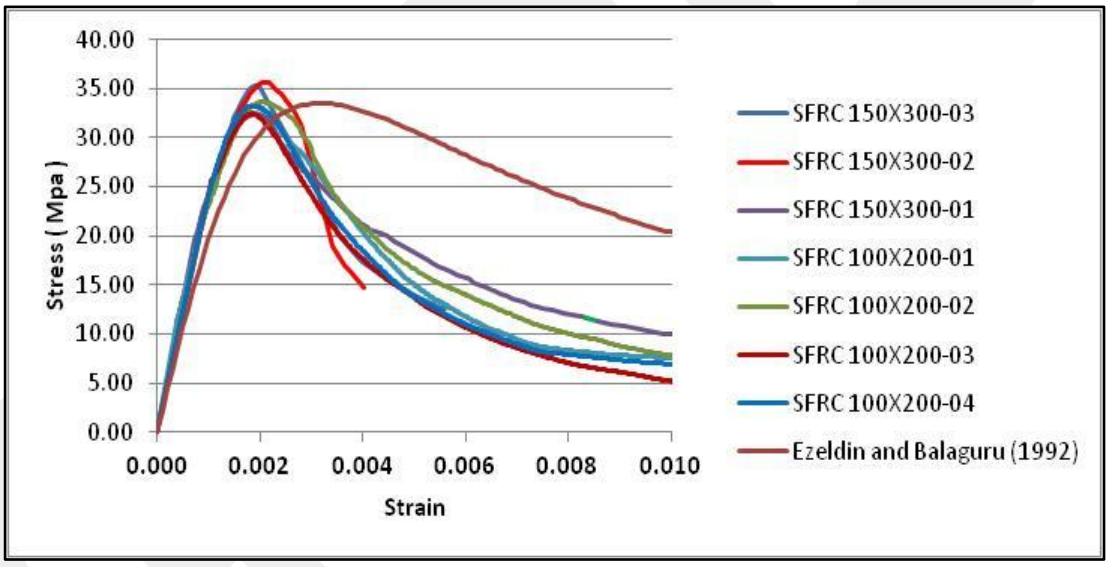

Figure 5-4 – Comparison of stress-strain curves of the tested SFRC specimens to the model proposed by Ezeldin and Balaguru (1992)

The names of the specimens are described by numbers to eliminate the crowdedness of the comparison diagrams. The names and corresponding numbering for the specimens are shown in Table 5-1.

Table 5-1 – SFRC cylinder specimens' descriptions

Name of Specimens	Descriptive Names in Diagrams
SFRC150×300-01	1
SFRC150×300-02	2
SFRC150×300-03	3
SFRC100×200-01	4
SFRC100×200-02	5
SFRC100×200-03	6
SFRC100×200-04	7

The stress-strain curves of each SFRC cylinder specimen is compared to that of the three selected models (Ezeldin and Balaguru (1992), Nataraja et al. (1999), and Wang (2006)) in terms of initial stiffness, strain at maximum stress, area under the stress-strain diagram at maximum stress, 90, 80, 70, 60, and 50% of maximum stress on the post-peak branch of stress-strain curves. Initial stiffness for stress-strain curves was obtained by calculating the slope between two points, 50 and 80% of the maximum stress on the ascending branch of the stress-strain curve as shown in Figure 5-5 - As an example, the diagram for the area at 70% of maximum stress on the post-peak branch of stress-strain curves is shown in Figure 5-6.

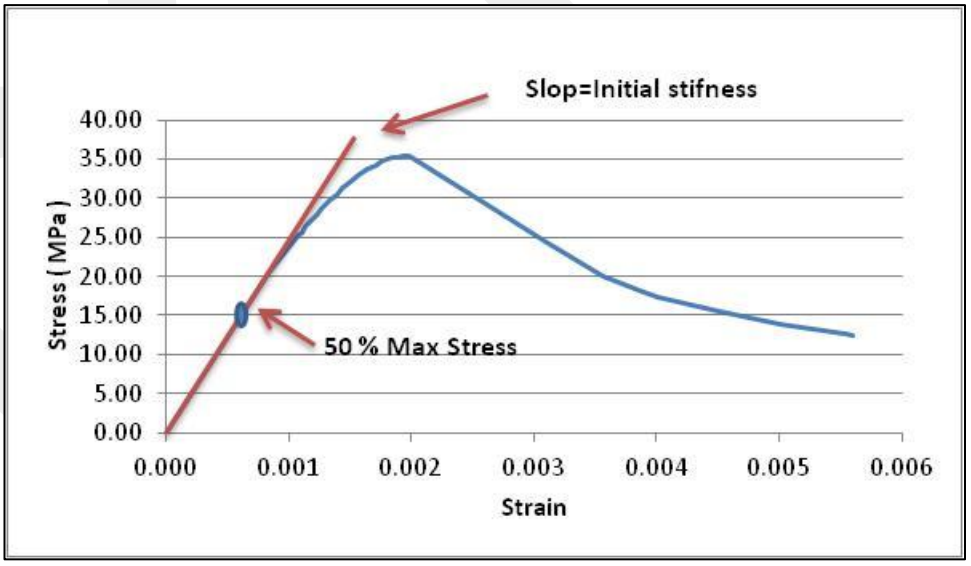

Figure 5-5 – Method of computing initial stiffness of stress-strain curves

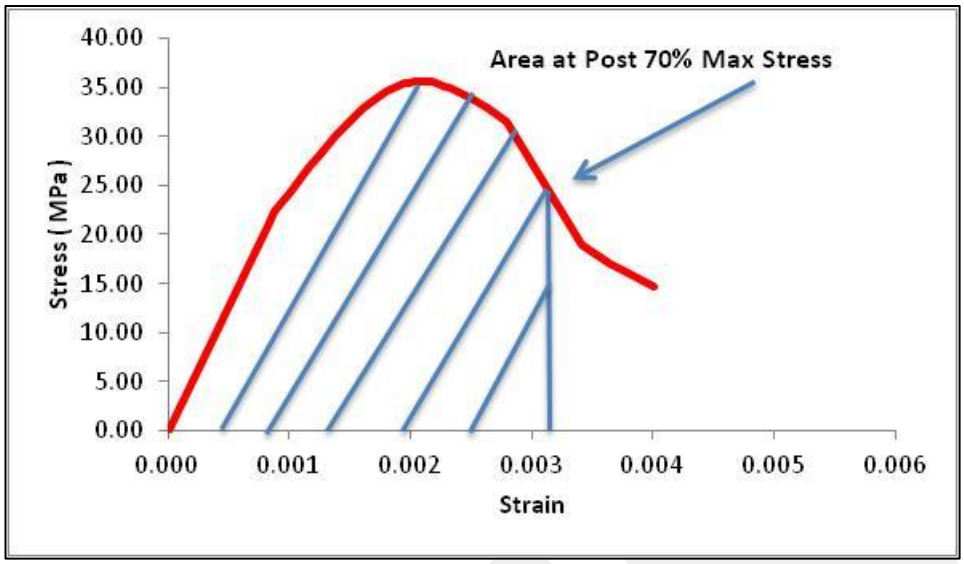

Figure 5-6 – Method of computing the area at 70% of maximum stress on the post-peak branch of stress-strain curve

An excel spreadsheet was used to calculate the values used in the comparisons. The results of the comparisons are shown in Figure 5-7 to Figure 5-14.

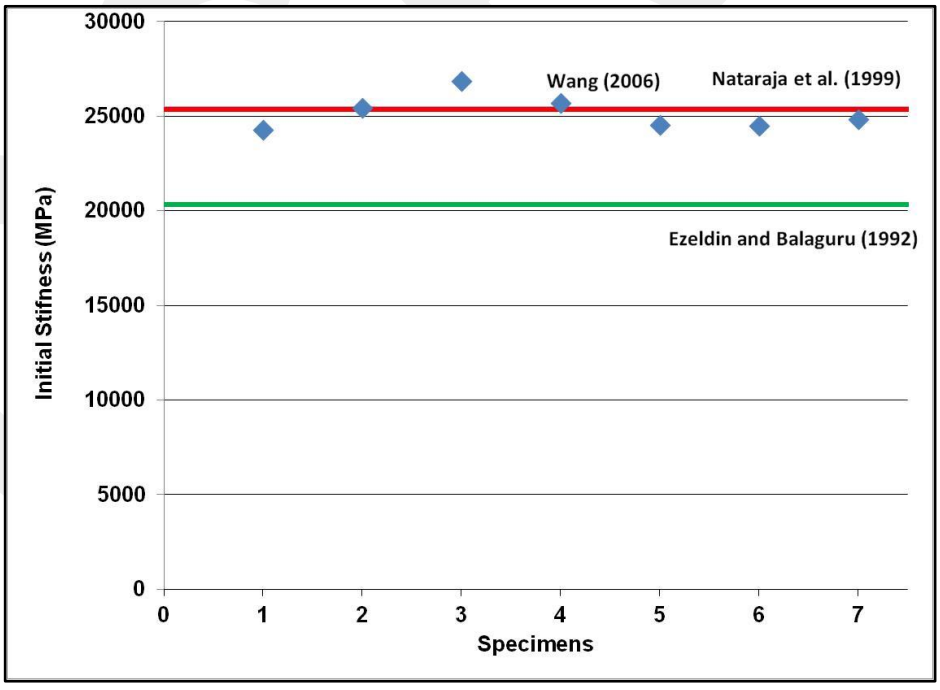

Figure 5-7 – Initial stiffness comparisons of tested SFRC specimens and used models

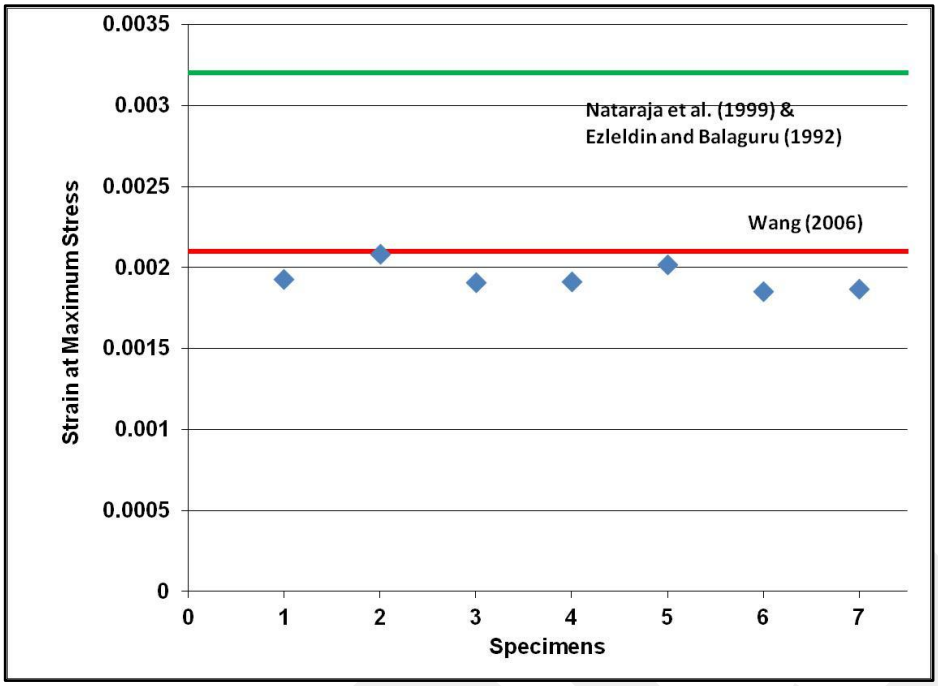

Figure 5-8 – Strain at maximum stress comparisons of tested SFRC specimens and used models

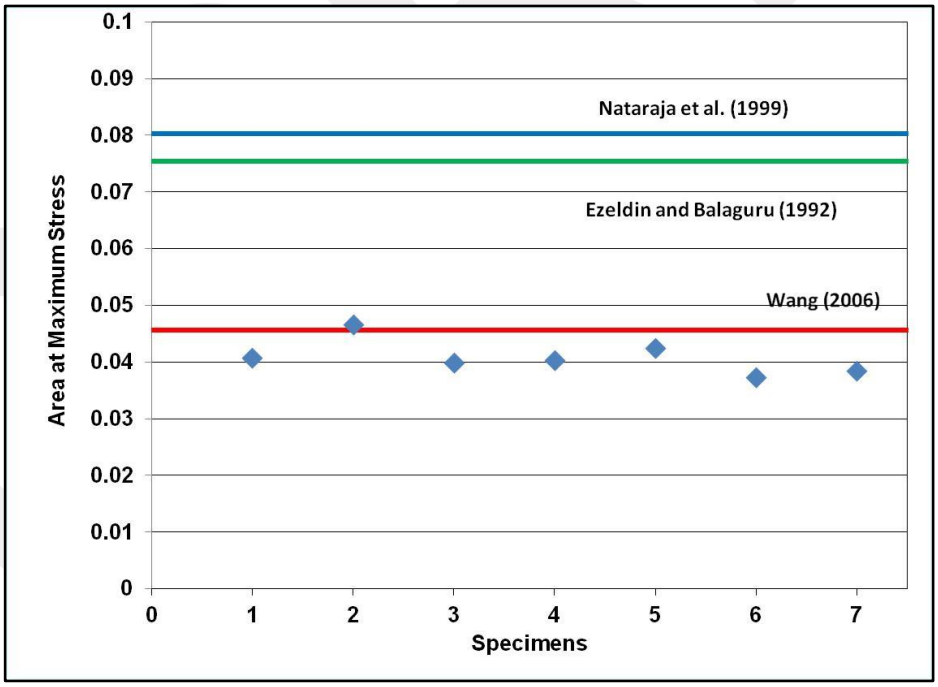

Figure 5-9 – Area under the stress-strain diagram at maximum stress comparisons of tested SFRC specimens and used models

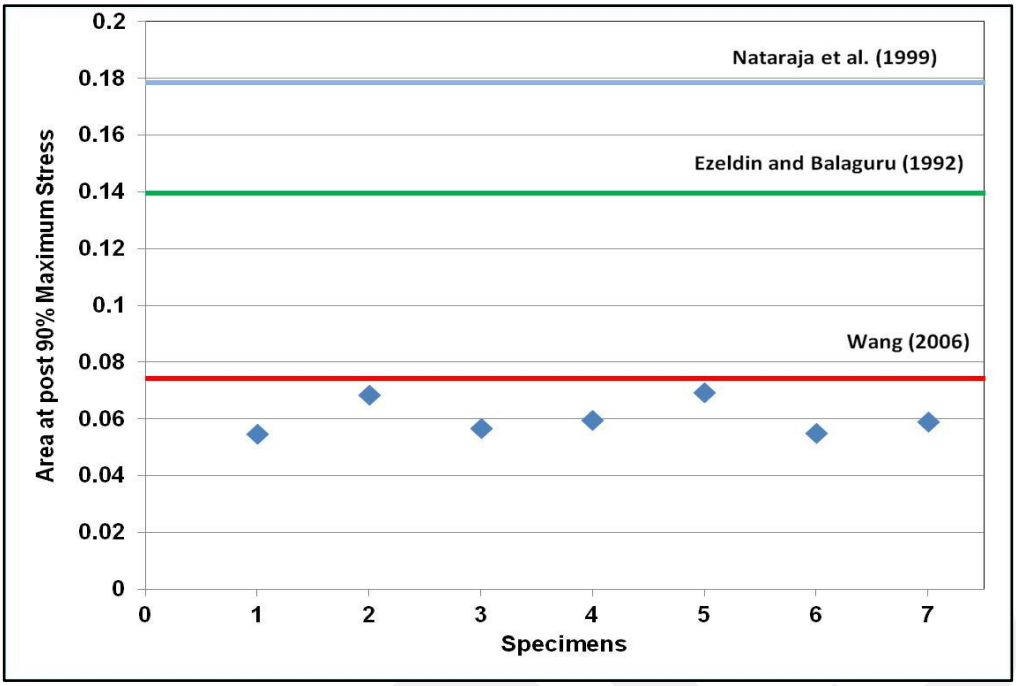

Figure 5-10 – Area under at 90% of maximum stress on descending branch of stress-strain diagram comparisons of tested SFRC specimens and used models

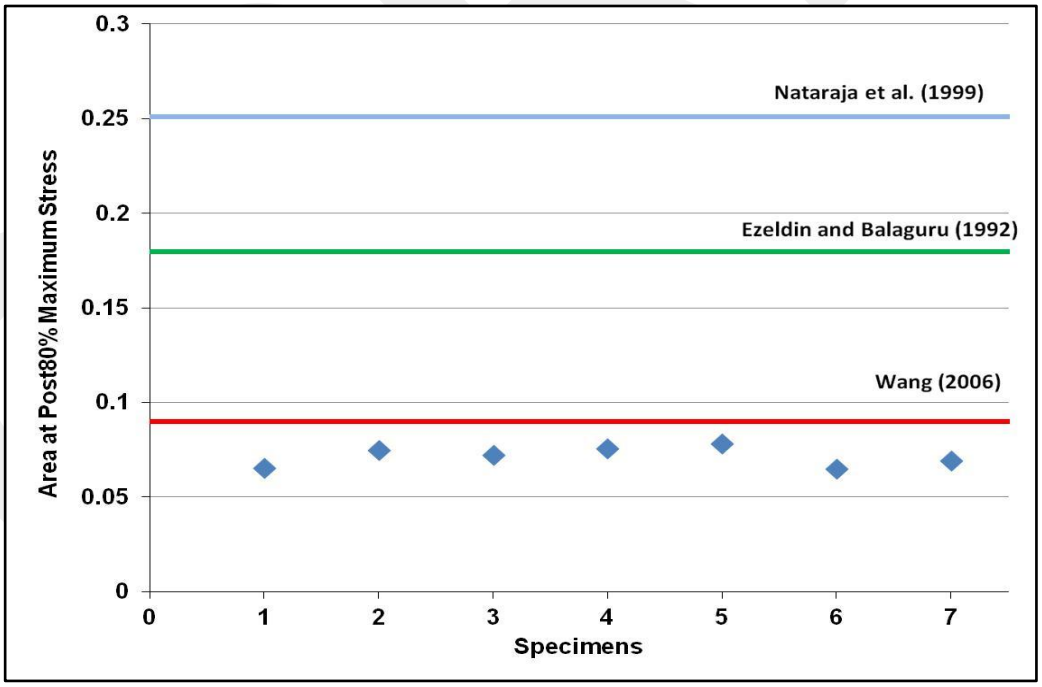

Figure 5-11 – Area under at 80% of maximum stress on descending branch of stress-strain diagram comparisons of tested SFRC specimens and used models

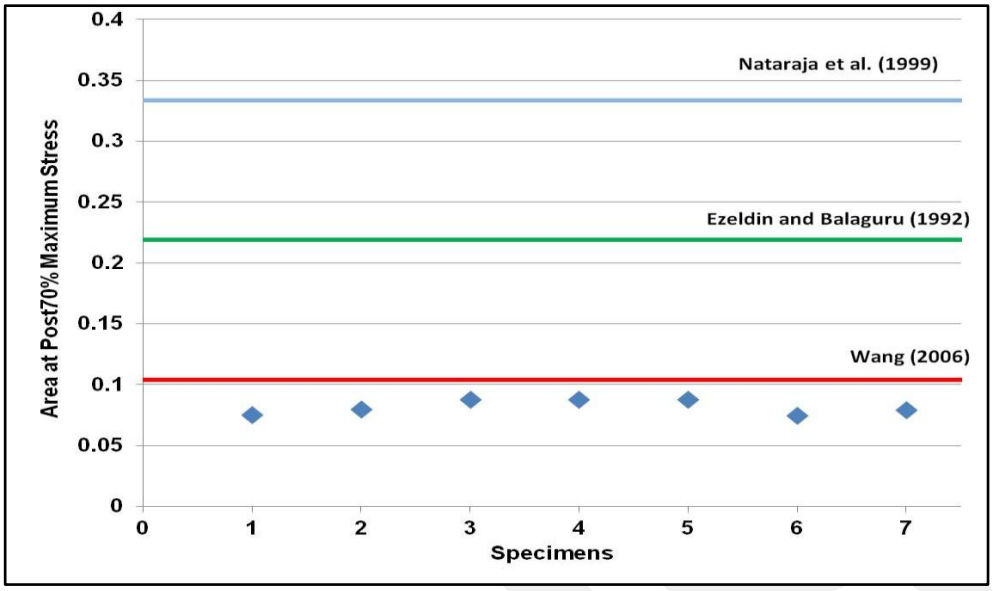

Figure 5-12 – Area under at 70% of maximum stress on descending branch of stress-strain diagram comparisons of tested SFRC specimens and used models

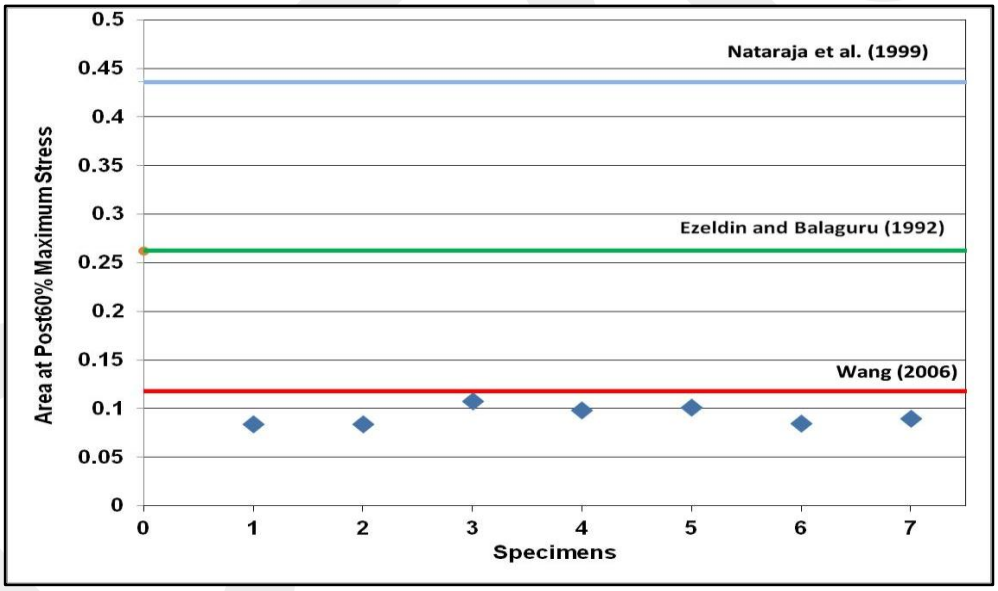

Figure 5-13 – Area under at 60% of maximum stress on descending branch of stress-strain diagram comparisons of tested SFRC specimens and used models

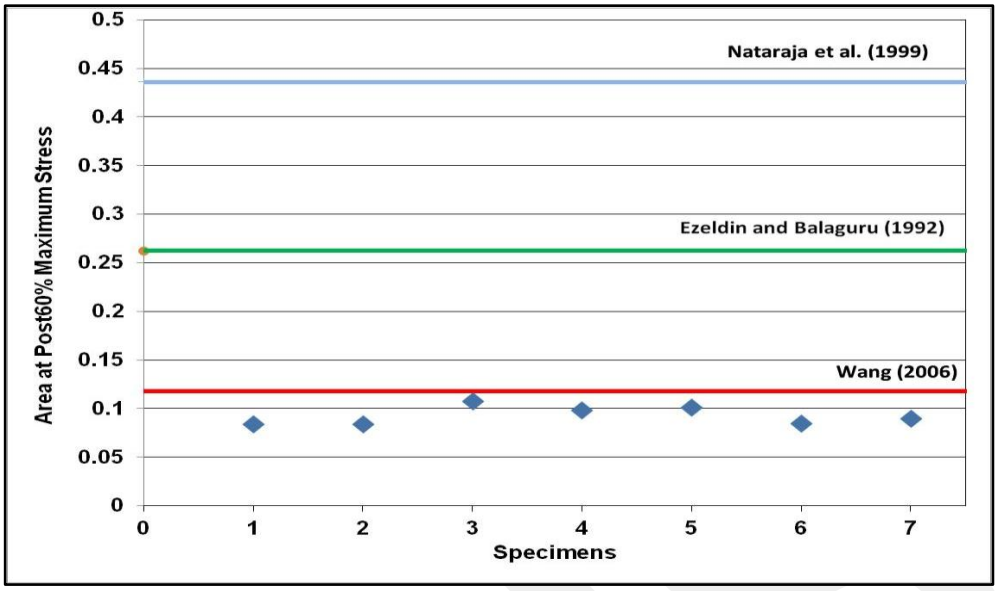

Figure 5-14 – Area under at 50% of maximum stress on descending branch of stress-strain diagram comparisons of tested SFRC specimens and used models

The figures indicate that the model proposed by Wang (2006) estimated compressive stress-strain relationships of the tested specimens better than the other models, Ezeldin and Balaguru (1992) and Nataraja et al. (1999). Therefore, Wang (2006) was selected as the model to be used in the analytical work related to the flexural behavior of the tested SFRC specimens.

5.2.3 CC Model and Comparisons

The literature review showed that CC compression models proposed by Popovics (1973) produced good predictions to estimate the load-deflection behavior of CC beams under flexure. Therefore, this model for CC was used in the analytical part of this research. For 24 MPa specified concrete compression strength, the stress-strain relationships of this model is shown in Figure 5-15..

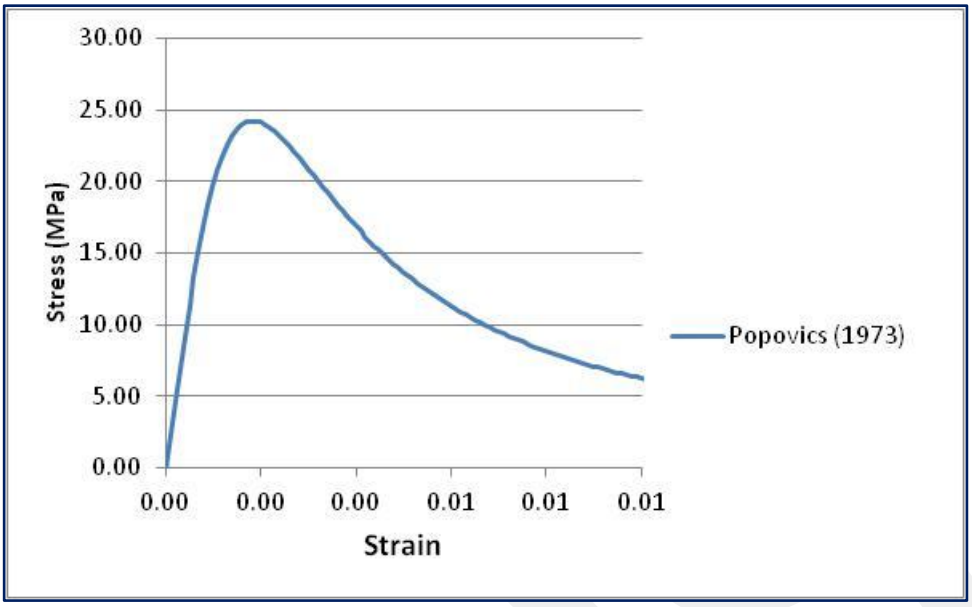

Figure 5-15 – CC compression model for 24 MPa concrete compression strength

This model was compared to the data of the tests performed in the scope of this research. The comparison of the used model and the tested CC specimens are shown in Figure 5-16. This figure indicates that the tested specimens may be estimated well with a reasonable accuracy using the model proposed by Popovics (1973).

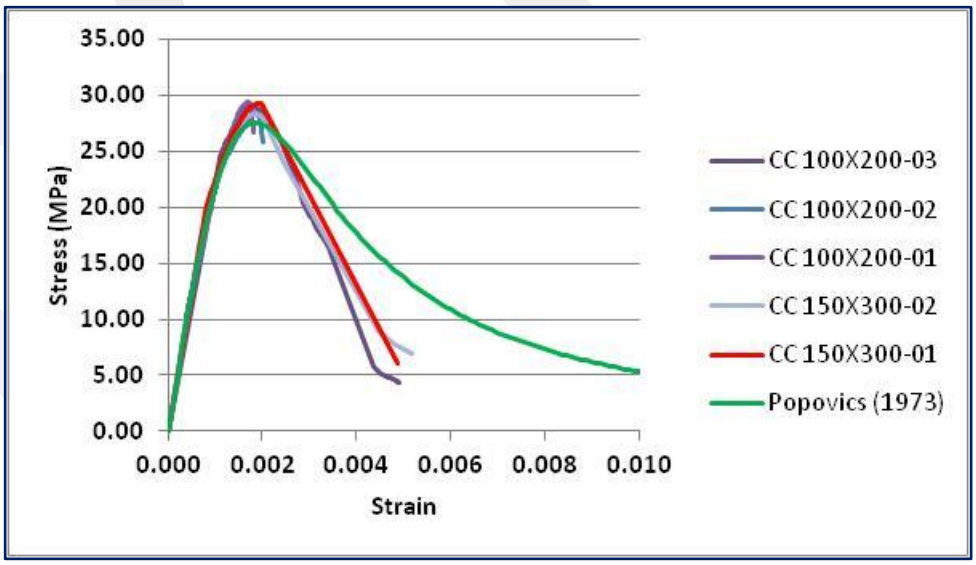

Figure 5-16 – Comparison of stress-strain curves of the tested CC specimens to the model proposed by Popovics (1973)

The name of the specimens are described by numbers to eliminate the crowdedness of the comparison diagrams. The names and corresponding numbering for the specimens are shown in Table 5-1.

Table 5-2 – CC cylinder specimens' descriptions

Name of Specimens	Descriptive Names in Diagrams
CC100×200-01	1
CC100×200-02	2
CC100×200-03	3
CC150×300-01	4
CC150×300-02	5

The stress-strain curves of each CC cylinder specimen is compared to that of the model (Popovics (1973)) in terms of initial stiffness, strain at maximum stress, area under the stress-strain diagram at maximum stress, 90, 80, 70, 60, and 50% of maximum stress on the post-peak branch of stress-strain curves. Initial stiffness for stress-strain curves was obtained by calculating the slope between two points, 50 and 80% of the maximum stress on the ascending branch of the stress-strain curve as shown in Figure 5-5. As an example, the diagram for the area at 70% of maximum stress on the post-peak branch of stress-strain curves is shown in Figure 5-6.

An excel spreadsheet was used to calculate the values used in the comparisons. The results of the comparisons are shown in Figure 5-17 to Figure 5-24.

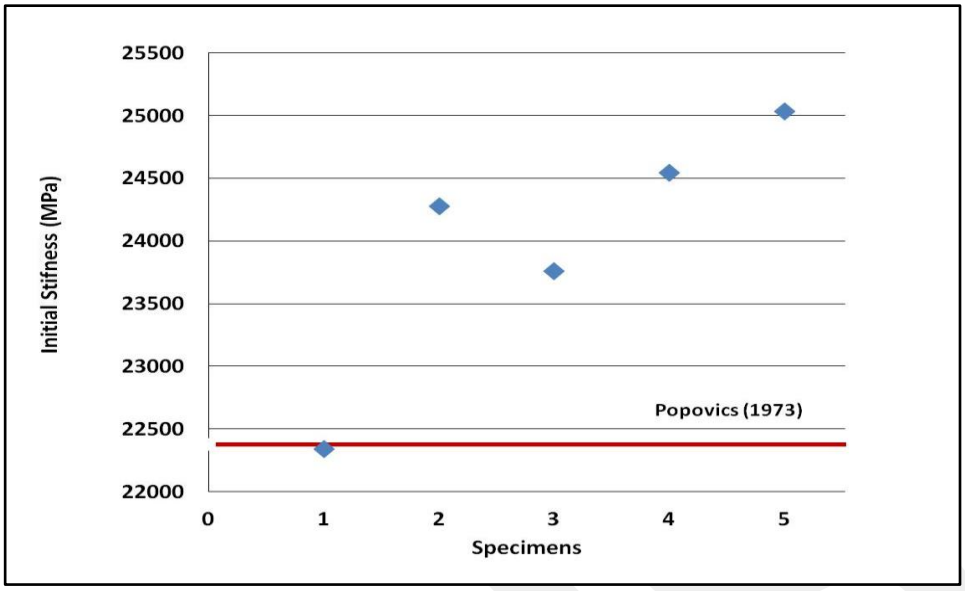

Figure 5-17 – Initial stiffness comparisons of tested CC specimens and used model

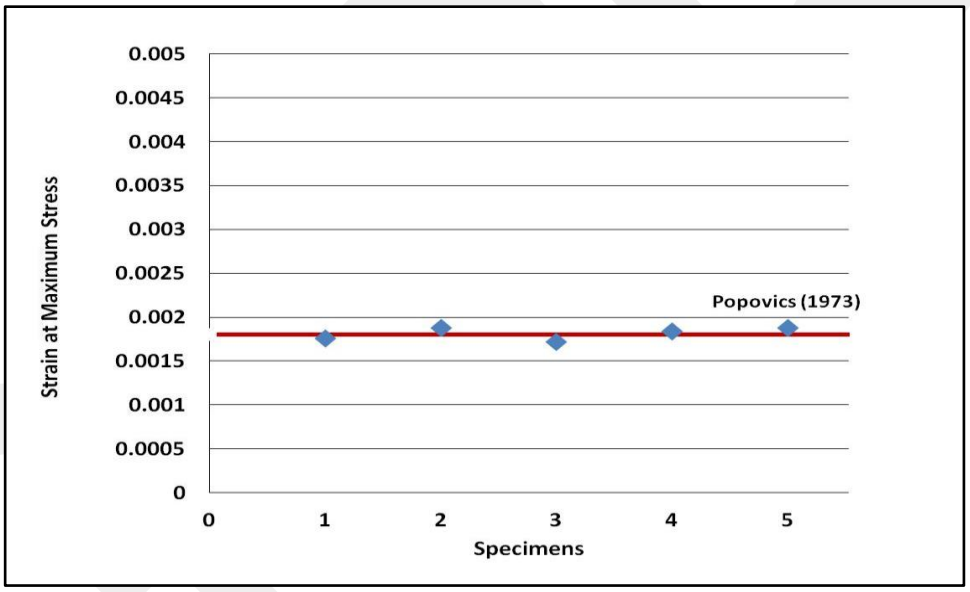

Figure 5-18 – Strain at maximum stress comparisons of tested CC specimens and used model

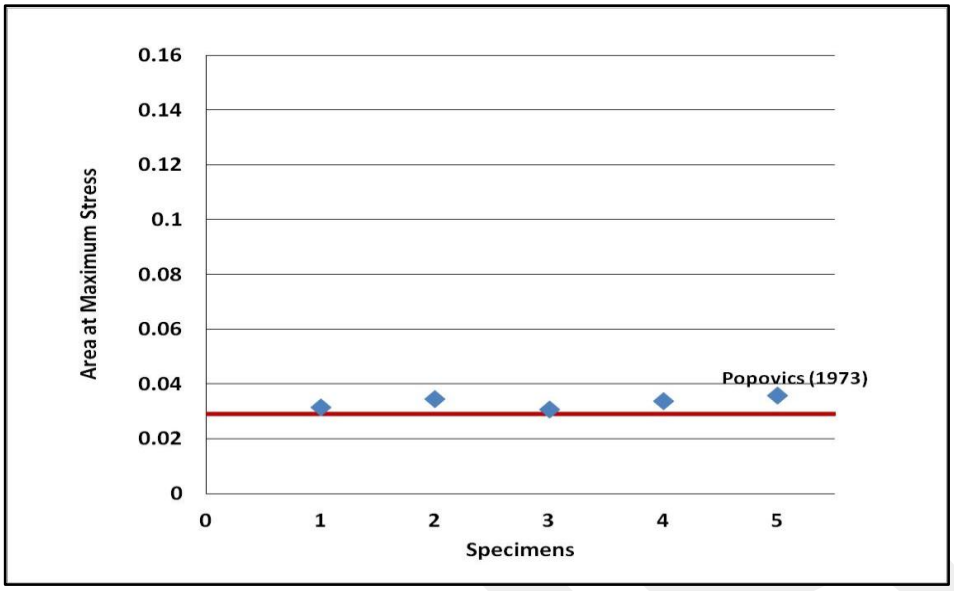

Figure 5-19 – Area under the stress-strain diagram at maximum stress comparisons of tested CC specimens and used model

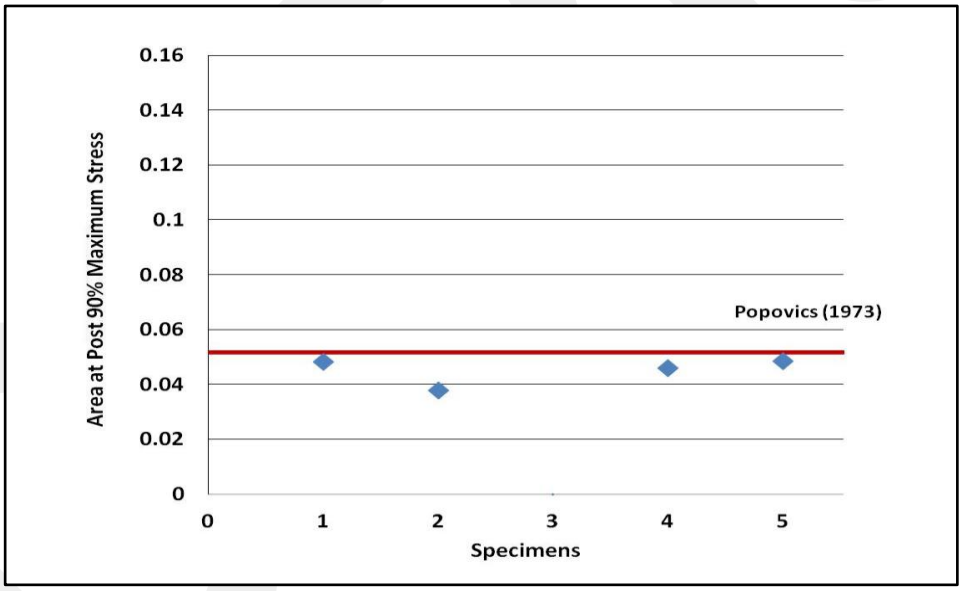

Figure 5-20 – Area under at 90% of maximum stress on descending branch of stress-strain diagram comparisons of tested CC specimens and used model

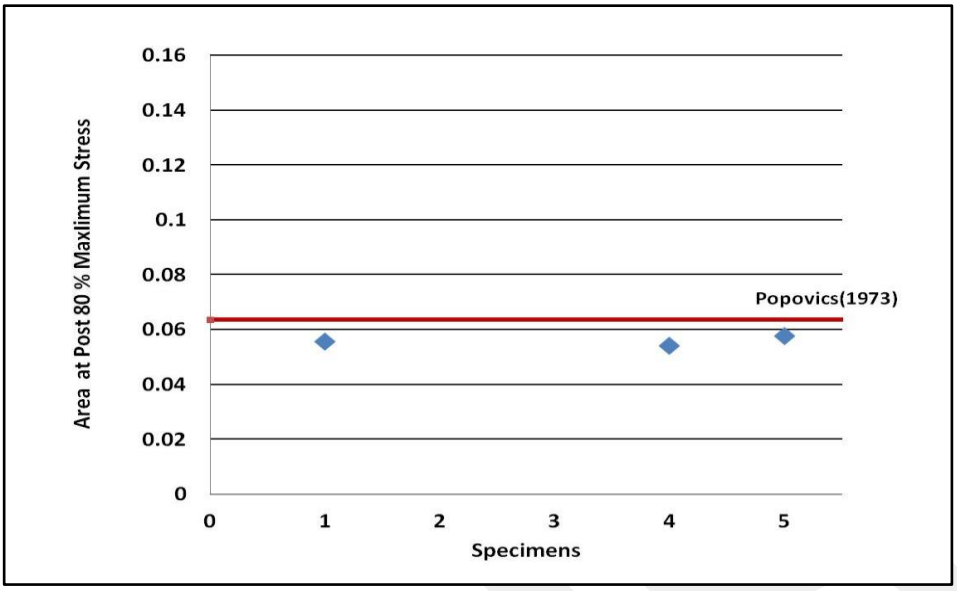

Figure 5-21 – Area under at 80% of maximum stress on descending branch of stress-strain diagram comparisons of tested CC specimens and used model

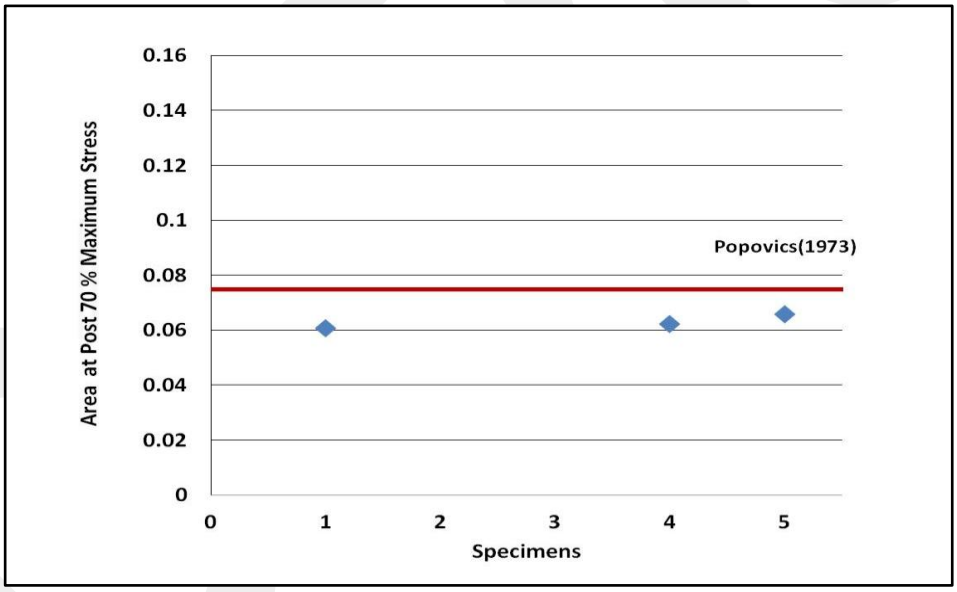

Figure 5-22 – Area under at 70% of maximum stress on descending branch of stress-strain diagram comparisons of tested CC specimens and used model

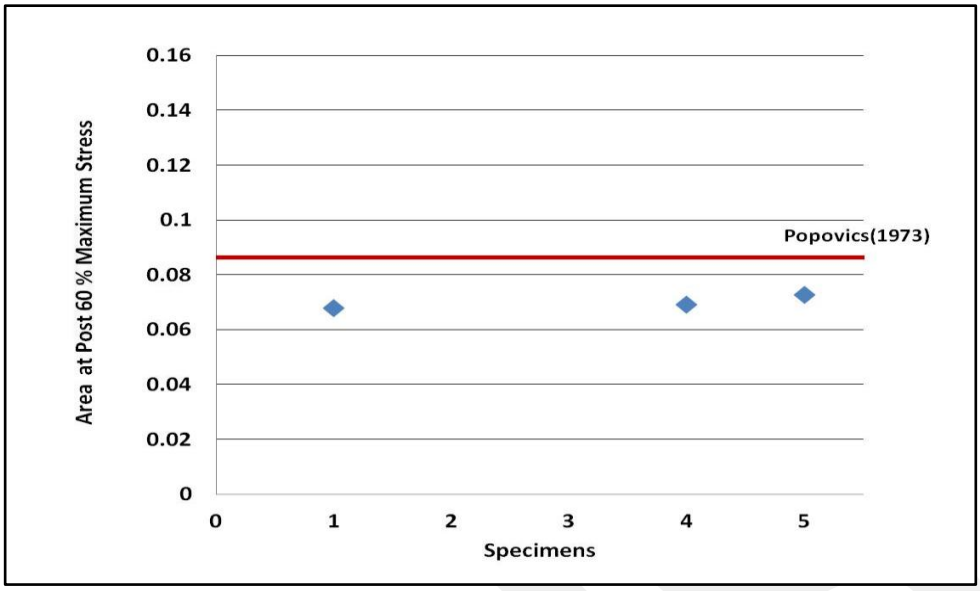

Figure 5-23 – Area under at 60% of maximum stress on descending branch of stress-strain diagram comparisons of tested CC specimens and used model

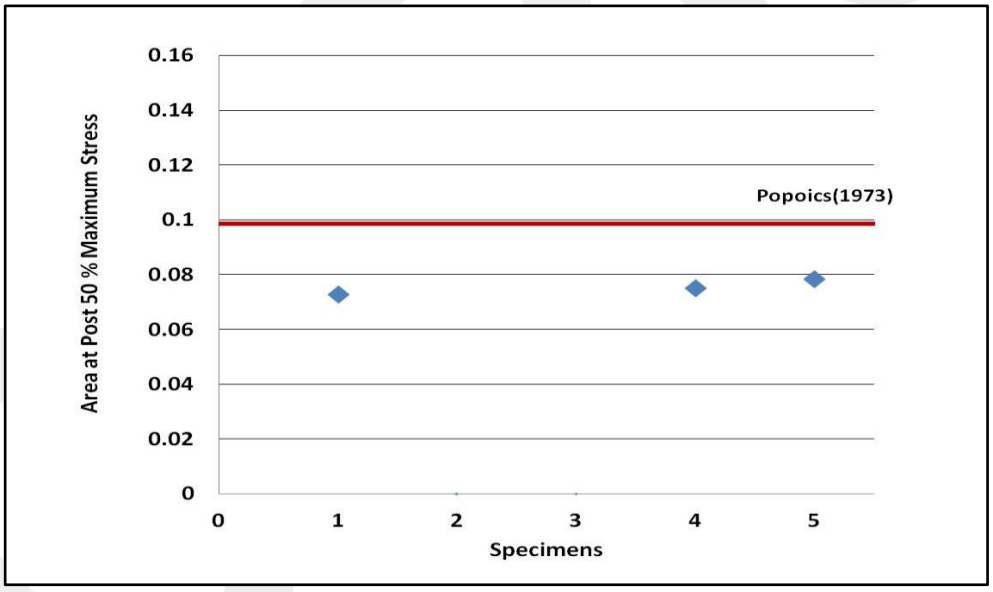

Figure 5-24 – Area under at 50% of maximum stress on descending branch of stress-strain diagram comparisons of tested CC specimens and used model

These figures indicate that the model proposed by Popovics (1973) estimated the test results reasonably well.

5.3 Stress-Strain Relationships in Tension

5.3.1 Test Results

The load-strain curves of the tested specimens in tension obtained in Chapter 4 were used to find the stress-strain relationships of SRFC of the tested specimens. In order to convert the load values recorded in the test to the stress values of solely SFRC, the measured stress-strain relationships of ϕ12 reinforcing bars changed to load-strain diagrams by multiplying the area of the bar with the stress values of the diagram. Using an excel spreadsheet, the load-strain diagram of the reinforcing bar was subtracted from the load-strain curves of the tested specimens. The resulting diagram's load is then divided by the square cross-sectional area of the tension specimen. The stress-strain diagrams of solely SFRC obtained using the above method for tested specimens are shown in Figure 5-25.

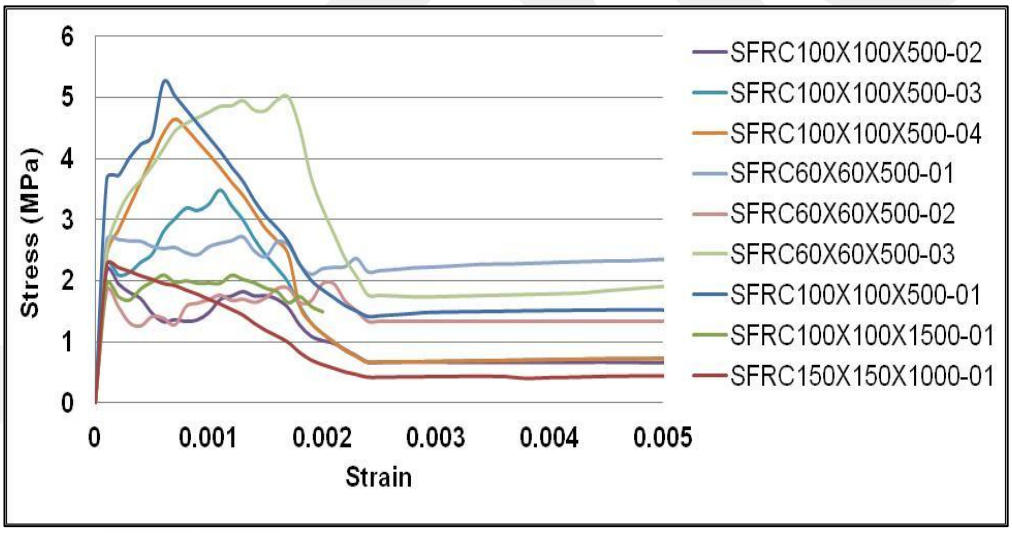

Figure 5-25 – Stress-strain curves of solely SFRC for the tested specimens

The stress-strain behavior can also be presented by bond factor (Sabeena 2013) diagram which may be drawn by dividing the stress values of the curves by stress at initial cracking. The above figure is redrawn in terms of bond factor as shown in Figure 5-26.

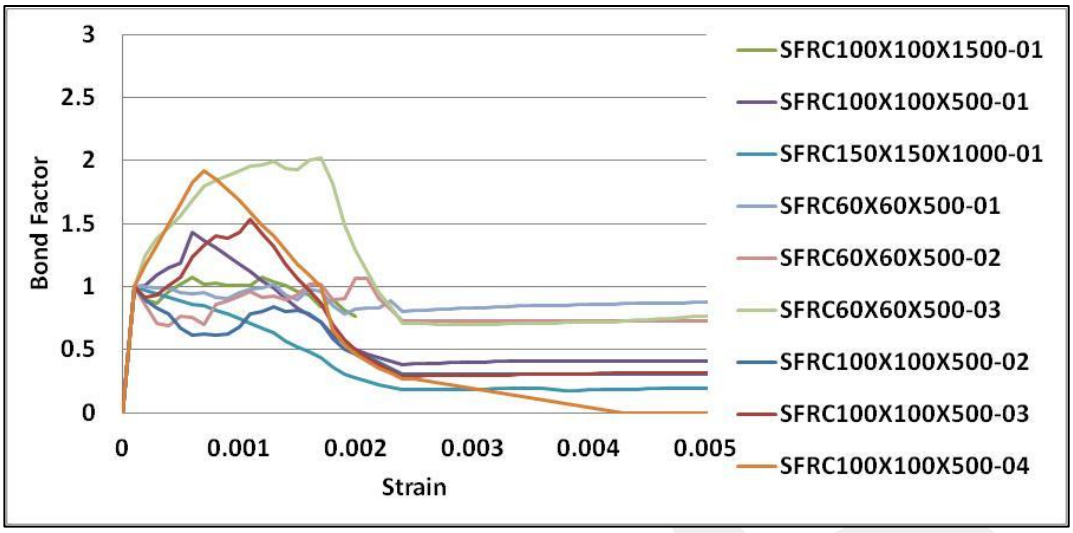

Figure 5-26 – Bond factor-strain curves of solely SFRC for the tested specimens

The stress-strain and bond factor-strain curves for SFRC specimens having the same cross-sections (60×60,100×100, 150×150 mm) are separately shown in Figure 5-27 to Figure 5-32. For all of these figures related to SFRC specimens, after cracking the load carrying capacity increased and later it dropped gradually to a residual tensile strength (post-crack strength) value which was kept constant thereafter. The ratio of the residual tensile strength to the cracking tensile strength was varying between 0.25 and 0.75 for SFRC specimens in tension, higher for specimens having smaller cross-sections and lower for specimens having larger cross-sections.

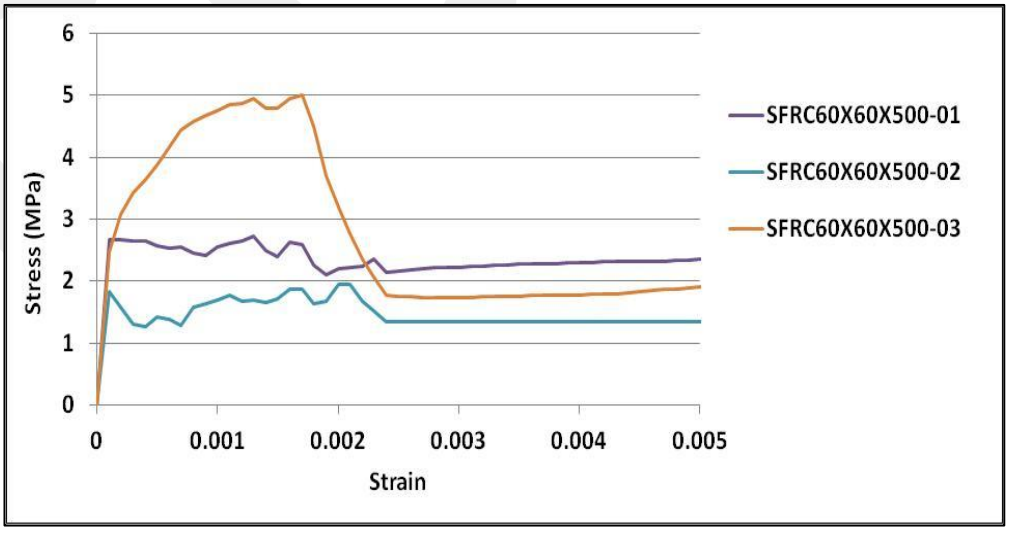

Figure 5-27 – Stress-strain curves of solely SFRC for specimens having 60×60 mm cross-section

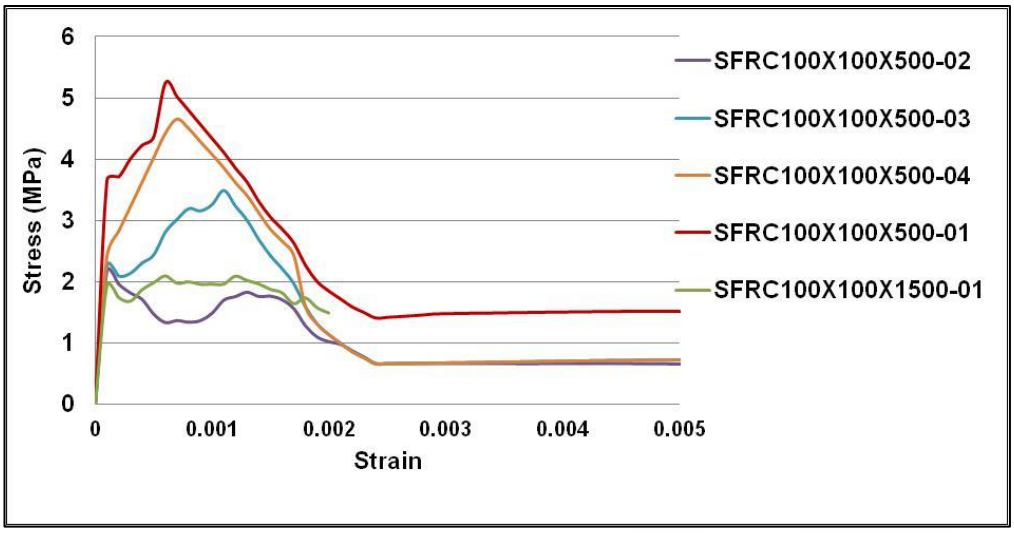

Figure 5-28 – Stress-strain curves of solely SFRC for specimens having 100×100 mm cross-section

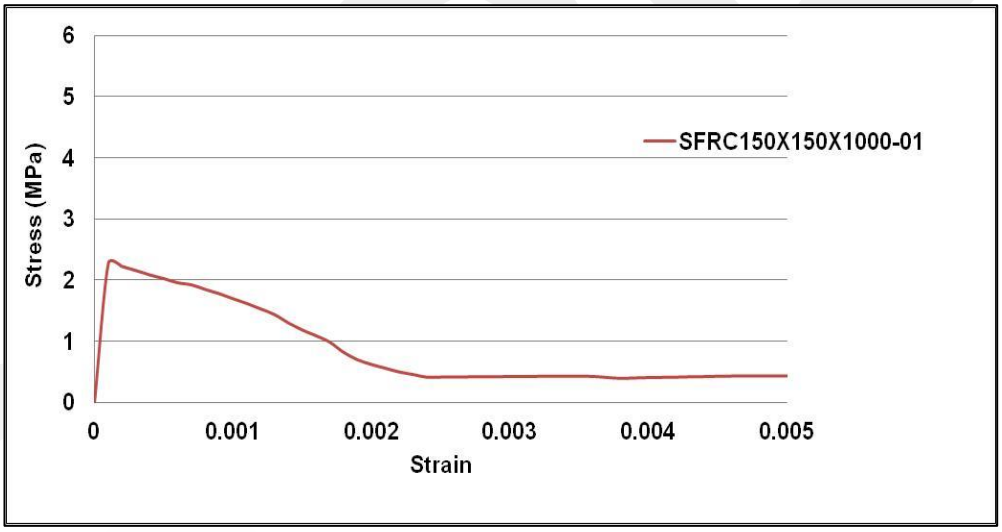

Figure 5-29 – Stress-strain curves of solely SFRC for specimens having 150×150 mm cross-section

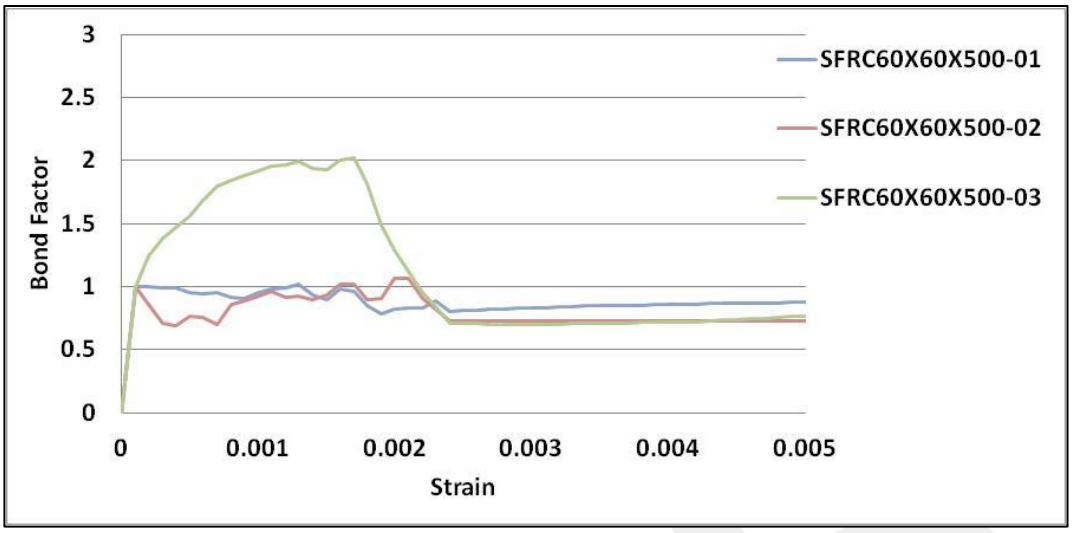

Figure 5-30 – Bond factor-strain curves of solely SFRC for specimens having 60×60 mm cross-section

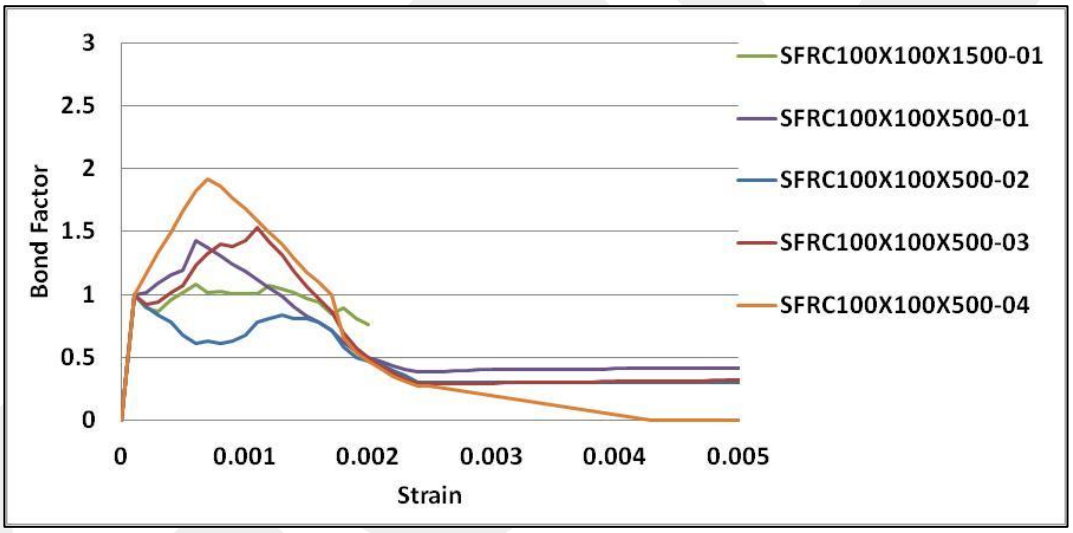

Figure 5-31 – Bond factor-strain curves of solely SFRC for specimens having 100×100 mm cross-section

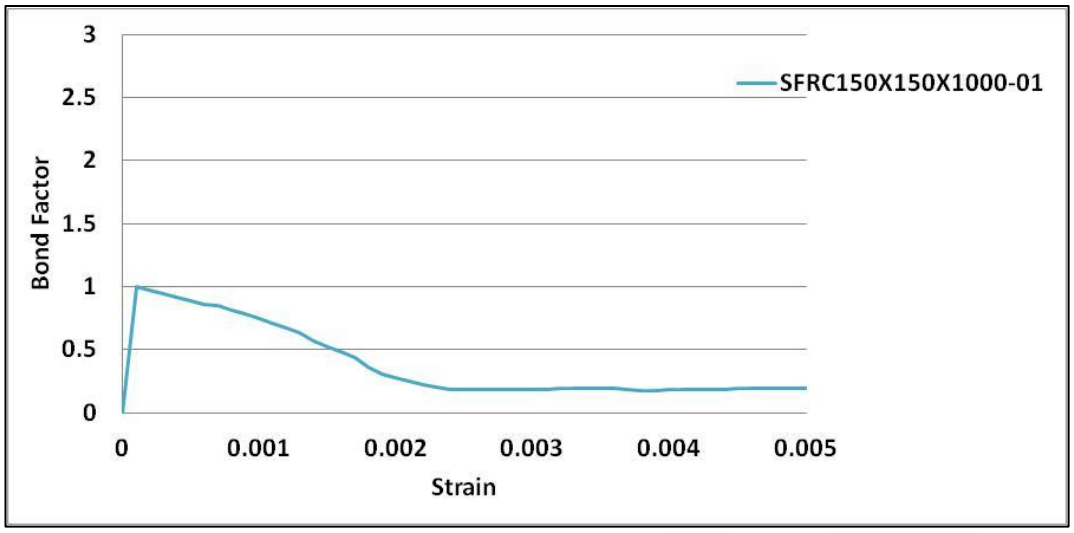

Figure 5-32 – Bond factor-strain curves of solely SFRC for specimens having 150×150 mm cross-section

The load-strain curves of the tested specimens in tension obtained in Chapter 4 were used to find the stress-strain relationships of CC of the tested specimens. In order to convert the load values recorded in the test to the stress values of solely CC, the measured stress-strain relationships of ϕ12 reinforcing bars changed to load-strain diagrams by multiplying the area of the bar with the stress values of the diagram. Using an excel spreadsheet, the load-strain diagram of the reinforcing bar was subtracted from the load-strain curves of the tested specimens. The resulting diagram's load is then divided by the square cross-sectional area of the tension specimen. The stress-strain diagrams of solely SFRC obtained using the above method for tested specimens are shown in Figure 5-33.

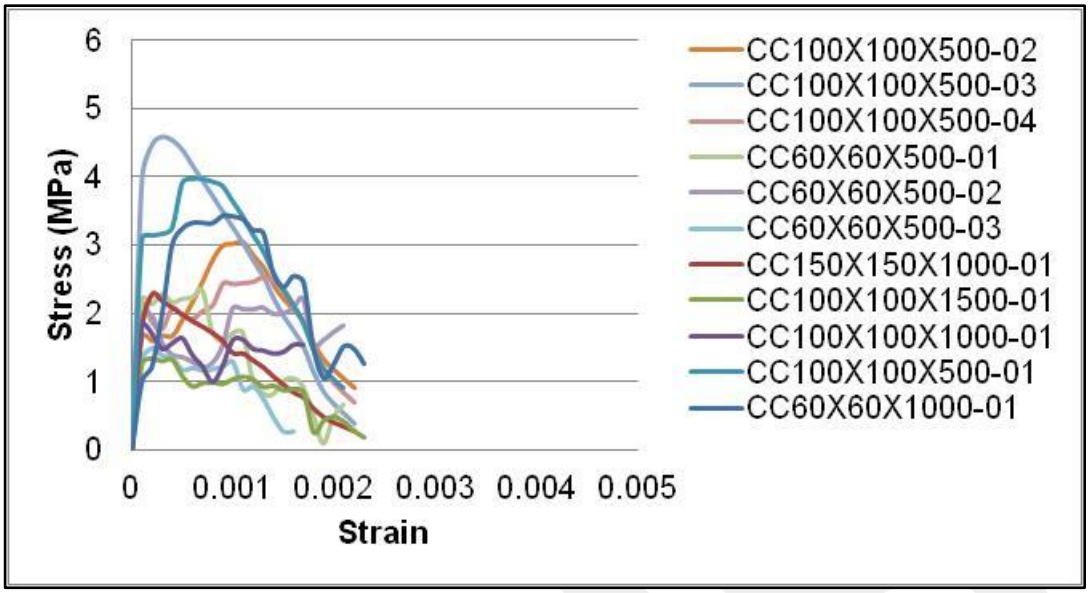

Figure 5-33 – Stress-strain curves of solely CC for the tested specimens

The stress-strain behavior can also be presented by bond factor diagram which may be drawn by dividing the stress values of the curves by stress at initial cracking. The above figure is redrawn in terms of bond factor as shown in Figure 5-34.

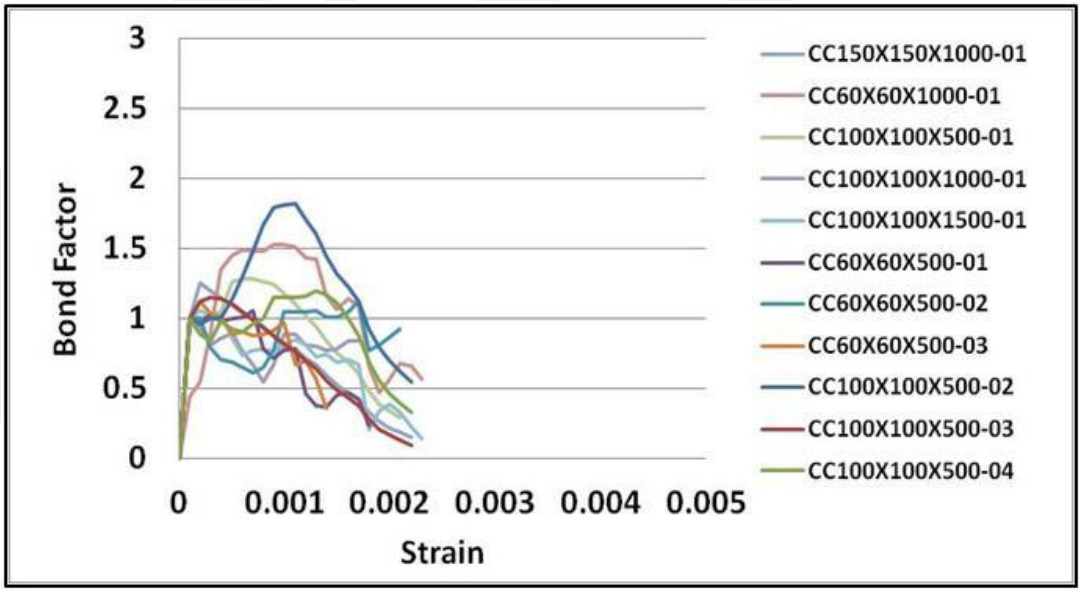

Figure 5-34 – Bond factor-strain curves of solely CC for the tested specimens

The stress-strain and bond factor-strain curves for CC specimens having the same cross-sections (60×60,100×100, 150×150 mm) are separately shown in Figure 5-35

to Figure 5-40. For all of these figures related to CC specimens, after cracking the load carrying capacity dropped gradually to zero, no load is carried by CC thereafter.

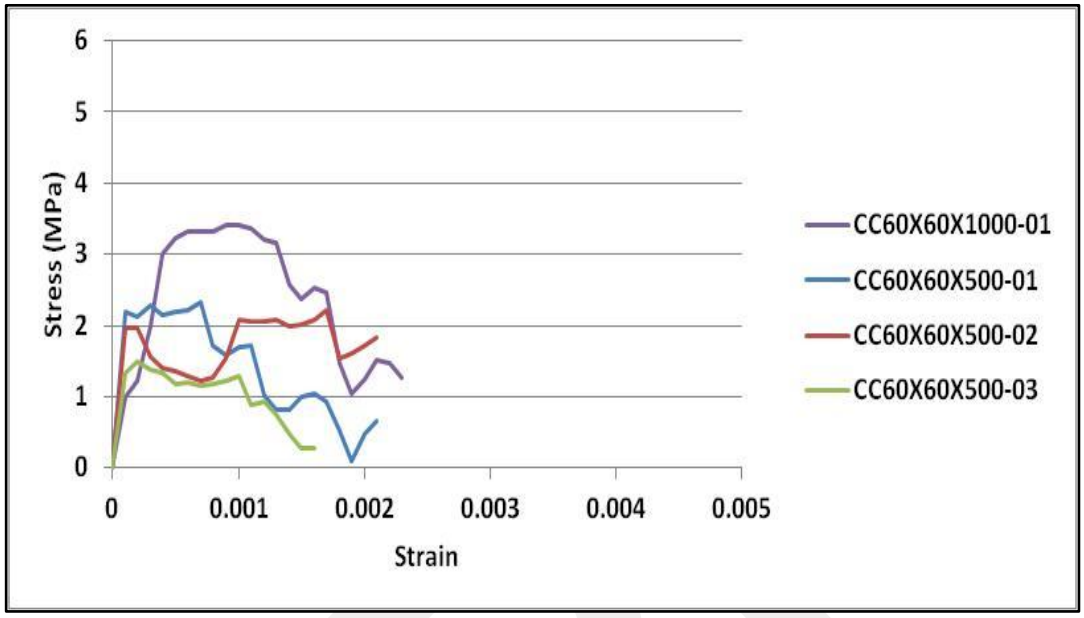

Figure 5-35 – Stress-strain curves of solely CC for specimens having 60×60 mm cross-section

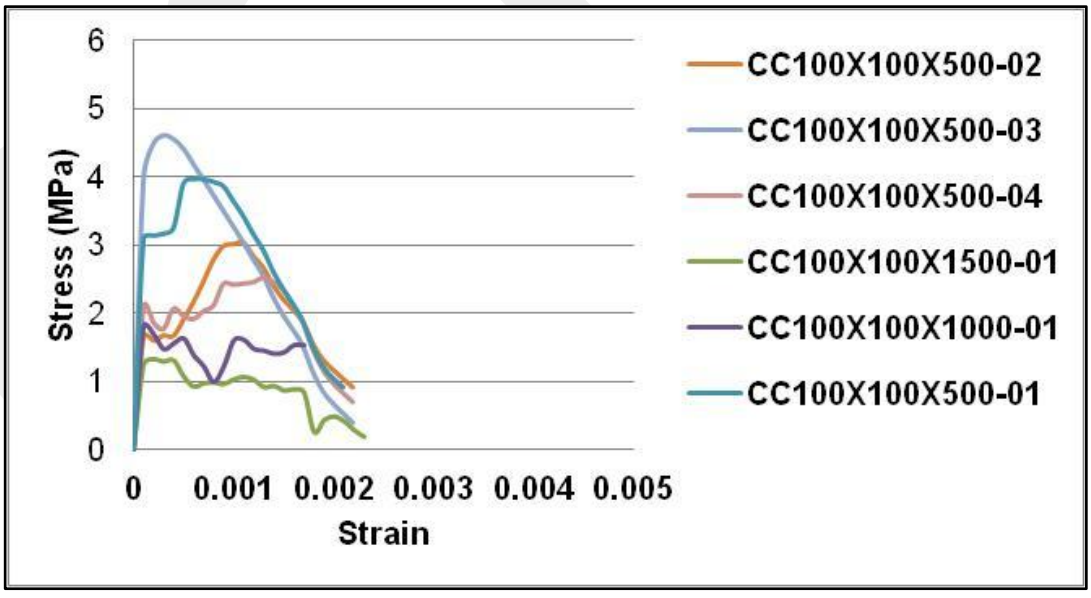

Figure 5-36 – Stress-strain curves of solely CC for specimens having 100×100 mm cross-section

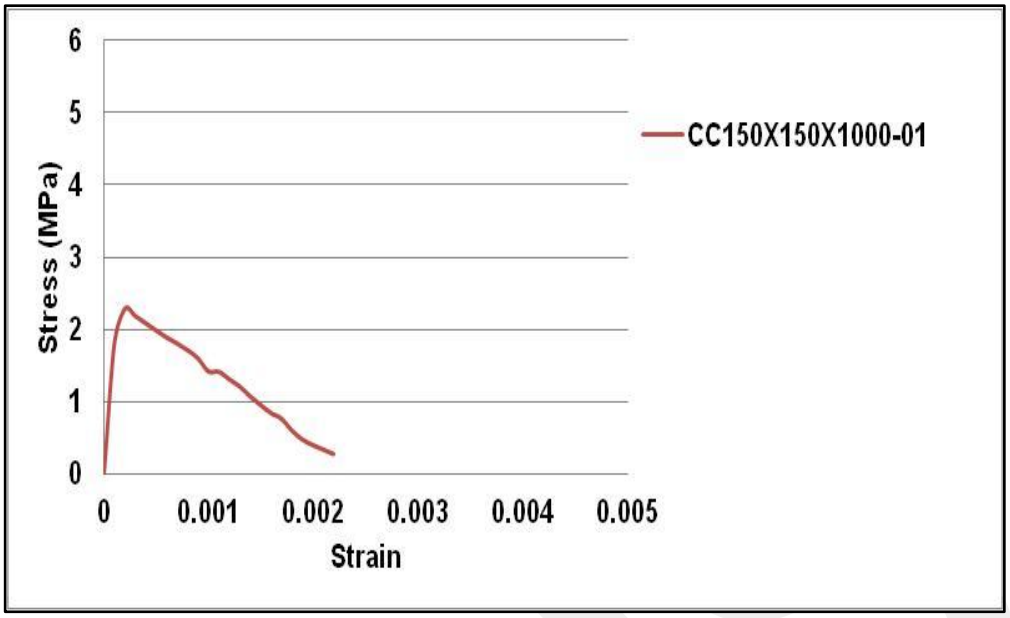

Figure 5-37 – Stress-strain curves of solely CC for specimens having 150×150 mm cross-section

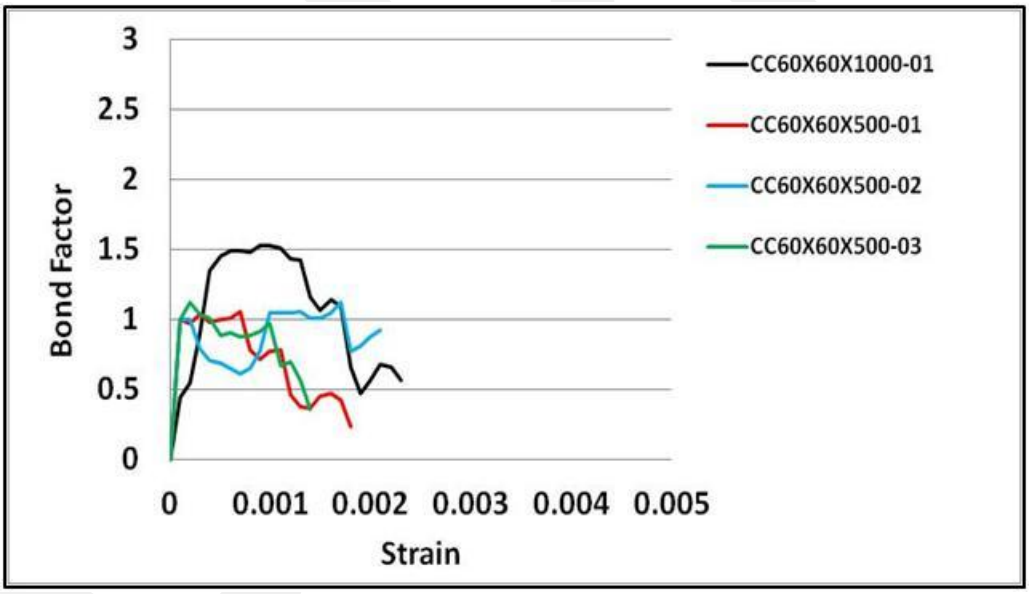

Figure 5-38 – Bond factor-strain curves of solely CC for specimens having 60×60 mm cross-section

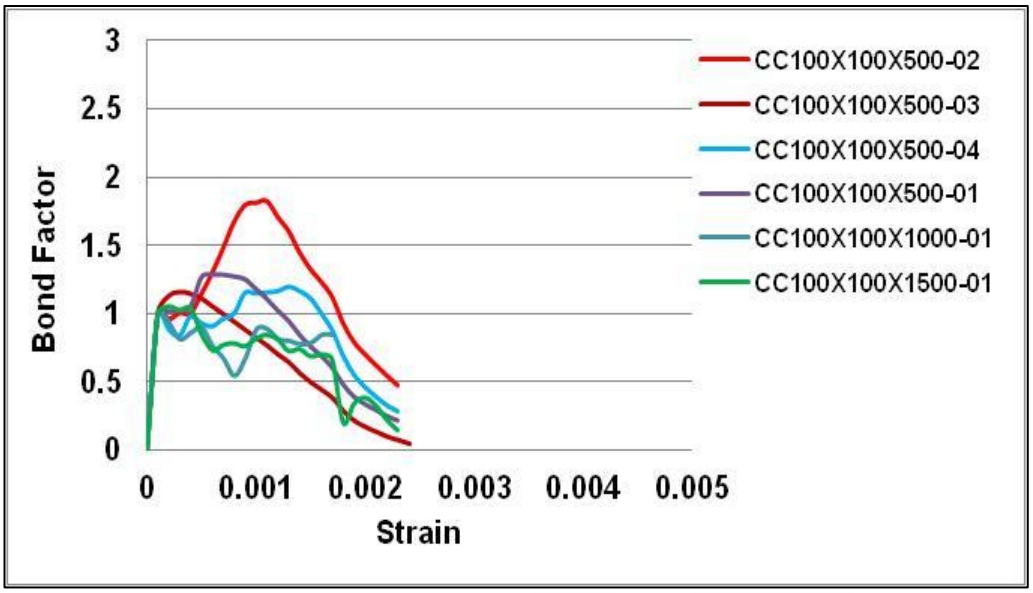

Figure 5-39 – Bond factor-strain curves of solely CC for specimens having 100×100 mm cross-section

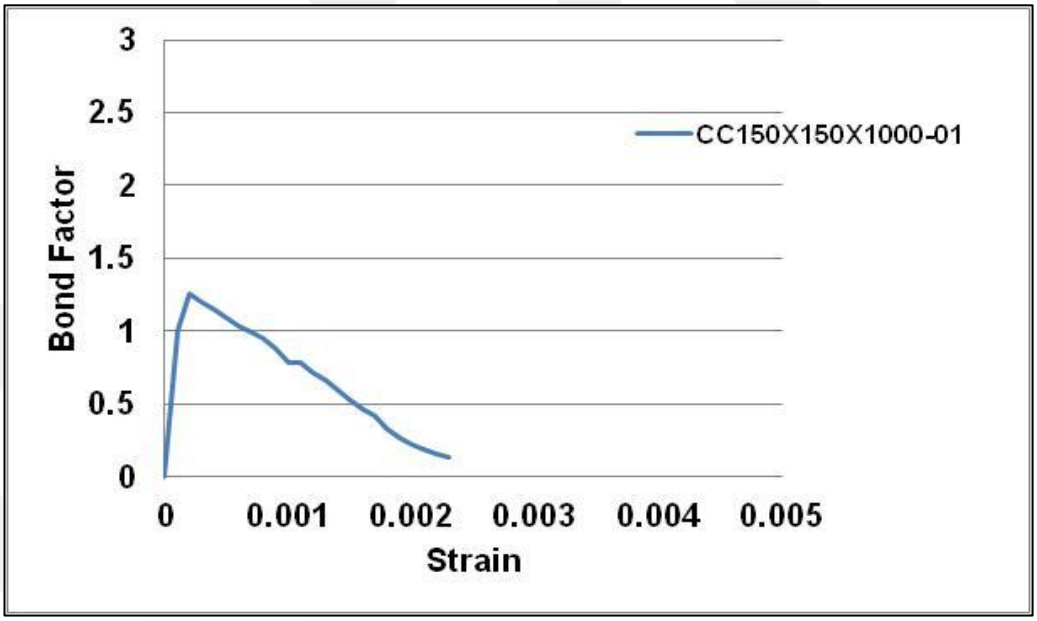

Figure 5-40 – Bond factor-strain curves of solely SFRC for specimens having 150×150 mm cross-section

5.3.2 SFRC Models and Comparisons

The SFRC model in tension developed by Soranakom and Mobasher (2009) (Figure 2-6) was used in comparisons of the test results. In this model, two important parameters, μ (residual tensile stress as a fraction of the cracking tensile strength)

and ε_{tu} (ultimate tension strain), define the characteristics of the tension behavior. In this research, a parametric study was carried out to determine the values of μ and ε_{tu}. Two values, 0.5 and 0.75, were considered for the μ parameter and three values, 0.005, 0.01, and 0.015, were considered for the ε_{tu} parameter. Moreover, based on test results, the model proposed by Soranakom and Mobasher (2009) is modified to have the stress at ultimate tension strain to be equal to half of the residual tensile stress. The modified models for 3.25 MPa tensile strength that were used in the comparisons are shown in Figure 5-41 and Figure 5-42.

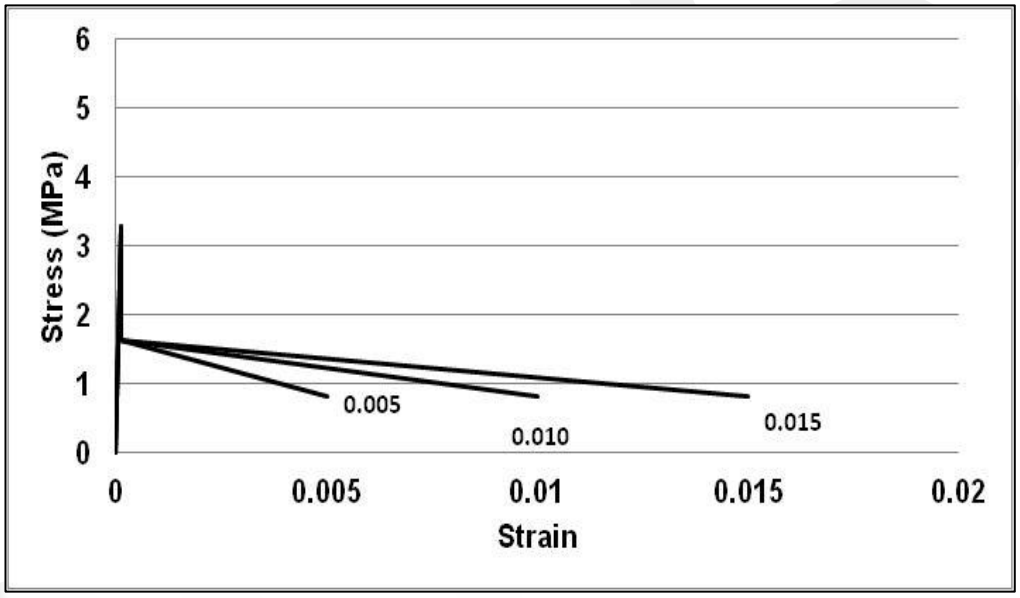

Figure 5-41 – Modified Soranakom and Mobasher (2009) model for μ=0.50 and ε_{tu}=0.005, 0.010, and 0.015

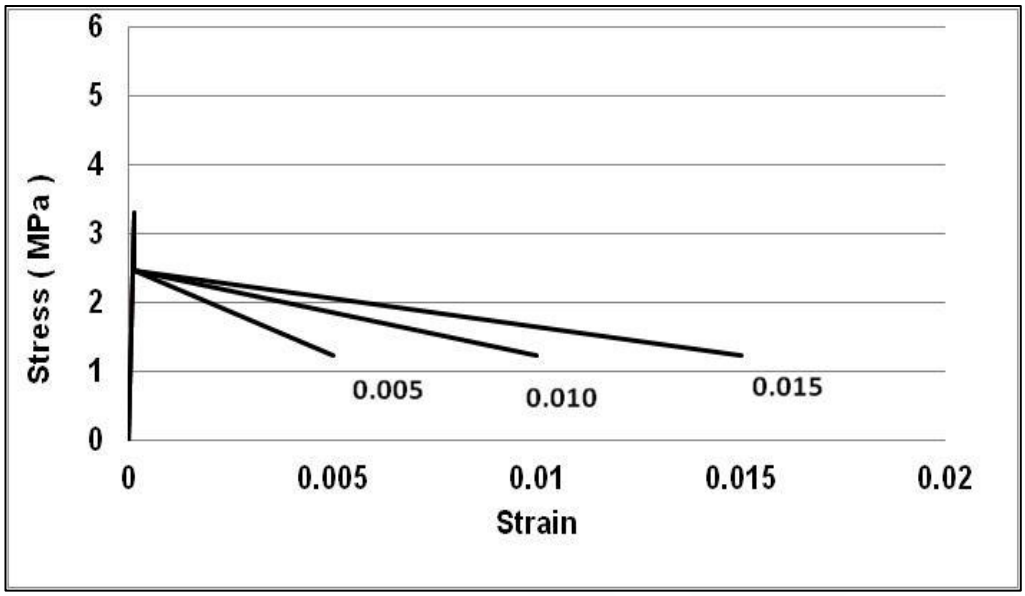

Figure 5-42 – Modified Soranakom and Mobasher (2009) model for μ=0.75 and ε_{tu}=0.005, 0.010, and 0.015

The comparisons of these models to the test results are shown in Figure 5-43 to Figure 5-48.

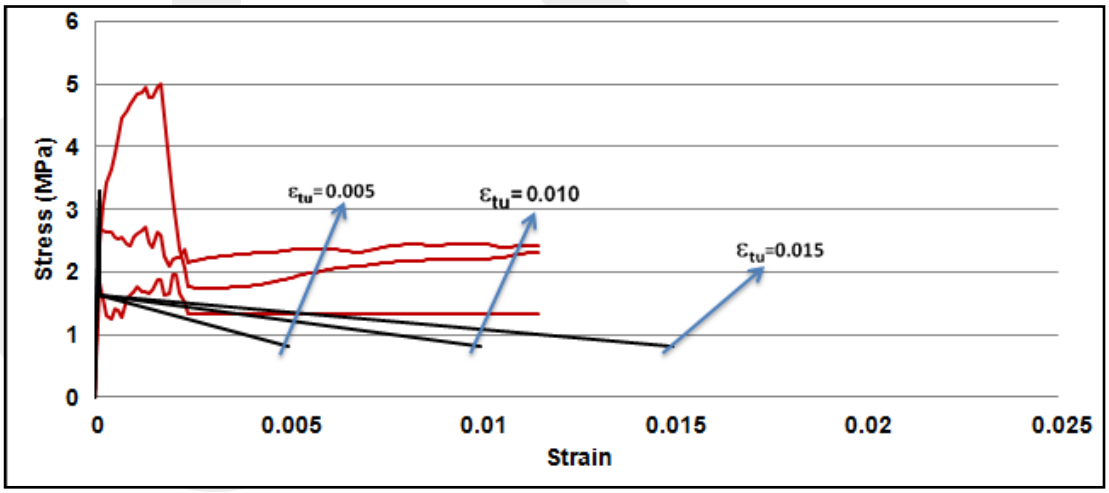

Figure 5-43 – Comparisons of stress-strain curves of tested SFRC specimens having 60×60 mm cross-section to Modified Soranakom and Mobasher (2009) model for μ=0.50 and ε_{tu}=0.005, 0.010, and 0.015

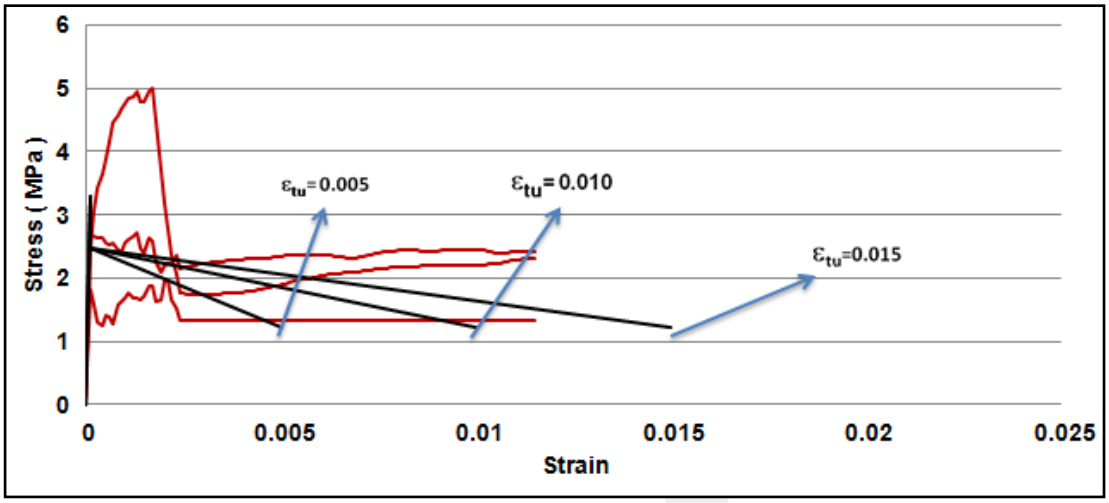

Figure 5-44 – Comparisons of stress-strain curves of tested SFRC specimens having 60×60 mm cross-section to Modified Soranakom and Mobasher (2009) model for μ=0.75 and ε_{tu}=0.005, 0.010, and 0.015

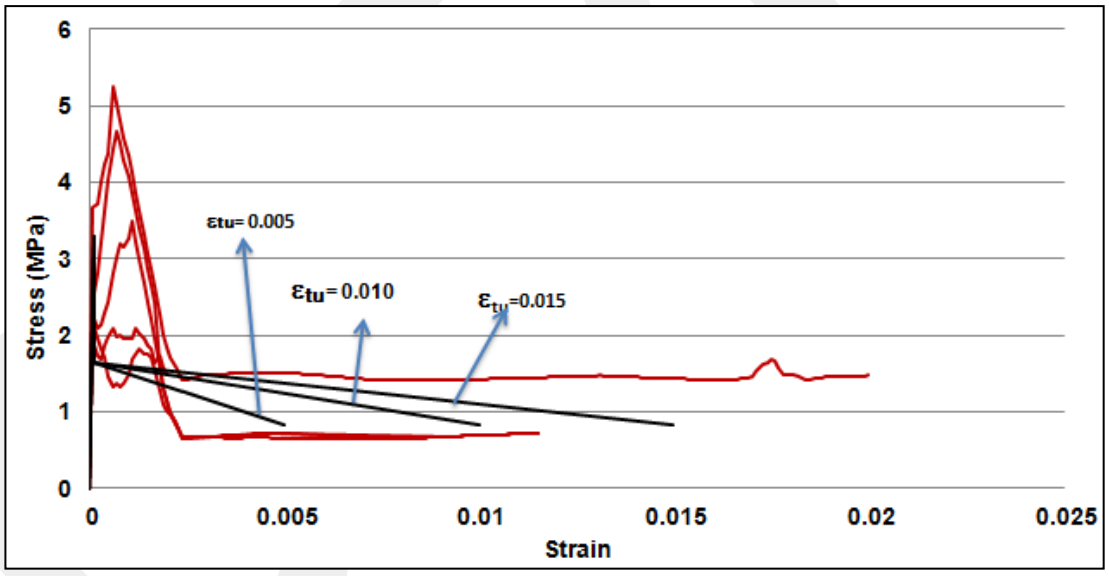

Figure 5-45 – Comparisons of stress-strain curves of tested SFRC specimens having 100×100 mm cross-section to Modified Soranakom and Mobasher (2009) model for μ=0.50 and ε_{tu}=0.005, 0.010, and 0.015

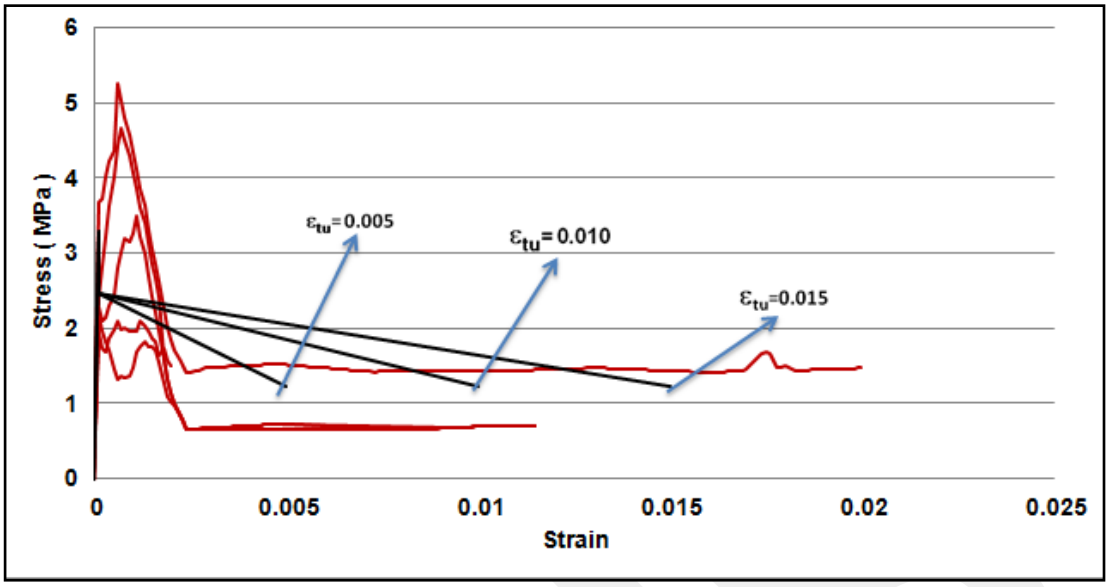

Figure 5-46 – Comparisons of stress-strain curves of tested SFRC specimens having 100×100 mm cross-section to Modified Soranakom and Mobasher (2009) model for μ=0.75 and ε_{tu}=0.005, 0.010, and 0.015

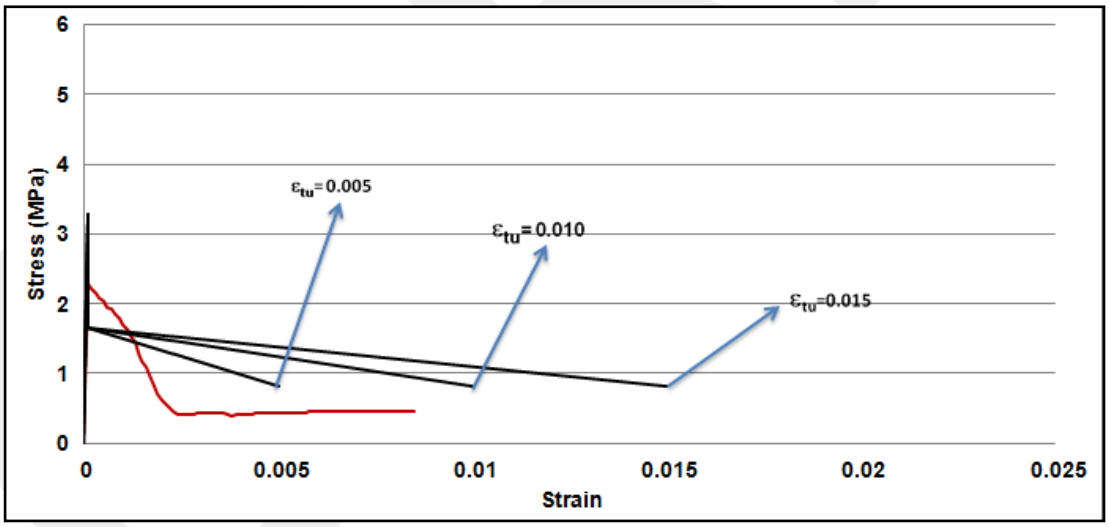

Figure 5-47 – Comparisons of stress-strain curves of tested SFRC specimens having 150×150 mm cross-section to Modified Soranakom and Mobasher (2009) model for μ=0.50 and ε_{tu}=0.005, 0.010, and 0.015

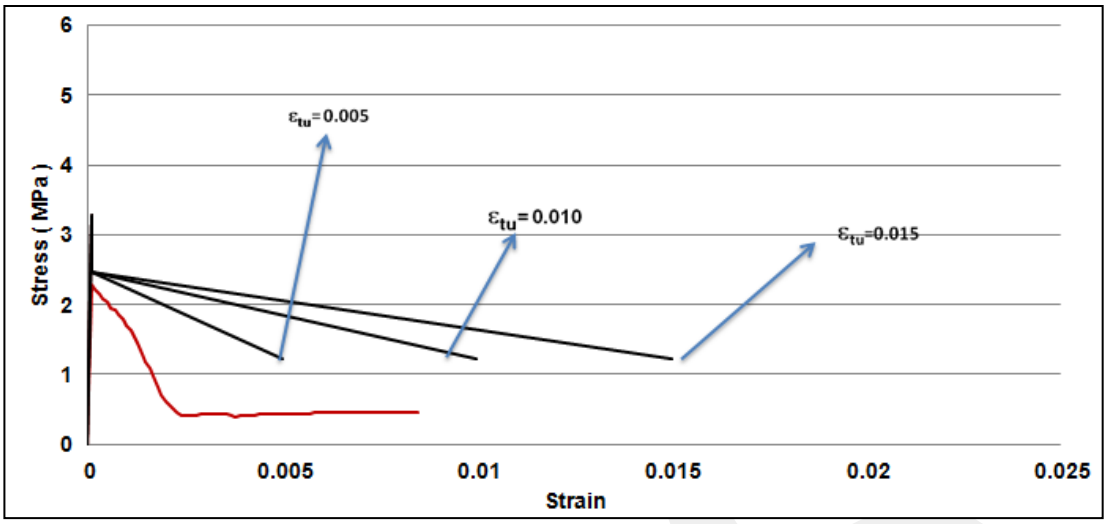

Figure 5-48 – Comparisons of stress-strain curves of tested SFRC specimens having 150×150 mm cross-section to Modified Soranakom and Mobasher (2009) model for μ=0.75 and ε_{tu}=0.005, 0.010, and 0.015

5.4 Estimation of Load-Deflection Curves and Comparisons

The flexural behavior of the tested SFRC specimens were estimated using the SFRC compression model proposed by Wang (2006) and modified SFRC tension model proposed by Soranakom and Mobasher (2009) for various μ (0.50 and 0.75) and ε_{tu} (0.005, 0.010, and 0.015) values. For this purpose, a program was developed using excel spreadsheet. The predicted load-deflection curves using the above models are shown in Figure 5-49 and Figure 5-50.

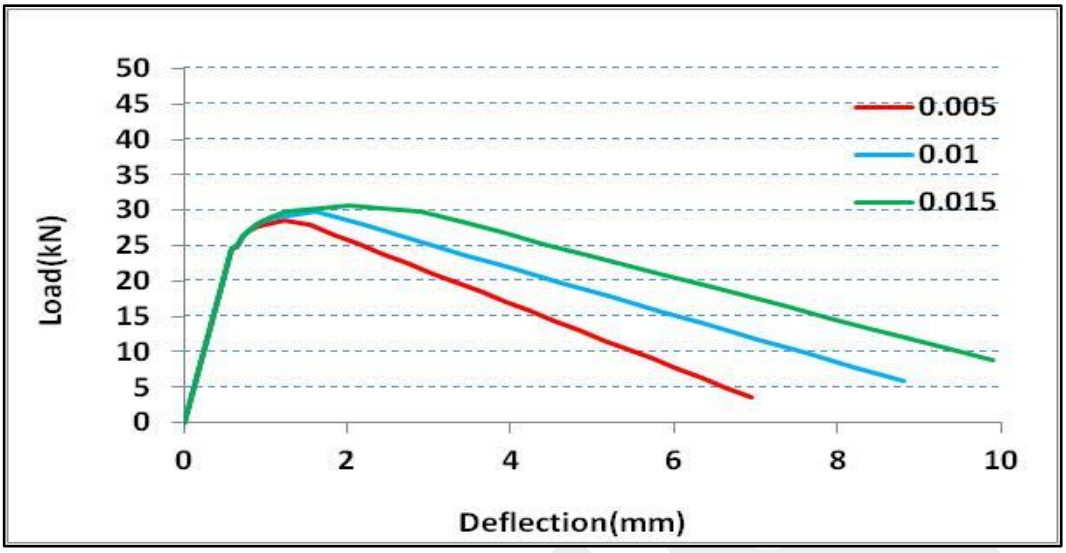

Figure 5-49 – Estimated curves using selected models for μ=0.50 and ε_{tu}=0.005, 0.010, and 0.015

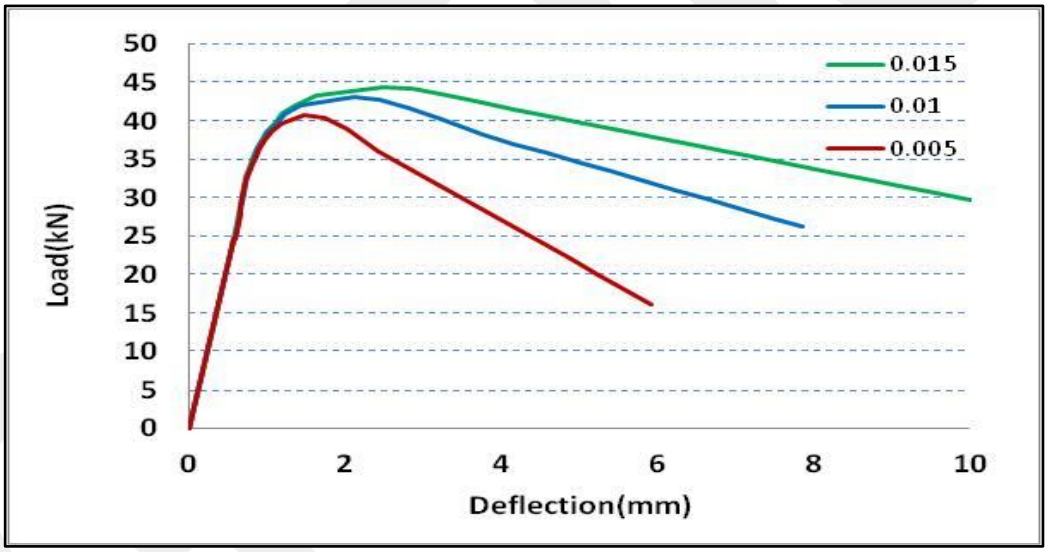

Figure 5-50 – Estimated curves using selected models for μ=0.75 and ε_{tu}=0.005, 0.010, and 0.015

These estimated curves were compared to the load-deflection behaviors of flexural SFRC specimens (3 specimens for first batch and 3 specimens for fourth batch) shown in Figure 4-11 and Figure 4-12. The comparisons were performed for initial stiffness, ultimate load, area under the load-deflection diagram at ultimate load and 70% of ultimate load on the post-peak branch of load-deflection curves. The

comparison values were calculated for each specimen based on the percent difference of estimated and test value divided by the test value as shown the equation below:

$$Percent\ Difference = abs\left(\frac{Value_{test} - Value_{estimated}}{Value_{test}}\right) * 100\% \qquad \text{Equation 5-1}$$

The names of the specimens are described by numbers to eliminate the crowdedness of the comparison diagrams. The names and corresponding numbering for the specimens are shown in Table 5-3.

Table 5-3 – SFRC flexural specimens' descriptions

Name of Specimens	Descriptive Names in Diagrams
SFRC150×150×600-01	1
SFRC150×150×600-02	2
SFRC150×150×600-03	3
SFRC150×150×600-04	4
SFRC150×150×600-05	5
SFRC150×150×600-06	6

Comparisons related to the initial stiffness of μ=0.50 and 0.75 are shown in Figure 5-51, and Figure 5-52, Table 5-4, and Table 5-5. These tables and figures indicate that the initial stiffness of the specimens were not affected by the tensile behavior of SFRC.

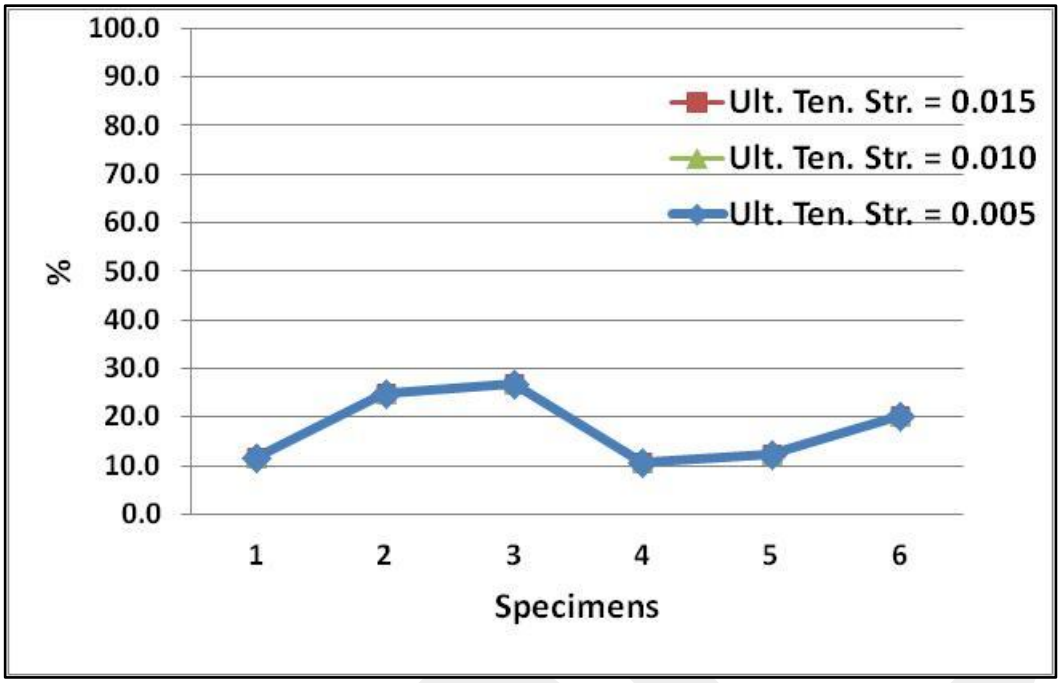

Figure 5-51 – Comparisons of initial stiffness of SFRC flexural specimens and predictions for μ=0.50

Table 5-4 – Comparisons of initial stiffness of SFRC flexural specimens and predictions for μ=0.50

ε_{tu}	1 (%)	2 (%)	3 (%)	4 (%)	5 (%)	6 (%)
0.005	11.78	24.82	26.88	10.67	12.38	20.25
0.01	11.78	24.82	26.88	10.67	12.38	20.25
0.015	11.78	24.82	26.88	10.67	12.38	20.25

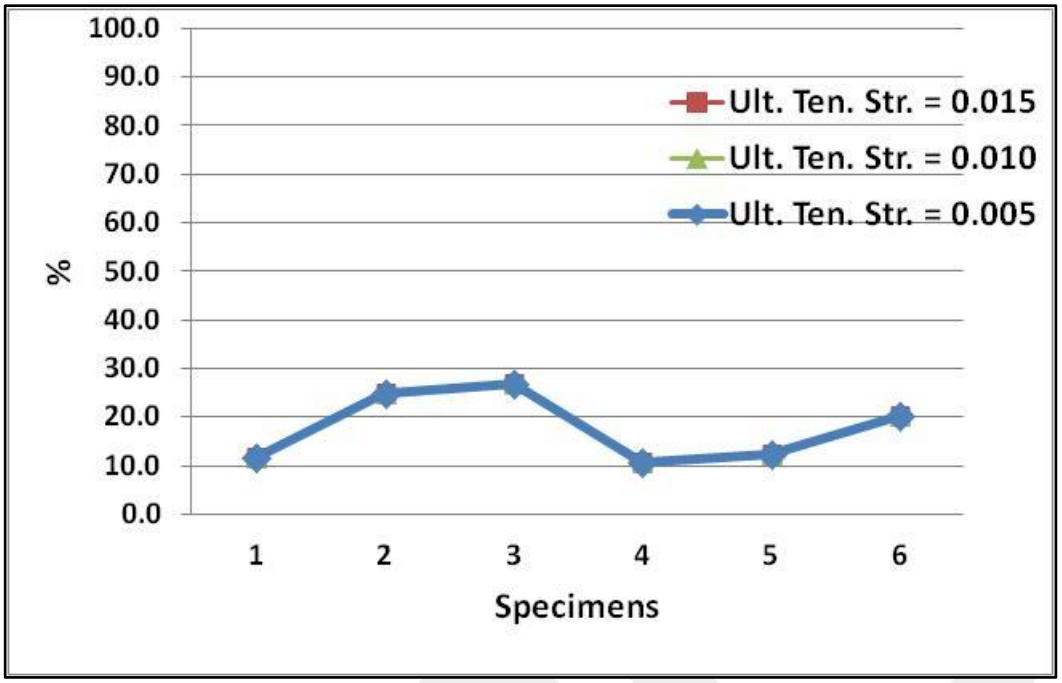

Figure 5-52 – Comparisons of initial stiffness of SFRC flexural specimens and predictions for μ=0.75

Table 5-5 – Comparisons of initial stiffness of SFRC flexural specimens and predictions for μ=0.75

ε_{tu}	1 (%)	2 (%)	3 (%)	4 (%)	5 (%)	6 (%)
0.005	11.78	24.819	26.878	10.669	12.378	20.253
0.01	11.78	24.819	26.878	10.669	12.378	20.253
0.015	11.78	24.819	26.878	10.669	12.378	20.253

Comparisons related to the ultimate load of μ=0.50 and 0.75 are shown in Figure 5-53, Figure 5-54, Table 5-6, and Table 5-7. These tables and figures indicate that the ultimate load of SFRC with μ=0.50 and ε_{tu}=0.015 results better estimations compared to other estimates. The estimates with μ=0.75 and ε_{tu}=0.005 were predicting the Specimens 1, 2 and 4 best whereas the estimates with μ=0.75 and ε_{tu}=0.010 were predicting the Specimen 3, and estimates with μ=0.75 and ε_{tu}=0.015 were predicting the Specimen 5 and 6 best.

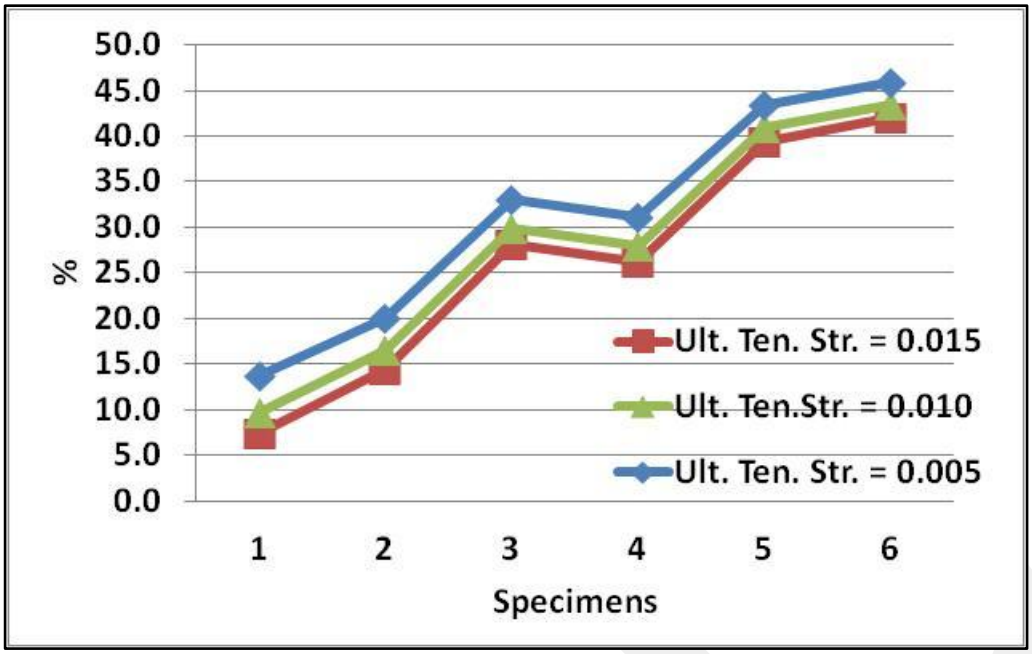

Figure 5-53 – Comparisons of ultimate load of SFRC flexural specimens and predictions for μ=0.50

Table 5-6 – Comparisons of ultimate load of SFRC flexural specimens and predictions for μ=0.50

ε_{tu}	1 (%)	2 (%)	3 (%)	4 (%)	5 (%)	6 (%)
0.005	13.7	20.1	33.1	31.2	43.5	45.9
0.01	9.7	16.5	30.0	28.0	40.9	43.5
0.015	7.4	14.4	28.2	26.2	39.4	42.0

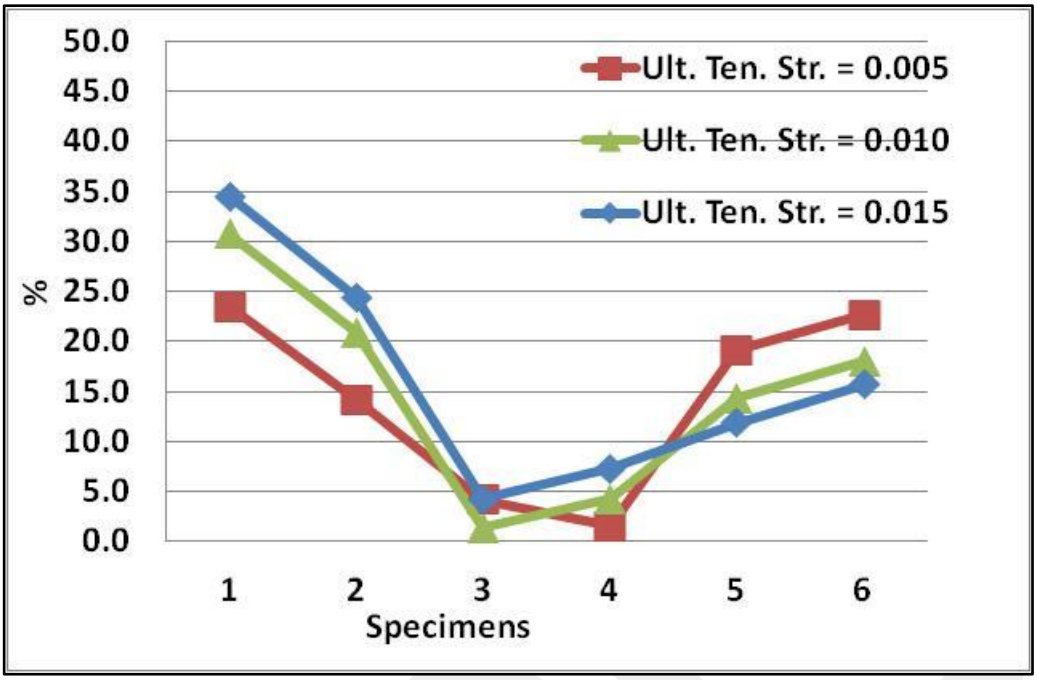

Figure 5-54 – Comparisons of ultimate load of SFRC flexural specimens and predictions for μ=0.75

Table 5-7 – Comparisons of ultimate load of SFRC flexural specimens and predictions for μ=0.75

ε_{tu}	1 (%)	2 (%)	3 (%)	4 (%)	5 (%)	6 (%)
0.005	23.5	14.3	4.2	1.5	19.1	22.7
0.01	30.8	21.0	1.4	4.2	14.4	18.1
0.015	34.6	24.5	4.3	7.3	11.9	15.7

Comparisons related to the area at ultimate load of μ=0.50 and 0.75 are shown in Figure 5-55, Figure 5-56, Table 5-8, and Table 5-9. These tables and figures indicate that the estimates with μ=0.50 and ε_{tu}=0.010 were predicting the Specimens 1 and 2 best whereas the estimates with μ=0.50 and ε_{tu}=0.005 and 0.015 were better predicting the Specimens 3, 4, 5, and 6. The first three (μ=0.75) ones which had ultimate tension strain = 0.005, and last three ones which had ultimate tension strain = 0.015 were the best among the others.

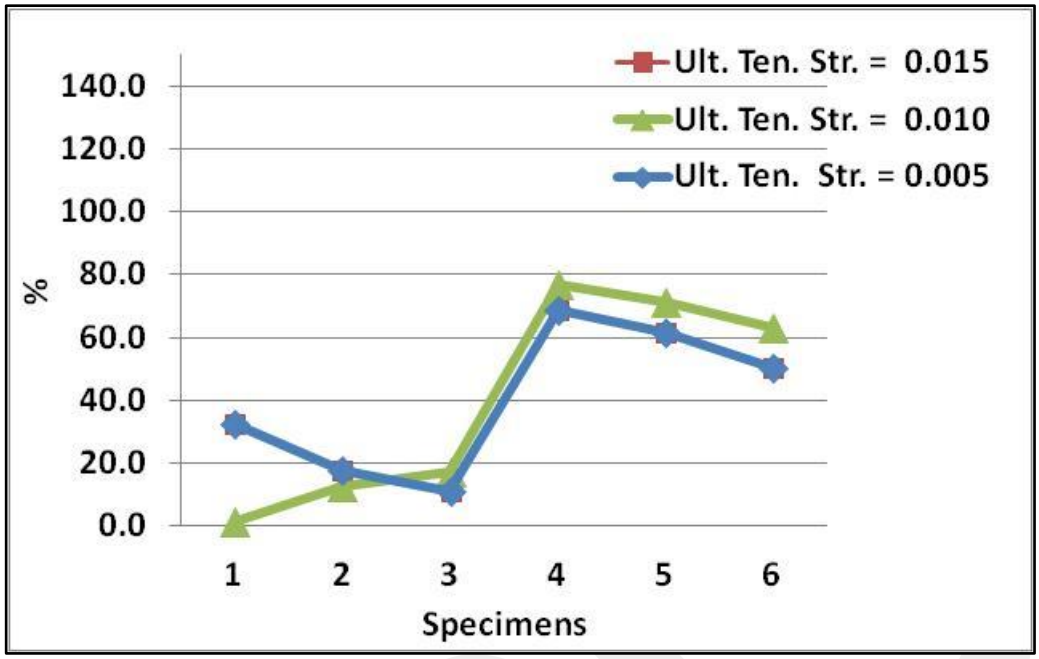

Figure 5-55 – Comparisons of area at ultimate load of SFRC flexural specimens and predictions for μ=0.50

Table 5-8 – Comparisons of area at ultimate load of SFRC flexural specimens and predictions for μ=0.50

ε_{tu}	1 (%)	2 (%)	3 (%)	4 (%)	5 (%)	6 (%)
0.005	32.5	17.8	11.4	68.6	61.6	50.5
0.01	1.6	12.5	17.3	76.7	71.5	63.3
0.015	32.5	17.8	11.4	68.6	61.6	50.5

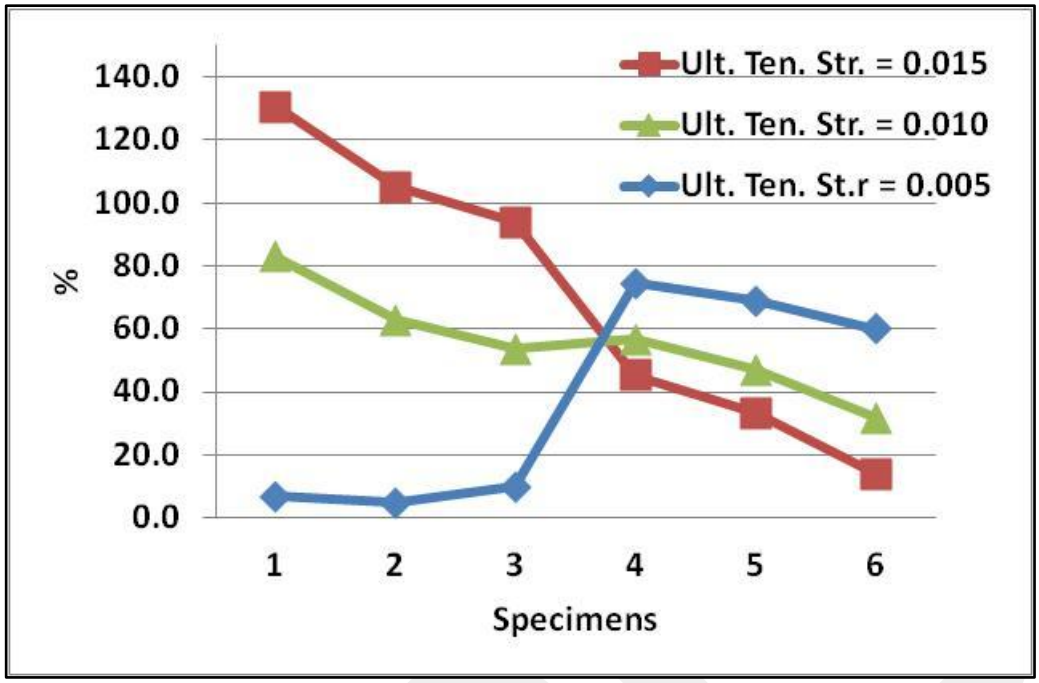

Figure 5-56 – Comparisons of area at ultimate load of SFRC flexural specimens and predictions for μ=0.75

Table 5-9 – Comparisons of area at ultimate load of SFRC flexural specimens and predictions for μ=0.75

ε_{tu}	1 (%)	2 (%)	3 (%)	4 (%)	5 (%)	6 (%)
0.005	7.0	4.9	10.0	74.6	69.0	60.1
0.01	82.9	62.7	53.8	56.6	47.0	31.7
0.015	130.4	104.9	93.8	45.3	33.2	14.0

Comparisons related to the area at 70% of ultimate load on the post-peak branch of load-deflection curves of μ=0.50 and 0.75 are shown Figure 5-57, Figure 5-58, Table 5-10, and Table 5-11. These tables and figures indicate that the first three for μ = 0.50 which had ultimate tension strain = 0.010 and last three which had ultimate tension strain = 0.005, 0.010, and 0.015 are better than the others. The first three for μ = 0.75 which had ultimate tension strain = 0.005 and last two which had ultimate tension strain = 0.015 and last one which had ultimate tension strain = 0.010 are better than the others, because they have values less than the others.

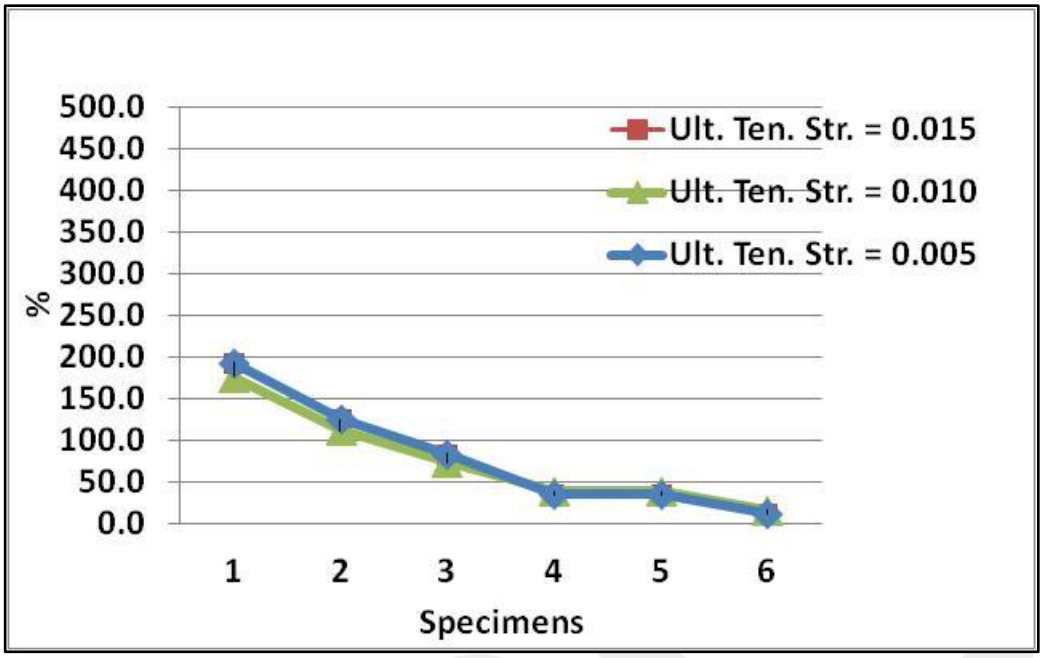

Figure 5-57 – Comparisons of area at 70% of ultimate load on the post-peak branch of SFRC flexural specimens and predictions for μ=0.50

Table 5-10 – Comparisons of area at 70% of ultimate load on the post-peak branch of SFRC flexural specimens and predictions for μ=0.50

ε_{tu}	1 (%)	2 (%)	3 (%)	4 (%)	5 (%)	6 (%)
0.005	194.2	126.0	84.5	35.4	35.1	12.1
0.01	177.1	112.9	73.8	39.1	38.9	17.2
0.015	194.2	126.0	84.5	35.4	35.1	12.1

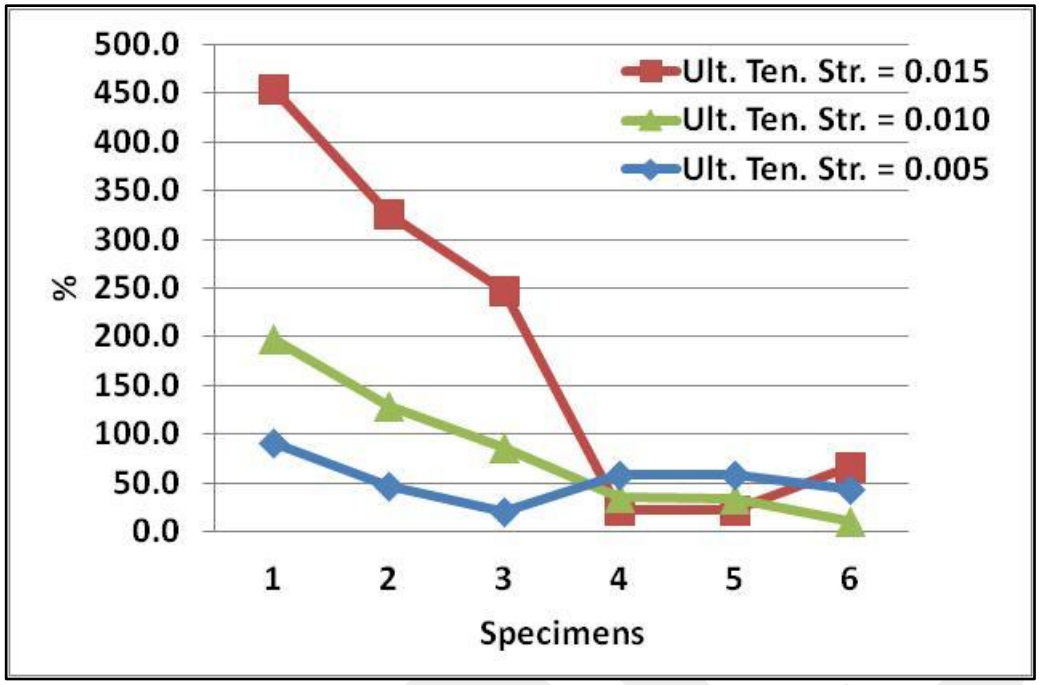

Figure 5-58 – Comparisons of area at 70% of ultimate load on the post-peak branch of SFRC flexural specimens and predictions for μ=0.75

Table 5-11 – Comparisons of area at 70% of ultimate load on the post-peak branch of SFRC flexural specimens and predictions for μ=0.75

ε_{tu}	1 (%)	2 (%)	3 (%)	4 (%)	5 (%)	6 (%)
0.005	91.5	47.2	20.1	57.9	57.8	42.8
0.01	197.5	128.6	86.6	34.6	34.4	11.1
0.015	455.4	326.8	248.4	22.0	22.5	66.0

6 SUMMARY, CONCLUSION AND RECOMMENDATIONS

6.1 Summary

Compressive and tensile behaviors of steel fiber reinforced concrete have been investigated in this research. Test series consisted of 20 singly reinforced specimens. The main parameters in the testing program were the type of concrete , cross-section and length. Two sizes of cylinders were tested, four batches of concrete were casted, two batches using CC and another two using SFRC. Behaviors of tested specimens were obtained and evaluated in terms of ultimate load, initial stiffness, and post-peak slope. Experimental load-deflection relationships obtained in this research were compared to the load-deflection curves obtained using the written Excel program. The stress-strain relationships available in the literature for SFRC in tension and compression were utilized in the numerical analyses. The proposed stress-strain relationships in the literature were compared and evaluated based on how accurately they predict the test data obtained in this research.

6.2 Conclusions

Compressive and tensile behaviors of steel fiber concrete have been obtained in this research.The observations and conclusions are as follows:

- The increase in the ultimate load capacity of the compression specimens with the addition of steel fibers was not significant compared to that of CC however, the compressive strength of SFRC specimens was always greater than that of CC specimens.
- When the stress-strain relationships of CC and SFRC specimens are compared, although there was no significant difference in the ascending branches, the descending branches of SFRC specimens showed a more ductile behavior.

- Based on the comparisons of these stress-strain relationships of CC and SFRC specimens, no significant difference was observed between 100×200 and 150×300 mm cylinders.
- It was noted that the initial stiffness of SFRC increased when the cross-section increased, this was valid also for CC specimens.
- After cracking, the load carrying capacity dropped dramatically to zero for CC beams under flexure however, the load carrying capacity of the SFRC beams increased to a maximum value after cracking then dropped gradually.
- Tensile SFRC specimens had greater initial crack load, yield load, and crack spacing than those of tensile CC specimens for all types of cross-sections.
- For tension specimens, as the cross-section of CC and SFRC specimens increased, the initial crack load increased. However, the cross-sectional dimensions did not have any significant effects on the yield load of CC and SFRC specimens.
- For tension specimens, as the cross-section of CC and SFRC specimens increased, the crack spacing increased. The change in the length of the specimens also does not have any significant effect on the crack spacing of the CC and SFRC specimens.
- Based on the analytical study performed to estimate the load-deflection behavior of SFRC specimens, SFRC compression models presented by Wang (2006) resulted in the best estimate of test data in the scope of this research.
- Based on the analytical study to estimate the load-deflection behavior of SFRC specimens, Soranakom and Mobasher (2009) SFRC tension model with a μ value equal to 0.75 and ultimate tension strain = 0.010 mm can be used to estimate the tension behavior of SFRC members with a reasonable accuracy.
- It is noted that for compression, Wang (2006)'s model results in the best estimate for our research.

6.3 Recommendations

For future work, following recommendations are made:

- For tension specimens with reinforcing bars, the test set-up oriented in vertical direction shall be selected which produces no bending deformations due to the self weight of the specimens.
- For tension specimens with reinforcing bars, selecting the length of the concrete prisms as a variable does not affect the behavior. Therefore, this variable may be eliminated.

7 REFERENCES

ACI Committee 544, "Design Considerations for Steel Fiber Reinforced Concrete," ACI 544.4R-88, American Concrete Institute, ACI Farmington Hills, MI; USA, 1988.

ACI Committee 544 (1996) "State of the Art Report on Fiber Reinforced Concrete," ACI 544.1R-96, American Concrete Institute, ACI Farmington Hills, Michigan, USA, 1996.

American Society for Testing and Materials, ASTM A820, "Standard Specification For Steel Fiber Reinforced Concrete," ASTM, Pennsylvania, USA, 1996.

American Society for Testing and Materials, ASTM C39, "Standard Test Method of Compressive Strength of Cylindrical Concrete Specimen," ASTM, USA, 2013.

American Society for Testing and Materials, ASTM C78 "Standard Test Method for Flexural Strength of Concrete (Using Simple Beam with Third-Point Loading)," ASTM, 2013.

Aoude, H., Cook, W. D., and Mitchell, D., "Innovative structural applications using SCC and SFRC", Recent Advances in Concrete Technology "RAC07", Washington, District of Columbia, September 19-21, 2007, pp. 565-572.

Baram, E. and Tugba, A. "Flexural Strength Design Criteria for Concrete Beams Reinforced with High-Strength Steel Strands," Advances in Structural Engineering, Vol. 15, No.10, 2012.

Barros, J.A.O. and Fiqueras, J. A., "Flexural behavior of SFRC," Testing and modelling. Journal of Materials in Civil Engineering, Vol. 11, No.4, 1999, pp. 331-339.

Bentur, A. and Mindes, S., "Fiber Reinforced Cementitious Deposits," Elsevier, 1990.

BS EN 14889-1: Fibers for Concrete - Part 1: "Steel Fibers-Definitions, Specifications and Conformity," British Standards Institution, London, 2006.

Bentz, E. C., "Explaining the Riddle of Tension Stiffening Models for Shear Panel Experiments," Journal of Structural Engineering, ASCE, V. 131, No. 9, Sept. 2005, pp. 1422-1425.

CEB-FIB Model Code, Bulletin d'Information No.213/214. Comite Euro-International du Beton, Thomas Telford (ed.) London, 1993.

Carreira, D.J. and Chu, K. M., "Stress-strain relationship for plain concrete in compression," ACI Journal Vol.82, No.6, 1985, pp. 797-804.

Cement & Concrete Association of New Zealand (CCANZ), "Fiber Reinforced Concrete," Information Bulletin: IB 39, December 2009, 19 pp.

Desayi, P. and Krishnan, S., "Equation for the Stress-Strain Curve of Concrete," ACI Journal, Proceedings V.61, No.3, Mar.1964, pp. 345-350.

Dhakal, R. P., "Post-peak Response Analysis of SFRC Columns Including Spalling and Buckling," Structural Engineering and Mechanics, Vol.22, No.3, 2006, pp. 311-330.

Edward G. Nawy D. Eng., P.E., C. Eng "Fiber Reinforced Composites " Concrete Construction Handbook, 2008, pp. 22-2-22-25

Ezeldin, A. S. and Balaguru, P. N., "Normal high-strength fiber reinforced concrete under compression," Journal of Materials in Civil Engineering, Vol. 4, No.4, 1992, pp. 415-427.

Frank, V. J., Lee, S.C., and Cho, J., "Model for Post-Yield Tension Stiffening and Rebar Rupture in Concrete Members," Engineering Structures, V. 33, No. 5, May 2011, pp. 1723-1733.

Fanella, D. A. and Naaman, A. E., "Stress-Strain Properties of Fiber Reinforced Mortar in Compression," ACI Journal, ProceedingsVol.82, No.4, 1985, pp.475-483.

Gopalaratnam, V. S. and Shah. S. P. "Softening Response of Plain Concrete in Direct Tension," ACI Journal, May-June, 1985, pp.310-323.

Hognestad, E., "A Study of Combined Bending and Axial Load in Reinforced Concrete Members," University of Illinois Engineering Experimental Station Bulletin 399:120, 1951.

Henager, C. H., Charles, H., and Doherty T., J., "Analysis of Reinforced Fibrous Concrete Beams," ACI 544.4R-88, American Concrete Institute, ACI Farmington Hills, MI; 1976, 18 pp.

Abrishami, H. H. and Mitchell, D., "Influence of Steel Fibers on Tension Stiffening," ACI Structural Journal, November-December 1997, pp. 769-776.

Japanese Concrete Institute, "Method of Test For Flexural Strength and Flexural Toughness of Fiber Reinforced Concrete," JCI – SF4, Japan Concrete Institute, 1984.

Deluce J. R. and Frank J. Vecchio, F. J., "Cracking Behavior of Steel Fiber-Reinforced Concrete Members Containing Conventional Reinforcement" ACI Structural Journal, May-June 2013, pp. 481-490.

Lok, T. S. and Xiao, J. R., "Tensile Behavior and Moment Curvature Relationship of Steel Fiber Reinforced Concrete," Magazine of Concrete Research, 50, No.4, 1998, pp. 359-368.

Luiz, A. J., Vanessa, E. S. B., Alice, R. B., Ramos, V. M. D., Daniel, L. A., El Debs, M. K., and Fernando, R. P., "Stress-Strain Curves for Steel Fiber-Reinforced Concrete in Compression," Revista Materia, Vol. 15, No. 2, 2010, pp. 260-266.

Mebarkia S. and Vipulanandan C., "Compressive Behavior of Glass Fiber-Reinforced Polymer Concrete," Journal of Material of Civil Engineering, Vol. 4, No. 1, 1992, pp. 91-105.

N. Ganesan, P.V. Indira, and M. V. Sabeena, "Tension Stiffening and Cracking of Hybrid Fiber-Reinforced Concrete", ACI Materials Journal/ November-December 2013, p.715-722.

Nataraja, M. C., Dhang, N., and Gupta, A. P., "Stress-Strain Curves for Steel-Fiber Reinforced Concrete under Compression," Cement & Concrete Composites, 1999, pp. 383-390.

National Research Council (CNR), "Guide for the Design and Construction of Fiber-Reinforced Concrete Structures," CNR-DT 204/2006, CNR, November 2007, 57 pp.

Nawy, E. G. and Blair, K., "Further Studies on Flexural Crack Control in Structural Slab Systems," Proceedings of the International Symposium on Cracking, Deflection, and Ultimate Load of Concrete Slab Systems, Nawy, E. G., ACI SP-30, 1971, pp.1-30 1-42. American Concrete Institute, Farmington Hills, MI.

Nawy, E. G. and Neuwerth, G. E., "Fiber Glass Reinforced Concrete Slabs and Beams," J. Struct. Div., ASCE, 103, 1977, pp. 421-440.

Olivito, R.S. and Zuccarello, F.A., "An Experimental Study on the Tensile Strength of Steel Fiber Reinforced Concrete," Composites: Part B, Vol. 41, 2010, pp. 246-255.

Popovics, S., "A Review of Stress-Strain Relationship for Concrete," ACI Journal, Vol. 67, No. 3, Mar. 1970.

RILEM, Final recommendations of TC 162-TDF, "Test and Design Method For Steel Fiber Reinforced Concrete,σ - ε Design Method," Materials and Structures, Vol. 36, 2003, pp. 560-565.

Romualdi, J.P. and Batson, G.B., "Mechanics of Crack Arrest in Concrete," Proc. ASCE, Eng. Mech. J., 89(EM3), 1963, pp. 147-168.

Romualdi, J. P. and Mandel, J. A., "Tensile Strength of Concrete Affected by Uniformly Distributed Closely Spaced Short Lengths of Wire Reinforcement," J. ACI, Vol. 61, No. 6, 1964, pp. 657-671.

Sargin, M., "Stress-Strain Relationship for Concrete and The Analysis of Structural Concrete Sections," Solid Mechanics Division, University of Waterloo, Waterloo, Ontario, Canada, Study No.4, 1971.

Shah, S. P. and Rangan, B. V., "Fiber Reinforced Concrete Properties," ACI J. Proc., Vol. 68, No. 2, 1971, pp. 126-135.

Soranakom, C., Yekani-Fard. M., and Mobasher, B., "Development of Design Guidelines for Strain-Softening Fiber Reinforced Concrete," International Symposium of Fiber Reinforced Concrete: Design and Application BEFIB 2008, Sept. 2008, pp. 513-523.

Soroushian, P. and Lee, C.D., "Constitutive Modeling of Steel Fiber Reinforced Concrete Under Direct Tension And Compression," R. N. Swamy, B. Barr (Eds), Fiber Reinforced Cements and Concretes, Recent Developments: 1989, pp. 363-375.

Swamy, R. N., "Fiber Reinforcement of Cement and Concrete", J. Mater. Struct., 1975, 8 (45), 1975, pp. 235–254

Swamy, R. N., Mangat, P. S., and Rao, C. V. "The Mechanics of Fiber Reinforcement of Cement Matrices in Fiber Reinforced Concrete", ACI SP-44, 1974, pp. 1–28.

The Concrete Institute, "Fiber Reinforced Concrete ", 2007.

Tulin L. G. and Gerstle K. H., "Discussion of Equation for Stress-Strain Curve of Concrete by P. Desayi and S. Krishnan," ACI Journal, 61(9), 1964, pp. 701- 716.

Vipulanandan C. and Paul E., "Performance of Epoxy and Polyester Polymer Concrete," ACI Mater. J., 1990, 87 (3), pp. 241–251.

Wang, C., "Experimental Investigation on Behavior of Steel Fiber Reinforced Concrete," Master's Thesis, 2006, University of Canterbury.

Zollo, R. F., "Fiber-reinforced Concrete: an Overview after 30 years of Development," Cement and Concrete Composites, Vol. 19, 1997, pp. 107-122.